FÍSICA
REVISTA CUBANA DE FÍSICA
Sociedad Cubana de Física
y Facultad de Física,
Universidad de La Habana
VOL.36 NO.2
DICIEMBRE, 2019

FÍSICA PARA TODOS

Revista Cubana de Física
ISSN 0253-9268
Online ISSN 2224-7939

REVISTA CUBANA DE FÍSICA
Vol. 36, No. 2 (Diciembre 2019)
ISSN 0253 9268 Online 2224 7939

Portada: Images from the First Summer School "Física para Todos" for High School students (July 8 - 12, 2019)

Todos los artículos en formato -e: www.revistacubanadefisica.org

La Revista Cubana de Física es una publicación semestral de la Sociedad Cubana de Física

WHAT MAKES THE REVISTA CUBANA DE FÍSICA RELEVANT TO OUR GEOGRAPHIC REGION?

¿QUÉ HACE A LA REVISTA CUBANA DE FÍSICA RELEVANTE PARA NUESTRA REGIÓN GEOGRÁFICA?

E. Altshuler

Editor in Chief, Revista Cubana de Física

It is fair to say that the Revista Cubana de Física has established a presence in the context of Latin America and the Caribbean[1]. Its "regional relevance" –a central requisite to enter the Web of Science for a publication which is not 100% written in English– shapes itself in many ways. For example, our section "Momentos de la Física en Cuba" typically deals with historical analysis of Physics in our island[2], but also serves, for instance, call the attention of policy-makers to the "critical shrinking" of our discipline[3]. Other sections like "Física para Físicos y No-Físicos", "Nuesta Física en Noticias", "Obituarios" and "Coordenadas" deal with subjects related not only to Cuban, but also to Latin American physics[4]. These sections are commonly –but not always– written in Spanish.

However, our *pièce de résistance* continues to be the original contributions –either full papers or original communications. Those also add up to the "regional relevance" of our journal, but perhaps in a subtler way: while a large percentage of those papers are written in English, a significant proportion is authored by Latin American physicists –Cubans, of course, heavily represented. Those facts have contributed to the steady increase in our bibliometric indices over the last few years.

Let us briefly analyze the original contributions to the Revista Cubana de Física from 2015 to 2019 (the present issue is not included in the statistics, neither special numbers). 46% of the original papers are written by all-Cuban teams, while 30% are produced by Cubans in collaboration with foreign partners, especially from México. The reminding 24% of the papers is totally written by non-Cuban researchers, roughly half of them from Latin American countries: México, Colombia, Venezuela and Ecuador. I might speculate that the relatively large contribution of México can be linked to the many Cuban physicists that have emigrated to than country over the last decades, while the also significant contribution from Colombia can be explained by the lack of a local journal analogous to the Revista Cubana de Física. Interestingly, the origin of the other 12% of papers written by non-Cuban scientists is quite diverse: the authors work in India, Jordan, Germany, Norway, Spain, France, Morocco, Oman, Saudi Arabia and the US.

Figure 1. *The paradox of the tailor and the client.* This illustration is taken from the editorial "La paradoja del sastre y el cliente" (O. de Melo, Rev. Cubana Fis. 32, 71 (2015)), containing a critical analysis of the decision to cut off to 4 years many undergrad programs by the Cuban Ministry of Higher Education.

The subject statistics of the papers published since 2015 (using the names of the Cuban Physical Society commissions) is: Condensed Matter: 25%, Theoretical Physics: 24%, Instrumentation and Metrology: 17%, Biological and Medical Physics: 11%, Physics teaching: 11%, Nuclear, Atomic and Molecular physics: 7%, and Optics and Spectroscopy: 5%. So, following a long tradition in Cuban Physics, Theory and Condensed matter dominate the scenario, although the limited possibilities of classification may have increased their

[1] E. E. Ramírez-Miquet and E. Altshuler "Where is our journal right now? Up-to-date bibliometrics and progress of Revista Cubana de Física". Rev. Cubana Fis. **36**, 2 (2019)

[2] L. M. Méndez-Pérez, P. Muné-Bandera y E. J. Roca-Oria "Celebrando el cuadrágesimo quinto aniversario de la Primera graduación de físicos en la universidad de Oriente". Rev. Cubana Fis. 32, 124 (2015)

[3] C. Cabal-Mirabal: "SOS Física: ocho desafíos para la Física cubana contemporánea". Rev. Cubana Fis. 36, 87 (2019)

[4] M. Sánchez-Colina "Olimpiadas universitarias de Física: De Cuba hacia Latinoamérica". Rev. Cubana Fis. 34, 2 (2017)

[5] Papers on granular matter, for example, have been either classified as "Condensed Matter" or "Instrumentation", to put one example.

numbers in detriment of what might be called "Statistical Physics" or "Complex Systems"[5], for example.

It can be said that the Revista Cubana de Física has become a "double-edged" Physics journal. On the one hand, half of the original papers come from totally Cuban teams, and the rest are quite eclectic regarding their origin, with a substantial Latin-American contribution. In spite of that, 64% of those papers are written in English. On the other hand, most contributions written in Spanish deal with hot topics of Cuban physics and physicists, including their relation with other Latin American physics communities.

In summary, the Revista Cubana de Física has tried to maintain a delicate balance between "universal" Physics and relevance to our region. I do hope that our long-standing effort will finally be noticed, opening our way to become a "full member" of the Web of Science. Whatever the output is, we will continue doing our best to keep improving: Cuban and Latin American physicists deserve it.

ABSORPTION AND REFLECTANCE SPECTROSCOPIC CHARACTERIZATION OF CANCEROUS AND PRE-CANCEROUS CERVICAL TISSUE

CARACTERIZACIÓN DE TEJIDO CERVICAL CANCEROSO Y PRE-CANCEROSO MEDIANTE ESPECTROSCOPIA DE ABSORCIÓN Y REFLECTIVIDAD

Y. P. Fernández Ramírez[a], W. Hoyos[b] and C. Rudamas[a†]

a) Laboratorio de Espectroscopia Óptica, Escuela de Física, Facultad de Ciencias Naturales y Matemática, Universidad de El Salvador, El Salvador. carlos.rudamas@ues.edu.sv†
b) FACSALEV, Universidad Dr. José Matías Delgado, El Salvador
† corresponding author

Recibido 30/5/2019; Aceptado 28/8/2019

Cancer diagnosis by non-invasive techniques is subject of cutting-edge research in biomedical field. This paper presents experimental results of absorption and reflectance spectroscopy for ex-vivo assessment of cancerous and pre-cancerous cervical tissue. Results show promising and provide a methodology to be integrated with the standard papsmear or screening and tests aimed at preventing deaths due to cervical cancer.

El diagnóstico del cáncer mediante técnicas no invasivas es objeto de investigaciones de punta en el campo biomédico. En este trabajo se presentan resultados experimentales de la aplicación de la espectroscopia de absorción y reflectancia para la evaluación ex-vivo de tejido cervical pre-canceroso y canceroso. Los resultados obtenidos pueden interpretarse como promisorios y develan una metodología que podría integrarse a la lectura convencional de papanicolaos o a campañas de tamizaje y prevención de muertes por cáncer cervicouterino.

PACS: Visible and ultraviolet sources (fuentes de luz visible y ultravioleta), 07.60.Rd; Spectroscopic and microscopic techniques in biophysics and medical physics (técnicas espectroscópicas y microscópicas en biofísica y física médica), 87.64.-t

I. INTRODUCTION

Cancer diagnosis is among the worldwide established priorities recognized by the World Health Organization (WHO). Nearly ten millions of people die every year as a consequence of cancer and its incidence continues to grow at accelerated rates, with estimations to be doubled by 2035 [1, 2]. This makes extremely important the implementation of efficient and cost-effective diagnosis procedures to better assess in early stages the tissue characteristics and prevent cancer from developing. The WHO foresees an increase in the diagnosed cases worldwide in the next decades with more than 80 % of new cases found in less-developed countries [3]. In a comprehensive study by Murillo *et al.*, cervical cancer is recognized as leading mortality cause in Latin American countries [4]. It is one of the most frequent cancers worldwide, with estimations of 266,000 deaths only in 2012 [5, 6].

There exist several techniques to address the study of cervical tissue in terms of morphology, composition, and other elements. The standard screening method is cervical cytology, also called "Pap test". This method helps detect abnormal cells in the cervix, which can develop into cancerous cells. In this way, screening reduces the risk of developing cervical cancer. If cancer is already present, early detection with screening improves the chances of recovery. However, cytologies are not always completely accurate [7]. Sometimes, test results can appear normal even if there is a cancer or abnormal cells in the lining of the cervix. Some women who receive cytology results may therefore be wrongly diagnosed. Optical techniques are pushing the development of non-invasive methods for cancer diagnosis and characterization as only light interacts with the tissue. These methods can be classified into two main groups: those which use light to excite or illuminate the biological sample and collect a response from the media (fluorescence microscopy [8], laser speckle imaging [9], spectroscopy-based methods [10], among others.) and those which aim at studying directly the internal structure of tissues (optical coherence tomography, photoacoustics [11], just to mention a few techniques.).

A potential implementation of optical techniques in cervical cancer diagnosis is found in the analysis of optical properties of cervical cells and tissue. By registering absorption and reflectance spectra from these samples, features of abnormal tissues can be identified as they are compared with model healthy tissue. Thereby, early diagnosis of cervical cancer can be performed by analyzing cells extracted from the cervix, thus avoiding other more invasive established methods such as biopsy. To the best of our knowledge, this intermediary protocol has not been exploited so far.

In this paper, we present a set of experimental analysis of cervical tissue using absorption and reflectance spectroscopy. In this context, the optical parameters of tissues are interrogated to study the main features leading to a clinical criteria. We aim thereby to describe the spectroscopic features of healthy, pre-cancerous and cancerous cervical tissue with

clinical perspective.

II. MATERIALS AND METHODS

In the experiments performed pre-cancerous and cancerous cervical tissues are studied by absorption and reflectance spectroscopy. Samples are collected during conventional cytological analysis of salvadoran female patients.

II.1. Sample collection procedures

Samples were collected using two different methods. In our investigation, we proceeded to the optical analysis of the collected cells which were previously classified with microscopy as healthy, pre-cancerous cervical intraepithelial neoplasia (CIN II) and cancerous carcinoma in-situ (CIN III). A smear test is performed on the patients following the standard procedure for this analysis [12]. In this method, a speculum is used to provide access to the cervix and a spatula is employed to smear the outer surface. This enables cells to get attached to the spatula surface, which are deposited in a glass plate for further lab treatment. In this procedure, the papsmear are colored with different dyes, which enable the identification of different cells and possible anomalies by microscopic observation. Cells are then subject to spectroscopic analysis to obtain their absorption and reflectance spectra.

For patients with clear identification of cells with cancerous features, a second sample collection using a colposcopy procedure is applied. In this method, a small portion of tissue is extracted from the cervical surface using a biospy Tischler punch. This tissue is also examined by using absorption and reflectance spectroscopic techniques.

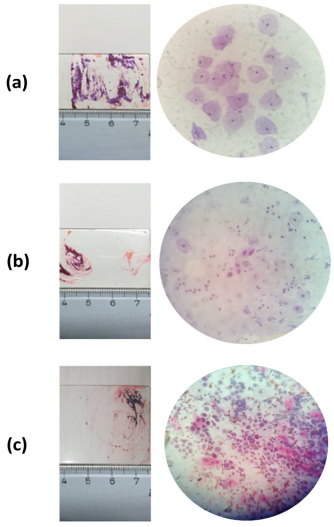

Figure 1. Optical imaging of the cell samples in between two plates and with x40 magnification. a corresponds to normal cells, b presents CIN II cells and c shows carcinoma *in-situ* CIN III cells.

The samples are represented in Fig. 1, where the studied cells are imaged with x40 magnification. The sample holders are also presented and scaled to illustrate how the cells are held in between two glass plates.

II.2. Optical set-up

In order to study our samples with the absorption and reflectance spectroscopies, an optical system projects light on the biological tissue to be evaluated. The light source is varied depending on the technique. For absorption spectroscopic measurements, a deuterium lamp is used and for reflectance measurements, a tungsten lamp is employed. Schemes of the optical setups employed are presented in Fig. 2 and Fig. 3.

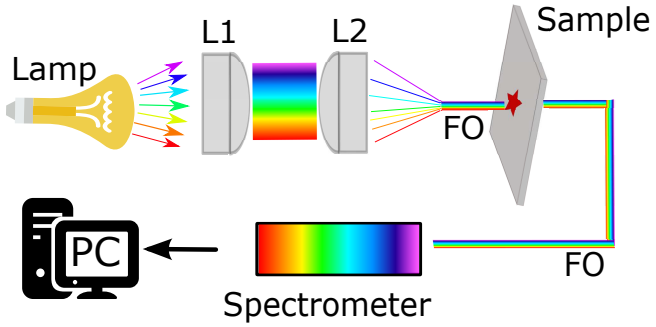

Figure 2. Optical setup employed for absorption spectroscopic measurement. L1 and L2 represent the set of lenses for beam shaping and FO is the optical fiber.

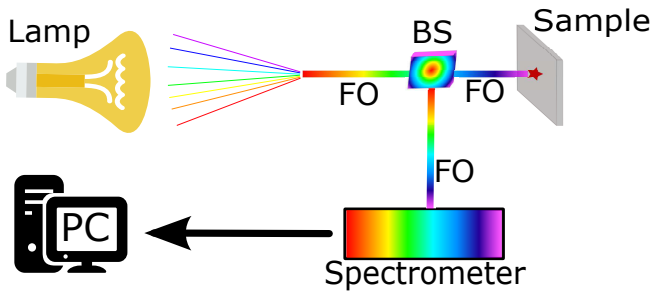

Figure 3. Optical setup employed for reflectance spectroscopic measurement. A beam splitter (BS) is used to derive the light towards the samples and the spectrometer simultaneously using the fiber optic (FO).

The spectrometer employed is an Ocean Optics model USB400. It is Czerny-Tuner configured with a focal distance of 42 mm at the input and 68 mm at the output. It has a plane diffraction grating with higher efficiencies between 300 and 400 nm and a spectral resolution of 1.5 nm in between 250 and 859 nm. It incorporates a cylindrical convex plane lens to reduce the image to the aperture of the detector. The detector operates in ambient temperature and integrates a Toshiba TCD130AP silicon charge-coupled device.

The information provided by the CCD device incorporated in the spectrometer is interfaced with the computer using an analog-to-digital converter and spectra are digitally registered using a USB port. Data acquistions are configured using the software SpectraSuite.

III. RESULTS

The absorption spectra for healthy (normal), pre-cancerous (cervical intraepithelial neoplasia, CIN II) and cancerous (carcinoma in-situ, CIN III) cells extracted from the cervical tissue are presented in Figure 4. They have two clearly formed

bands with maxima at 532 nm and 600 nm, which correspond to the absorption bands of hemoglobine [13]. The maximum located at 532 nm corresponds to the oxihemoglobin [14]. The spectral characteristics of this tissues are highlighted from the absorption measurements and the differences between a normal tissue and tissues with dysplasia are evident. Healthy tissues absorb much less of excitation light. The maximums remain at the same wavelengths and the spectral shape is the same in each type of cells. Moreover, as can be easily appreciated, absorption is higher in the pre-cancerous tissue with more advanced dysplasia associated (CIN III > CIN II) as compared to a normal tissue.

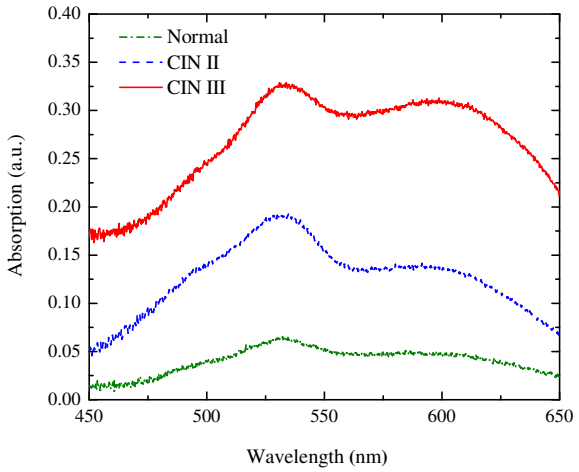

Figure 4. Absorption spectra of normal (healthy), CIN II and CIN III tissues. For better distinction among the plots, the reader is referred to the online version of the article where the plots appear in color.

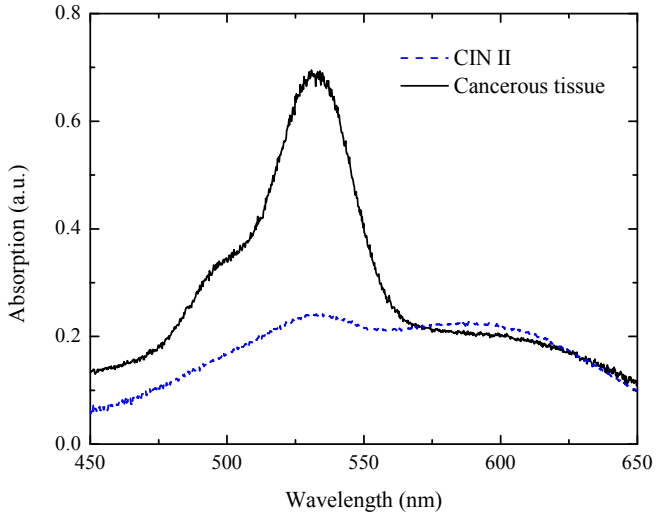

Figure 5. Comparison of the absorption spectra for cancerous cervical tissue and CIN II cells. For better distinction among the plots, the reader is referred to the online version of the article where the plots appear in color.

A comparison of a cancerous cervical tissue with a cervical intraepithelial neoplasia (CIN II) is presented in Figure 5. It can be appreciated the localization of the absorption maxima around 532 nm. It is clear the correlation existing between the abnormal tissue and its absorption features.

The absorption features shown in Figures 4 and 5 demonstrate that early assessment of the cervix using only the extracted cells is possible, thus avoiding the invasive nature of biopsies as much as possible and providing spectroscopic results on the degree of the cancer manifestation without extracting small portions of tissue, thus making the procedure less painful and still reliable. In addition, these cells samples can be directly examined in a microscope for further analysis in search for pathologies.

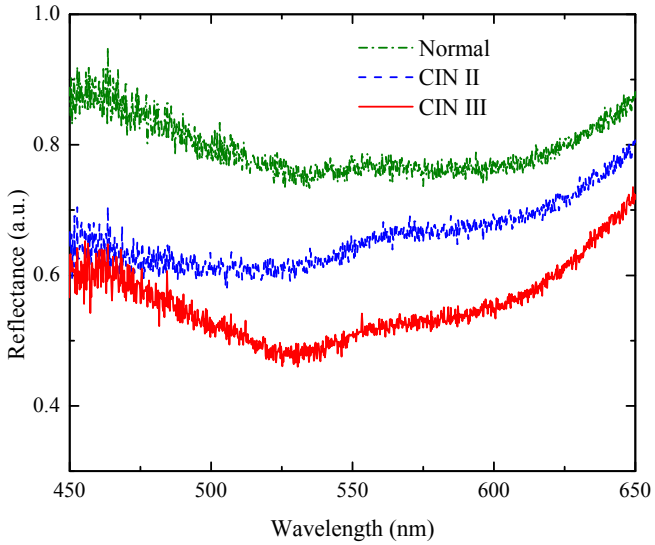

Figure 6. Reflectance spectra for cells with different classifications: healthy (normal), CIN II and CIN III. For better distinction among the plots, the reader is referred to the online version of the article where the plots appear in color.

For the absorption measurements the main contributions to the band are associated to the hemoglobin. This is explained by the fact that as cancer develops, other processes such as angiogenesis become relevant. Angiogenesis is a mechanisms ruling the formation of new blood vessels from existing vessels and is well related to the presence of cancer [15].

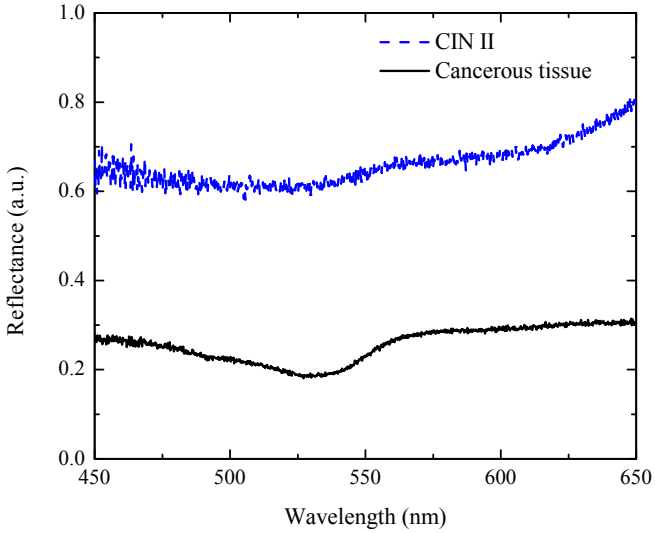

Figure 7. Comparison of reflectance spectra of cancerous tissue and cells (CIN II). For better distinction among the plots, the reader is referred to the online version of the article where the plots appear in color.

The reflectance spectra for cell samples extracted from cervical tissue are shown in Figure 6. As evidenced in these graphs, the results indicate an optical response aligned with the

absorption results presented in Figure 4. The more cancerous the cells are the less reflective and more absorptive they behave. Furthermore, the processes involved in the optical properties of these cells explain these results. As cells grow in size, their nuclei also grow, which turns to contribute significantly to the optical properties of the sample: it absorbs more light and reflects less [16].

The sample with cells issued from the smear test reflect more light than the extracted tissue as evidenced by the spectra from Figure 7, and maintain the spectral profile in the region 450-650 nm. Therefore, by using these reflectance features, early evaluation of the cervix can be performed, leading to quantification of the status of the cervical tissue. The threshold enabling the diagnosis is around 0.3 for the reflectance.

IV. CONCLUSIONS

Absorption and reflectance spectroscopies can potentially be employed to assess cervical cells and tissue. The spectral features provide information connected to degrees of development of cancer. The described methods enable this optical non-invasive technique to be considered in practical clinical assessment to enable an accurate diagnosis. Biopsies can be avoided using the methodology explained here and early detection of cervical cancer is enabled with non-invasive protocols.

ACKNOWLEDGMENTS

The authors wish to thank D. Madrid and D. Pleitez for providing the samples. Also we thank the other members of the research group who contributed to the discussion of the results. This work has been partially supported by the Council of Scientific Research (CIC-UES) in the framework of projects 05.31, 09.19 and 09.20.

REFERENCES

[1] F. Bray, J. Ferlay, I. Soerjomataram, R. L. Siegel, L. A. Torre and A. Jemal, CA Cancer J. Clin. **68**, 394 (2018).
[2] G. W. Prager, S. Braga, B. Bystricky *et al.*, ESMO Open **3**, e000285 (2018).
[3] L. G. C. Negrin, ecancer **9**, 577 (2015).
[4] R. Murillo, R. Herrero, M. S. Sierra and D. Forman. Cancer Epidemiol, **44S**, S121 (2016).
[5] J. Ferlay, I. Soerjomataram, R. Dikshit, S. Eser, C. Mathers, M. Rebelo, D. M. Parkin, D. Forman and F. Bray, Int. J. Cancer **136**, E359 (2015).
[6] D. Traynor, S. Duraipandian, C. M. Martin, J. J. O'Leary and F. M. Lyng, J. Biomed. Opt. **23**, 055001 (2018).
[7] S. Hosono, T. Terasawa, T. Katayama, S. Sasaki, K. Hoshi and C. Hamashima. Cancer Science **109**, 934 (2018).
[8] Z. Tao, X. Dang, X. Huang, M. D. Muzumdar, E. S. Xu, N. M. Bardhan, H. Song, R. Qi, Y. Yu, T. Li, W. Wei, J. Wyckoff, M. J. Birrer, A. M. Belcher and P. P. Ghoroghchian, Biomaterials **134** 202 (2017).
[9] A. Bennett, T. Sirkis, Y. Beiderman, S. Agdarov, Y. Beiderman and Z. Zalevsky, Biomed. Opt. Express **8**, 5359 (2017).
[10] A. C. Soares, J. C. Soares, F. M. Shimizu, M. E. Melendez, A. L. Carvalho and O. N. Oliveira Jr, ACS Appl. Mater. Interfaces **7**, 25930 (2015).
[11] J. Holmes, T. von Braunmühl, C. Berking, E. Sattler, M. Ulrich, U. Reinhold, H. Kurzen, T. Dirschka, C. Kellner, S. Schuh, and J. Welzel, Br. J. Dermatol. **178**, 1102 (2018).
[12] G. Guvenc, A. Akyuz, and C. H Açikel, J. Adv. Nurs. **67**, 428 (2011).
[13] B. D. Horecker, J. Biol. Chem. **148**, 173 (1943).
[14] W. G. Zijlstra and A. Buursma, Comp. Biochem. Physiol. **118**, 743 (1997).
[15] J. Folkman, Nat. Med. **1**, 27 (1995).
[16] O. C. Marina, C. K. Sanders and J. R. Mourant, Biomed. Opt. Express **3**, 296 (2012).

TEXTILES ELECTRÓNICOS DE BAJO COSTO BASADOS EN ARDUINO PARA INTRODUCIR CIRCUITOS ELÉCTRICOS Y PROGRAMACIÓN

ARDUINO-BASED LOW-COST ELECTRONIC TEXTILES TO INTRODUCE ELECTRIC CIRCUITS AND PROGRAMMING

E. Serrano-Pérez†

UNITEC MÉXICO - Campus Atizapán, Universidad Tecnológica de México, Boulevard Calacoaya 7, Capistrano, Cd. Adolfo López Mateos, Estado de México, México, 52970; edgar_serrano@my.unitec.edu.mx†
† autor para la correspondencia

Recibido 9/5/2019; Aceptado 29/8/2019

Se presenta una propuesta de proyecto de bajo costo para que alumnos de temprana edad se motiven por el estudio de la física en el área de la electricidad, los circuitos eléctricos y la programación de microcontroladores a través de la integración de elementos de bajo costo para animar visualmente prendas textiles y artículos de uso cotidiano. Durante el desarrollo del proyecto se parte desde el uso de los conceptos de la ley de Ohm y el estrecho vínculo que existe entre la representación de un número binario en el lenguaje Arduino hasta salida de voltaje del microcontrolador para encender o apagar cada uno de los ledes que se programan de manera secuencial.

A project for early age students is proposed in order to motivate the study of physics, mainly for the electricity area, electrical circuits and microcontroller programming through the integration of low-cost elements to animate visually textiles and common daily items. It includes the use of the concepts related to the Ohm law and the link that exists between the representation of a binary number in the Arduino language with the physical voltage output of the microcontroller to turn on or off each one of the led as result of a programming sequence.

PACS: Laboratory computer use (uso de computadoras de laboratorio), 01.50.Lc; Demonstration experiments and apparatus (experimentos demostrativos y aparatos), 01.50.My; Laboratory experiments and apparatus (experimentos de laboratorio y aparatos), 01.50.Pa

I. INTRODUCCIÓN

Durante el estudio de las ciencias y en particular de la física, los alumnos de secundaria afrontan dificultades para interpretar las leyes que rigen los fenómenos que se presentan en su entorno. Con frecuencia los alumnos se afrontan a la solución de problemas y casos de estudio basados en ecuaciones que tratan de describir de manera ideal un fenómeno físico. En particular, el estudio la Ley de Ohm permite a los estudiantes comprender la relación que existe entre voltaje, resistencia e intensidad de corriente en un circuito eléctrico, sin embargo se trata de conceptos abstractos y frecuentemente los estudiantes tienen poca experiencia previa al tratar el tema [1], para tratar de mejorar el proceso de aprendizaje en la introducción de la electricidad y los circuitos se propuso desarrollar una actividad que le permita a los estudiantes aprender y aplicar los conceptos de la física en un proyecto que englobe el uso de dispositivos electrónicos programables de bajo costo para decorar y animar visualmente prendas de vestir.

El auge de las tarjetas de desarrollo basadas en microcontroladores permite adaptar una gran cantidad de dispositivos electrónicos para ser utilizados como herramientas educativas en temas fundamentales como la electricidad y el magnetismo, además de incentivar la introducción hacia la programación de dispositivos electrónicos en edades tempranas durante el estudio de las ciencias, se ha observado el potencial de los textiles electrónicos para fomentar la exploración de circuitos eléctricos [2] y como un medio para atraer al género femenino al estudio de la física y las áreas de la ingeniería [3, 4]. Sin embargo, en los países en vías de desarrollo, la alta demanda de estudiantes frecuentemente no puede ser cubierta a través de la adquisición de kits prefabricados, por lo que la actividad descrita implica la adquisición de materiales accesibles y de bajo costo para promover el interés y el desarrollo de habilidades tecnológicas entre los estudiantes, como lo son ledes de distintos colores, resistencias de 330 Ω, una tarjeta Arduino Uno, cables de conexión y una tablilla de prototipos.

II. DESARROLLO

El primer módulo se llevó a cabo durante los meses de octubre y noviembre de 2018 y se desarrolló con 5 equipos de 3 personas. La actividad promovió que los alumnos pudieran ser capaces de verificar el diseño de un sistema a través de un experimento físico y con esto dar validez a los resultados obtenidos [5].

En un inicio, la gran mayoría de los estudiantes no tenía nociones para el cableado de circuitos eléctricos y la programación de microcontroladores, por lo que se buscó inicialmente que el código de programación fuera lo

más sencillo e intuitivo de entender para homogenizar el conocimiento del grupo. El programa utilizado como base para programar una simple secuencia de 5 luces led se muestra en la figura 1.

```
void setup() {
  pinMode(0, OUTPUT);
  pinMode(1, OUTPUT);
  pinMode(2, OUTPUT);
  pinMode(3, OUTPUT);
  pinMode(4, OUTPUT);
}
void loop() {
 digitalWrite(0, HIGH);
 digitalWrite(1, LOW);
 digitalWrite(2, LOW);
 digitalWrite(3, LOW);
 digitalWrite(4, LOW);
 delay(300);

 digitalWrite(0, LOW);
 digitalWrite(1, HIGH);
 digitalWrite(2, LOW);
 digitalWrite(3, LOW);
 digitalWrite(4, LOW);
 delay(300);

 digitalWrite(0, LOW);
 digitalWrite(1, LOW);
 digitalWrite(2, HIGH);
 digitalWrite(3, LOW);
 digitalWrite(4, LOW);
 delay(300);

 digitalWrite(0, LOW);
 digitalWrite(1, LOW);
 digitalWrite(2, LOW);
 digitalWrite(3, HIGH);
 digitalWrite(4, LOW);
 delay(300);

 digitalWrite(0, LOW);
 digitalWrite(1, LOW);
 digitalWrite(2, LOW);
 digitalWrite(3, LOW);
 digitalWrite(4, HIGH);
 delay(300);
}
```

Figura 1. Código fuente en lenguaje Arduino.

El reducido conjunto de instrucciones le permitió a los estudiantes conocer los conceptos de entradas y salidas digitales de un microcontrolador, además de los conceptos fundamentales de niveles lógicos para encender/apagar cada uno de los ledes a través de la corriente eléctrica que fluye desde cada uno de los pines del microcontrolador y que fluye a través de conductores de cobre.

Figura 2. Diseños textiles utilizando ledes, resistencias y una tarjeta Arduino.

Al analizar el programa, los estudiantes comenzaron a interpretar la estrecha relación que existe entre la sección de programación (software) con la parte física de los dispositivos (hardware). Cuando los estudiantes lograron programar la tarjeta Arduino y realizar sus circuitos eléctricos sugirieron incrementar el número de ledes conectados a la tarjeta para hacer una secuencia de luces más grande, por lo cual fue necesario que cada equipo modificara al programa base para controlar más ledes en diferentes secuencias de encendido de acuerdo a las necesidades de su diseño en particular. Cada equipo hizo su propio diseño con la única premisa de utilizar una secuencia de ledes adaptada a las necesidades de su diseño y colocarla como una parte interactiva del textil tal y como se muestra en la figura 2.

Es de resaltar el lado artístico de las estudiantes al realizar sus trabajos y diseños sobre textiles, por una parte las estudiantes combinaron diferentes elementos decorativos para realizar su textil electrónico, entre ellos se resalta el uso de pintura inflable, lentejuela, diamantina y elementos plásticos tridimensionales como hojas de plástico para decoración, además de realizar costura utilizando hilo tradicional mostrando agrado e interés por el diseño de sus propias creaciones, en general las estudiantes diseñaron elementos relacionados con los aspectos de la naturaleza como las flores y las mariposas.

Algunos de los estudiantes dedicaron más tiempo al detalle de sus diseños y algunos otros mostraron un mayor interés por el cableado de los ledes y sus circuitos utilizando la tarjeta Arduino sin poner mayor dedicación hacia su diseño textil. Por su parte, los estudiantes en general eligieron utilizar colores más oscuros en su textil electrónico. La temática de los alumnos en sus diseños fue relacionada con máquinas y automóviles, además de diversos dibujos animados, en contraste con los elementos de la naturaleza generalmente reflejados en las estudiantes. Los colores elegidos fueron desde tonalidades de grises hasta elementos rojos y azul oscuro. Algunos estudiantes comenzaron a proponer la integración de más dispositivos como sensores en su textil y la posibilidad de utilizar cables conductores como hilo de cobre para poder lavar sus prendas; surgió además la iniciativa de poder manipular el encendido de las secuencias a través de Bluetooth usando un celular.

El primer módulo culminó con la exposición de cada equipo frente al grupo, algunos alumnos comentaron que sus proyectos se desconectaban frecuentemente con facilidad debido al movimiento corporal con sus textiles por lo que se abrió la posibilidad de poder soldar los elementos y adquirir un mayor grado de fijación.

Con el inicio del segundo módulo en los meses de diciembre de 2018 y enero de 2019 se propuso la opción de utilizar una matriz de ledes de 8×8 que tiene integrado un controlador MAX7219 (aprox, $4.00 USD). La mayoría de los alumnos se mostró entusiasta con la nueva propuesta, pues con el uso de la matriz de ledes se presentó la posibilidad de generar patrones de símbolos y crear secuencias de animaciones en sus diseños.

Para facilitar la creación de sus animaciones se utilizó la herramienta de edición en línea Xantorohara, la cual es accesible a través de la web del autor, y se puede utilizar de manera gratuita. El uso del editor de animaciones permite simular previamente el comportamiento deseado del

sistema, con lo cual se facilita el proceso de aprendizaje de los alumnos al permitirles la libertad de hacer los cambios necesarios para adaptarse a sus propias variables y diseños particulares [6].

Se requirió que los alumnos obtuvieran el código para la tarjeta Arduino que se genera al diseñar sus propios patrones de animación con énfasis en formato byte con la finalidad de que al analizar su código pudieran identificar la relación que existe entre el código binario y la lógica digital para el encendido y apagado de los ledes.

La actividad les permitió a los estudiantes tener un primer acercamiento hacia un concepto clave y fundamental en el estudio de la electrónica y los sistemas digitales en ingeniería, como lo es la tabla de verdad, donde se trata de representar los valores de salida de un sistema a través de un conjunto de ceros y unos, tal y como se muestra en la Figura 3.

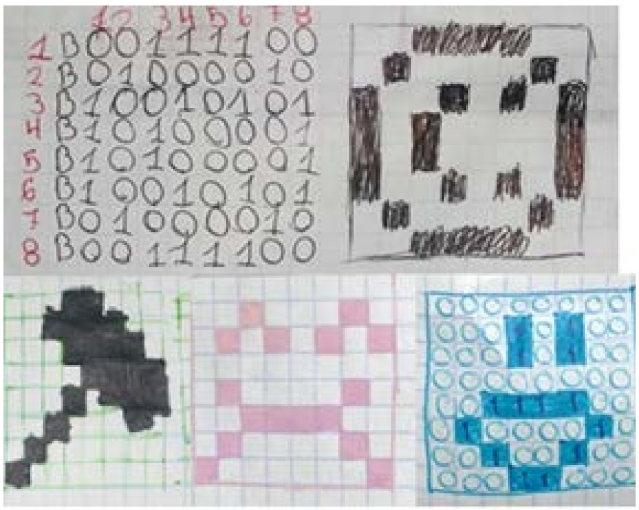

Figura 3. Representaciones de la tabla de verdad para una matriz de ledes 8×8.

La importancia de este concepto radica en que se observó que los alumnos fueron capaces de enlazar conocimientos multidisciplinarios para crear sus proyectos, en este caso, vincular el uso del código binario con su interpretación en lenguaje Arduino y su comportamiento físico a través de un voltaje en las terminales de los pines del microcontrolador.

Para poder identificar visualmente lo que ocurre con las terminales de la tarjeta se invoca el concepto de la ley de Ohm para conectar una resistencia de 330 Ω en serie con un led que consume alrededor de 15 mA cuando se conecta a una fuente de 5 volts. La representación que engloba los conceptos fundamentales se resumen en la tabla 1.

Tabla 1. Conceptos fundamentales en el desarrollo de circuitos eléctricos

Tabla de verdad	Lenguaje arduino	Voltaje	Interpretación visual
0	LOW	5 V	Encendido
1	HIGH	0 V	Apagado

La actividad resultó enriquecedora para los alumnos pues permitió vincular aspectos de la física entre los cuales se destacan la ley de Ohm, conceptos de corriente y resistencia eléctrica, además de introducir nociones de electrónica digital y la programación en edades tempranas a fin de que los alumnos comiencen a interesarse por las áreas de la ingeniería que sustentan sus pilares en ciencias fundamentales como la Física y las Matemáticas tal y como se aprecia en la figura 4. Los alumnos integraron la matriz de ledes en prendas de vestir como un elemento decorativo, otros más lo fijaron a sus celulares e incluso algunos lo adaptaron en unos lentes.

Figura 4. Integración de la matriz de ledes en los diseño de estudiantes.

Algunos alumnos que terminaron de manera anticipada el diseño de sus patrones visuales, la programación, y el armado de sus circuitos eléctricos comentaron la opción de agregar más matrices de ledes para crear diseños más grandes.

III. CONCLUSIONES

Es remarcable la gran creatividad que muestran los alumnos de temprana edad para desarrollar sus propios diseños y el surgimiento de nuevas ideas una vez que se logra alcanzar el objetivo primario, en este caso la introducción hacia los circuitos eléctricos y la programación. Los resultados fueron bastante alentadores al descubrir el potencial de los alumnos para crear prototipos inmersos en un proyecto que engloba la Ciencia, la Tecnología, la Ingeniería, las Artes y las Matemáticas (STEAM) que puede llevarse a cabo con dispositivos accesibles y de bajo costo.

REFERENCES

[1] ND Setyani, Suparmi, Sarwanto; J. Handhika, J. Phys.: Conf. Ser. **909**, 012051 (2017)..

[2] K. Peppler and D. Glosson, J. Sci. Educ. Technol. **22**, 751 (2013).

[3] L. Buechley, and B.M. Hill, LilyPad in the wild: how hardware's long tail is supporting new engineering and design communities, in Proceedings of the 8th ACM Conference on Designing Interactive Systems. 2010, ACM: Aarhus, Denmark. p. 199-207.

[4] D.A. Fields, Y. Kafai, T. Nakajima, J. Goode and J. Margolis, Equity & Excellence in Education **51**, 21 (2018).

[5] J.A. Lesteiro-Tejeda, D. Hernández-Delfín, and A.J. Batista-Leyva, Rev. Cubana Fis. **34** 5, (2017).

[6] P.A. Lonngi-Villanueva, and M.D. Ayala-Velázquez, Rev. Cubana Fis. **24**, 76 (2007).

ON THE POSSIBILITIES OF EXISTENCE OF PHOTOSYNTHETIC LIFE AROUND ALPHA CENTAURI B

SOBRE LAS POSIBILIDADES DE EXISTENCIA DE VIDA FOTOSINTÉTICA ALREDEDOR DE ALFA DEL CENTAURO B

G. Estrada-Rodriguez[a], A. Gonzalez-Noa[b] and R. Cárdenas[b†]

a) Maxwell Institute Graduate School in Analysis and its Applications, University of Edinburgh, United Kingdom
b) Planetary Science Laboratory, Universidad Central "Marta Abreu" de Las Villas, Santa Clara, Cuba; rcardenas@uclv.edu.cu†
† autor para la correspondencia

Recibido 15/10/2019; Aceptado 10/11/2019

We start with a brief description of the Alpha Centauri system and its main characteristics. Afterwards, we carry out calculations of several habitability metrics, such as the Π biological productivity and photosynthesis rates, in the oceans of the hypothetical exoplanets orbiting around Alpha Centauri B. By including a function of the temperature in a photosynthetic model, we describe the behavior of the metrics mentioned above for organisms with prokaryotic and eukaryotic cells that could potentially live in these exoplanets.

Comenzamos con una breve descripción del sistema Alpha del Centauri y sus características fundamentales. Luego, realizamos cálculos sobre varias métricas de habitabilidad, como la productividad biológica Π y las tasas fotosintéticas, en los océanos de los exoplanetas hipotéticos que orbitan alrededor de Alpha del Centauri B. Mediante la inclusión de una función de la temperatura en un modelo fotosintético, describimos el comportamiento de las métricas arriba mencionadas para organismos con células procariotas y eucariotas que pudieran potencialmente vivir en esos exoplanetas.

PACS: Astrobiology and extraterrestrial materials (astrobiología y materiales extraterrestres), 91.62.Fc; photochemistry, photosynthesis (fotoquímica, fotosíntesis), 92.20.ch

I. INTRODUCTION

The system Alpha Centauri comprises three stars. Alpha Centauri A is a yellow star, very similar to the Sun (spectral type G), and Alpha Centauri B is an orange type K star. Both spin around themselves in an orbit of approximately 80 years. Since they have similar masses, they move around one space point approximately equidistant between them, the center of mass. The third star is Proxima Centauri, which rotates around the two previous at a much bigger distance. There is a debate about the eccentricity of Proxima Centauri and if this star is actually related to the system. However, the three stars have similar parallax and proper movement. In the event that Proxima is related to the other two, its orbit would last for several hundreds of thousands of years. It is a small and red star that only can be seen through powerful telescopes.

Both Alpha Centauri A and Alpha Centauri B have high metallicity, so both should have circumstellar disks with a relatively high fraction of solid material, which would favor the formation of terrestrial planets. As Alpha Centauri B has less luminosity than Alpha Centauri A, the former has the zone of habitability closer to the star. For this reason, a planet located there would be less exposed to the gravitational negative disturbances that could come from the nearby binary star. In table 1 general properties of the Alpha Centauri system as compared with the Sun are shown.

Tabla 1. General properties of the stars that conform the triple system Alpha Centauri compared with the Sun

Parameter	Alpha Centauri A	Alpha Centauri B	Proxima Centauri	Sun	Unit of measurement
Age	4850	4850	4850	4650	Million years
Mass	1100	0.907	0.123	1	Solar masses
Radius	1227	0.865	0.145	1	Solar radiuses
Temperature	5790	5316	3040	5780	K
Luminosity	1519	0.44	0.000138	1	Solar luminosity
Hydrogen	71.5	69.4	69.5	73.7	%
Helium	25.8	27.7	27.8	24.5	%
Heavier elements	2.74	2.89	2.90	1.81	%

II. MATERIALS AND METHODS

We refer the reader to reference [1], where the process of formation of planetary systems around a star is simulated using the package of integration MERCURY. This package is designed to study the growth of planets around binary stars. Among the planets obtained, eleven were formed inside the habitability zone. In this section we present three habitability metrics used to quantify habitability in them: Earth Similarity Index (ESI), E model of photosynthesis, and Π model of biological productivity.

II.1. Earth Similarity Index

The Earth Similarity Index (ESI), introduced in [2], is given by:

$$ESI = \prod_{i=1}^{n} \left(1 - \left|\frac{x_i - x_{i0}}{x_i + x_{i0}}\right|\right)^{\frac{w_i}{n}}, \tag{1}$$

where:

- x_i is one property of the planet, for example the temperature at planet surface,
- x_{i0} is the value of that same property in current Earth,
- w_i is a weight exponent and
- n is the total number of properties that are used in calculation.

The properties of above mentioned eleven planets are shown in table 2.

II.2. E Model of Photosynthesis

The main characteristics of this model are presented in [3]. The rate P of the photosynthetic process in this model can be calculated as:

$$P = P_{Pot}\left(\frac{1}{E^*_{UV}}\right). \tag{2}$$

Here E^*_{UV} is the inhibitory dimensionless irradiance, while P_{pot} is the speed of the process in the absence of photo-inhibition, which is given in the following way:

$$P_{Pot} = P_s\left(1 - e^{-\left(\frac{E_{PAR}}{E_s}\right)}\right). \tag{3}$$

In the previous expression P_s is the maximum rate of photosynthesis in the absence of inhibition, E_{PAR} (W/m^2) is the irradiance of the photosynthetically active radiation (PAR), while E_s (W/m^2) is a parameter measuring the efficiency of photosynthesis, the smaller its value, the more efficiently the species uses PAR.

The inhibitory dimensionless irradiance of the ultraviolet light is be given by:

$$E^*_{UV} = \sum_{\lambda_i=176\text{ nm}}^{\lambda_i=340\text{ nm}} \varepsilon(\lambda_i)E(\lambda_i)\Delta\lambda, \tag{4}$$

where $\varepsilon(\lambda_i)$ (m^2/W) are the biological action spectra that quantify the effectiveness of the spectral exposition $E(\lambda_i)$ (W/(m^2·nm)). This means that $\varepsilon(\lambda_i)$ represents the inhibition of the photosynthesis caused by the ultraviolet light of wavelength λ_i.

Substituting 3 in 2 and normalizing by P_s we obtain:

$$\frac{P}{P_s} = \frac{1 - e^{-\left(\frac{E_{PAR}}{E_s}\right)}}{1 + E^*_{UV}} \tag{5}$$

This is a common form of expressing this model.

II.3. Π Model of Biological Productivity

The Π model of biological productivity reads as follows [4]:

$$\frac{\Pi}{\Pi_{max}} = \left(1 - \left(\frac{T_{opt} - T}{T_{opt} - 273}\right)^2\right)\left(\frac{P_{atm} - P_{min}}{P_{1/2} + (P_{atm} - P_{min})}\right). \tag{6}$$

In this equation T is temperature at planetary surface, P_{atm} is the atmospheric partial pressure of CO_2, P_{min} is the minimum partial pressure of CO_2 needed to sustain photosynthesis, and $P_{1/2}$ is the partial pressure giving $\Pi/\Pi_{max} = 1/2$. The function of temperature is an inverted parabola symmetric to the optimum temperature for life (taken equal to 25°C in this study).

As this study is based on an atmosphere with a similar composition to the one of the Earth, it was assumed that the dependence with the partial pressure of CO_2 in the atmosphere of the exoplanets would be similar to the one of the Earth. Then this model would depend only on temperature.

In table 3 we show results of previous application of the three habitability metrics presented in this section [5].

III. RESULTS AND DISCUSSION

When analyzing the results of the previous table it is observed that the tendency of the values of the rates of photosynthesis does not match the tendencies of the remaining metrics. This is because the E model of photosynthesis does not take into account the temperature, which is a very important magnitude for determining if an environment is capable to hold life.

Therefore, we propose a modification to the photosynthesis model by introducing a function of temperature:

$$\frac{P}{P_s} = \left(\frac{1 - e^{-\left(\frac{E_{PAR}}{E_s}\right)}}{1 + E^*_{UV}} \right) \left(1 - \left(\frac{T_{opt} - T}{T_{opt} - 273} \right)^2 \right) \quad (7)$$

The new results are shown in table 4, and are more coherent since the exoplanets that have an Earth Similarity Index between 0.9 and 1.0 are also the ones with higher biological productivity (Π model) and higher rates of photosynthesis.

By including this temperature function we see a major improvement in the behavior of the indexes for different kinds of organisms that, at the same time, have different optimum temperatures for their development. For example, the most beneficial mean temperature to attain a higher rate of biological productivity for thermophilic prokaryotic organisms can be taken as 51°, for eukaryotic organisms would be equal to 25°, and in multicellular organisms would be equal to 15°.

Tabla 2. Properties of the planets selected in the paper

Planet	Superficial Temperature (K)	Density (kg/m^3)	Radius (m)	Velocity of Escape	ESI
a1	291.75	6326.14	7737661.45	14546.43	0.924
a5	290.85	6182.42	7489052.58	13918.21	0.936
a6	271.46	6689.11	8376072.70	16192.04	0.875
a8	267.88	5995.90	7170038.50	13122.79	0.911
b2	336.46	5813.04	6861304.53	12364.76	0.864
b3	349.08	5150	3005075.99	5098.55	0.750
b4	285.27	6389.72	7848401.97	14828.57	0.926
b7	310.85	5150	5429452.60	9211.85	0.918
b8	364.98	5150	2385130.39	4046.72	0.688
c1	373.79	5150	4636756.26	7866.93	0.776
c3	282.77	6534.01	8101441.98	15478.52	0.911

Tabla 3. Habitability Metrics for Exoplanets around Alpha Centauri B

Planet	ESI	Superficial Temperature (K)	Π/Π_{max}	$\langle P/P_s \rangle$ Ocean water I	$\langle P/P_s \rangle$ Ocean water II	$\langle P/P_s \rangle$ Ocean water III
a1	0.924	291.75	0.56	0.72	0.52	0.37
a5	0.936	290.85	0.55	0.72	0.52	0.36
a6	0.875	271.46	0	0.69	0.48	0.35
a8	0.911	267.88	0	0.68	0.48	0.34
b2	0.864	336.46	0	0.78	0.57	0.40
b3	0.750	349.08	0	0.79	0.59	0.41
b4	0.926	285.27	0.44	0.71	0.51	0.36
b7	0.918	310.85	0.44	0.75	0.54	0.38
b8	0.688	364.98	0	0.79	0.60	0.42
c1	0.776	373.79	0	0.80	0.61	0.43
c3	0.911	282.77	0.37	0.71	0.50	0.36

Tables 5-7 collect results considering above mentioned temperatures.

Tabla 4. Habitability Metrics for Exoplanets around Alpha Centauri B considering the influence of temperature in photosynthesis

Planet	ESI	Superficial Temperature (K)	Π/Π_{max}	$\langle P/P_s \rangle$ Ocean water I	$\langle P/P_s \rangle$ Ocean water II	$\langle P/P_s \rangle$ Ocean water III
a1	0.924	291.75	0.56	0.69	0.49	0.35
a5	0.936	290.85	0.55	0.66	0.47	0.33
a6	0.875	271.46	0	0	0	0
a8	0.911	267.88	0	0	0	0
b2	0.864	336.46	0	0	0	0
b3	0.750	349.08	0	0	0	0
b4	0.926	285.27	0.44	0.52	0.37	0.26
b7	0.918	310.85	0.44	0.56	0.40	0.28
b8	0.688	364.98	0	0	0	0
c1	0.776	373.79	0	0	0	0
c3	0.911	282.77	0.37	0.44	0.31	0.22

Tabla 5. Habitability Metrics for Thermophilic Prokaryotic Organisms (T_{opt} = 51°C)

Planet	ESI	Superficial Temperature (K)	Π/Π_{max}	$\langle P/P_s \rangle$ Ocean water I	$\langle P/P_s \rangle$ Ocean water II	$\langle P/P_s \rangle$ Ocean water III
a1	0.924	291.75	0.36	0.44	0.31	0.22
a5	0.936	290.85	0.34	0.41	0.30	0.21
a6	0.875	271.46	0	0	0	0
a8	0.911	267.88	0	0	0	0
b2	0.864	336.46	0.57	0.73	0.54	0.38
b3	0.750	349.08	0.46	0.60	0.45	0.31
b4	0.926	285.27	0.25	0.30	0.21	0.15
b7	0.918	310.85	0.56	0.70	0.51	0.36
b8	0.688	364.98	0.22	0.29	0.22	0.15
c1	0.776	373.79	0.03	0.04	0.03	0.22
c3	0.911	282.77	0.20	0.24	0.17	0.12

Tabla 6. Habitability Metrics for Eukaryotic Organisms (T_{opt} = 25°C)

Planet	ESI	Superficial Temperature (K)	Π/Π_{max}	$\langle P/P_s \rangle$ Ocean water I	$\langle P/P_s \rangle$ Ocean water II	$\langle P/P_s \rangle$ Ocean water III
a1	0.924	291.75	0.56	0.69	0.49	0.35
a5	0.936	290.85	0.55	0.66	0.47	0.33
a6	0.875	271.46	0	0	0	0
a8	0.911	267.89	0	0	0	0
b2	0.864	336.46	0.57	0.73	0.54	0.38
b3	0.750	349.08	0	0	0	0
b4	0.926	285.27	0.44	0.52	0.37	0.26
b7	0.918	310.85	0.44	0.56	0.40	0.28
b8	0.688	364.98	0	0	0	0
c1	0.776	373.79	0	0	0	0
c3	0.911	282.77	0.37	0.44	0.31	0.22

From the tables above it is clear that the potential for the existence of the prokaryotic life is much bigger than for the eukaryotic or the multicellular one, that is, the number of suitable planets to develop this type of life is much bigger compared to the other two. Also, one observes that in table 5 and in table 7 the biological productivity (Π model) and the rates of photosynthesis do not coincide with the ESI. This happens because the optimal mean temperature for the realization of the photosynthesis in these cases was assumed to be 51° and 15° respectively, which differ with the one of the Earth, which is around 25°.

IV. CONCLUSIONS

In order to describe the habitability in exoplanets of terrestrial type successfully, they should satisfy several parameters at the same time. For the results to have more precision and the model to recreate a habitable planet of terrestrial type, the model should take into account the temperature.

The results demonstrate that the less complex is the form of life, the greater are the possibilities that any of these exoplanets have it.

Tabla 7. Habitability Metrics for Multicellular Organisms (T_{opt} = 15°C)

Planet	ESI	Superficial Temperature (K)	Π/Π_{max}	$\langle P/P_s \rangle$ Ocean water I	$\langle P/P_s \rangle$ Ocean water II	$\langle P/P_s \rangle$ Ocean water III
a1	0.924	291.75	0.57	0.69	0.49	0.35
a5	0.936	290.85	0.58	0.70	0.50	0.35
a6	0.875	271.46	0	0	0	0
a8	0.911	267.89	0	0	0	0
b2	0.864	336.46	0	0	0	0
b3	0.750	349.08	0	0	0	0
b4	0.926	285.27	0.58	0.69	0.49	0.35
b7	0.918	310.85	0	0	0	0
b8	0.688	364.98	0	0	0	0
c1	0.776	373.79	0	0	0	0
c3	0.911	282.77	0.52	0.62	0.44	0.31

REFERENCES

[1] M. Guedes, E. Rivera, E. Davis, G. Laughlin, E. Quintana and D. Fischer, Astrophys. J. **679**, 1582 (2008).

[2] D. Schulze-Makuch, A. M´endez, A. G. Fairén, P. von Paris, C. Turse, G. Boyer, A. F. Davila, A. Resendes de Sousa, M. Antonio, D. Catling, and L. N. Irwin, Astrobiol. **11,** 1041 (2011).

[3] J. Fritz, P. Neale, R. Davis and J. Pelloquin. Marine Ecol. Prog. Series **365**, 1 (2008).

[4] T. Volk, Am. J. Sci. **28**, 763 (1987).

[5] A. González-Noa, R. Cardenas and J. Hearnshaw. Rev. Cubana Fis. **30**, 81 (2013).

THERMAL REDUCTION OF Cu^{2+} IN PRESENCE OF Ag^{+} IN CLINOPTILOLITE: STRUCTURAL STUDY BY EXAFS AND HR-XRD

REDUCCIÓN TÉRMICA DE Cu^{2+} EN PRESENCIA DE Ag^{+} EN CLINOPTILOLITA: ESTUDIO ESTRUCTURAL POR EXAFS Y HR-XRD

B. Concepción-Rosabal[a†], I. Rodríguez-Iznaga[b] ,V. Petranovskii[c], F. Chávez Rivas[d], S. J. A. Figueroa[e], A. Pentón-Madrigal[b]

a) Instituto de Ciencia y Tecnología de Materiales (IMRE) - Universidad de La Habana, Cuba; beatriz@imre.uh.cu†
b) Facultad de Física- IMRE, Universidad de La Habana, La Habana, Cuba
c) Centro de Nanociencias y Nanotecnología (CNyN) – Universidad Nacional Autónoma de México. Carretera Tijuana-Ensenada, Km 107. Ensenada, B.C. México
d) Escuela Superior de Física y Matemáticas, Instituto Politécnico Nacional (IPN), C.P. 07738, México, D.F., México
e) Brazilian Synchrotron Light Laboratory (LNLS)/Brazilian Center of Energy and Materials (CNPEM), CP 6192, 13083-970, Campinas, SP, Brazil
† corresponding author

Recibido 14/5/2019; Aceptado 12/11/2019

Cu^{2+}–Ag^{+} bimetallic systems were exchanged and then thermally reduced in natural clinoptilolite (CLI) from Tasajeras deposit (Cuba). The systems were characterized by means of extended X-ray absorption fine structure (EXAFS) and high resolution X-ray diffraction (HR-XRD) experiments. The EXAFS signals of the bimetallic systems showed changes in the Cu^{2+} coordination as a result of their reduction at 150°C, which doesn't happen to CuCLI monometallic one. The presence of silver facilitates the reduction of Cu^{2+} in bimetallic systems forming only clusters. At higher reduction temperature (450°C) all mono- and bi-metallic samples exhibit mainly metallic particles of Cu and Ag with higher aggregation. These results are confirmed by HR-XRD studies. Aggregation of reduced copper species is restricted in the presence of silver.

Sistemas bimetálicos de Cu^{2+}–Ag^{+} fueron intercambiados y seguidamente reducidos térmicamente en la clinoptilolita natural (CLI) del yacimiento de Tasajeras (Cuba). Estos sistemas fueron caracterizados a través de experimentos de estructura fina de la absorción de rayos X en la región extendida (EXAFS, acrónimo en inglés) y difracción de rayos – X de alta resolución (HR-XRD, acrónimo en inglés). Las señales de EXAFS de los sistemas bimetálicos mostraron cambios en la coordinación del Cu^{2+} como resultado de su reducción a 150°C, lo cual no sucede en el sistema monometálico de CuCLI. La presencia de la plata facilita la reducción del Cu^{2+} en los sistemas bimetálicos, formándose solamente clústeres a esta temperatura. A mayor temperatura de reducción (450°C) todas las muestras mono- y bi-metálicas exhiben principalmente partículas de Cu y Ag metálico con mayor agregación. Estos resultados se confirman por estudios de HR-XRD. La agregación de las especies de cobre reducidas es restringida en presencia de la plata.

PACS: Zeolites, clusters in zeolites, structural properties, (zeolitas, clústeres en zeolitas, propiedades estructurales) 82.75.z, 82.75.Mj, 82.75.Vx; X-ray absorption spectroscopy (EXAFS) (espectroscopia de absorción de rayos X), 61.05.cj; X-ray diffraction (XRD) (difracción de rayos X), 61.05.cp

I. INTRODUCTION

Modified zeolites with metal nanospecies (ions, clusters, nanoparticles, etc.) are of interest due to their unique and improved properties to develop new materials as catalyts, drugs, bactericides and others [1–9]. Among other metals, Cu and Ag are outstanding due to both catalytic properties and olygodynamic activity. Thus, it is well-known that zeolites modified with copper cations are among the most selective and active catalysts to nitrogen monoxide (NO) reduction [1, 10–13]. It is also recognized that the type of supported metallic nanospecies, their aggregation and stability define the properties and use of modified zeolites.

Numerous studies on zeolites modified with only one metal are available in the literature. The properties of the metal species experience important changes in multimetallic systems with respect to monometallic one [1, 14–17]. In this sense, it was shown that both stability and catalytic activity in NO-reduction to Cu^{2+} catalysts supported on mordenite increase when silver is present [1]. It has been reported that Zn^{2+} has a positive effect to Cu^{2+} reduction on clinoptilolite zeolite [15].

Early structural studies [14] on thermal reduced bimetallic Cu^{2+}–Ag^{+} systems exchanged in clinoptilolite from the Tasajeras deposit (Cuba) were performed by means of UV-Vis reflectance diffuse spectroscopy and conventional X – ray diffraction. The obtained results showed a significant inter influence of both metals during the reduction process and formation of different reduced species, which was associated with a synergetic effect of the different concurrent species. UV-Vis spectra showed evidences on exchanged Cu2+ through the characteristic band of this cation associated with d-orbital transitions. A band of charge-transfer complex due to the interaction of this cation with oxygen both of ligand water molecules and of zeolite framework was observed as well, which in turn lead to the formation of

$Cu(_2^+)$-δ/CLI($_2$−)+δ and $Ag(^+)$-δ/CLI(−)+δ complexes. Besides this, it was revealed the occurrence of both copper and silver particles possessing plasma resonance absorbance at higher temperature (450oC), which is in line with reported X – ray diffraction results [4, 5]. Also, X – ray diffraction has shown peak intensities changes fundamentally associated with differences in nature, amount and position of the extra-framework ions in zeolite channels [4, 5, 18].

This work presents a study concerning the thermal reduction under hydrogen flow of a bimetallic Cu^{2+}–Ag^+ system exchanged on natural clinoptilolite from Tasajeras deposit, Cuba. The influence of silver on Cu2+ reduction was studied by means of High Resolution X – Ray Diffraction (HR-XRD) and Extended X-ray absorption fine structure (EXAFS).

II. EXPERIMENTAL

The purified zeolite material, with a particle size of 40 – 90 μm, was obtained from the zeolitic rock of Tasajeras deposit (Cuba). It is a mixture of about 78 % clinoptilolite-heulandite, 5 % mordenite and 17 % of others phases (montmorillonite, quartz, feldspar and iron oxides). The elemental chemical composition of the purified zeolite material was reported previously in [14]. Herein this zeolite is referred as the purified zeolite or natural clinoptilolite (CLI).

Copper/Silver-CLI bimetallic systems were prepared by Cu^{2+} and Ag^+ simultaneous ion-exchange using 0.1 mol/L $Cu(NO_3)_2/AgNO_3$ mixed solutions with different Cu/Ag ratios (see Table 1) and 1g/4mL liquid/solid ratio, at room temperature. After this, they were reduced at two different temperatures, 150°C and 450°C, in a hydrogen flow. The CuCLI monometallic system was also obtained in similar mode, but using 0.1mol/L $Cu(NO_3)_2$ solution, and reduced under same conditions to provide a reference from which the effects of silver addition could be investigated. The number after the sample name indicates the reduction temperature.

Table 1. Copper and silver content for exchanged zeolites samples. The number in the bimetallic samples indicates the used Cu−Ag ratio.

Samples	CuCLI	$AgCu_3CLI$	$AgCu_9CLI$
Cu (wt %)	3.40	1.44	1.50
Ag (wt %)	-	3.80	2.23

X - ray absorption spectroscopy experiments at Cu−K and Ag−K absorption edges were performed in transmission mode and at room temperature in the XAFS2 beamline of the LNLS, Campinas, Brazil [19]. The monochromator was calibrated with metallic foils placed between the second and third ionization chamber for each measured absorption edge. Samples of CuO and $AgNO_3$ were used as references. For each sample the energy scans were conducted three times for statistic improvement. Durapore Membrane Filters with 0.2 μm pore size were used to deposit the powders. The EXAFS analysis was performed using the Iffefit software package [20].

HR-XRD experiments were conducted in transmission mode at MCX beamline ELETTRA using energy of 12.399 keV and collected at room temperature. The samples were disposed in borosilicate glass capillaries (0.5 mm diameter), data were collected by means of a Pilatus detector, with fixed measuring time of 150 s, using a double crystal monochromator of Si (111).

III. RESULTS AND DISCUSSION

III.1. EXAFS EXPERIMENTS

Figure 1a shows the average $\chi(k)\cdot k^2$ signal calculated from the absorption spectra of the studied samples. The EXAFS signals of the CuCLI and $CuCLI_15_0$ samples show the same period and amplitude, this is an evidence of no changes in the local environment in this thermal treatment. The signal period is associated with Cu distances to its nearest neighbors, as shorter the period longer distances are expected. As commented for figure 1a, the reduction at 150°C does not affect the Cu coordination related to the as obtained sample (CuCLI). On the other hand, when the sample is reduced at 450°C the period of the EXAFS signal is reduced and matches the one of metallic Cu, but the signal exhibits lower amplitude. This result could be interpreted by the occurrence of Cu nanoparticles, by the important contribution that copper atoms in surface done when are in form of nanosized clusters. The EXAFS equation has a term that is direct related with the coordination number (N), if for any reason this number decreases (i.e. for metallic copper in bulk form: $N = 12$ copper for first nearest neighbors) the amplitude of the signal decreases consequently. If we assume that copper are segregate from the zeolite, this atoms could aggregate to form a nanoparticle that has an important amount of free surface. The copper atoms in the surface of this nanoparticles has a lower amount of first nearest neighbors, for this reason the average coordination number (that is the one obtained in the EXAFS fit) will decrease, given a reduction in the amplitude. Temperature effects (disorder) that can also affect the EXAFS amplitude can be consider in this case, but their effects are lower for nanoparticles bigger than 1 nm [21] , that are our case as we will show in the following. This Cu nanoparticles produced by the thermal treatment should be outside the zeolites channels.

The figure 1b shows a different behavior for the $AgCu_3CLI$ sample. In this case the amplitude and the period of the EXAFS signal of the reduced sample at 150°C ($AgCu_3CLI_15_0$) are quite different to the unreduced one, in particular for large k (wavenumber) values. These changes in amplitude and period should result as a variation in the coordination number of Cu^{2+} or as a contribution of metallic Cu emerging clusters. This result suggests that the addition of Ag^+ may facilitate the reduction of Cu^{2+} without favoring the formation of elemental copper (Cu^o), this can be sustained consider the hydrogen spillover phenomena [22]. Hydrogen reduction in silver it is expected to happen at lower temperatures (< 150°C) than in copper, then once reduced, the metallic silver could help into copper reduction by means of the spillover effect. The sample $AgCu_3CLI_45_0$ exhibits close the same behavior described for $CuCLI_45_0$. The fact that there are only changes in amplitude and not in phase

for $AgCu_3CLI_45_0$, is an evidence of the absence of alloy formation. It should be highlight that Ag:Cu alloy is not thermodynamically allowed for bulk system [23]. Finally, the $AgCu_9CLI$ sample exhibits the same behavior as that described for the $AgCu_3CLI$ sample as function of both reduction temperatures (Fib. 1c).

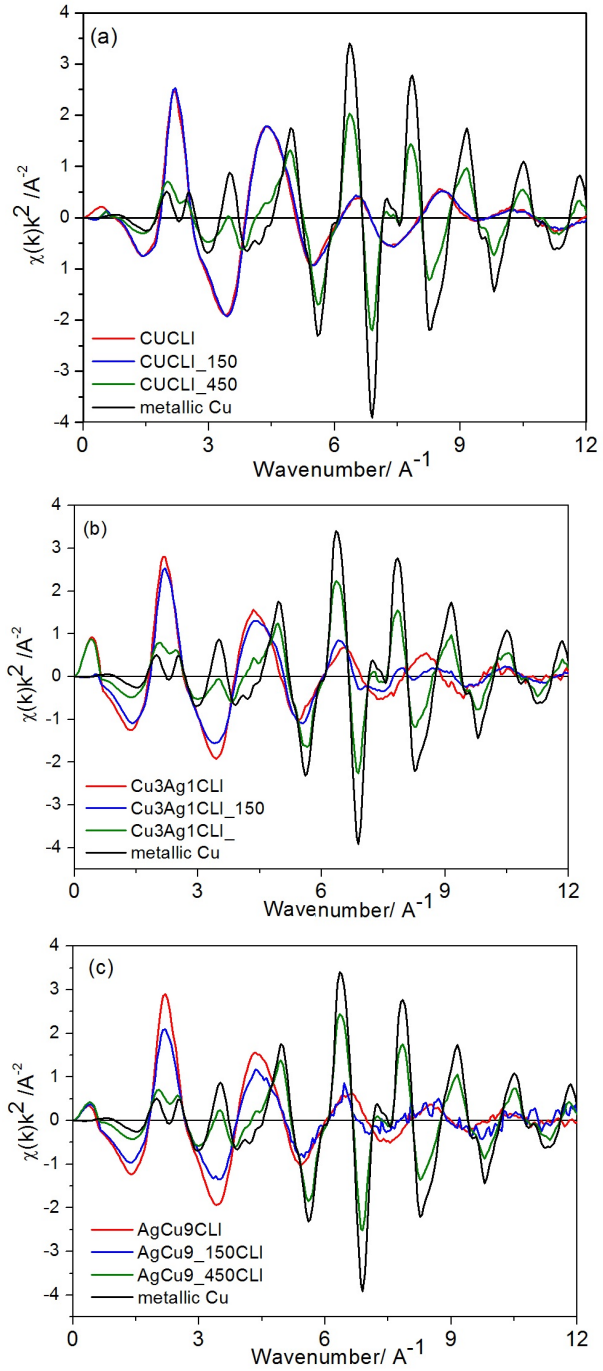

Figure 1. a) Average $\chi(k)\cdot k^2$ data calculated from the Cu–K absorption edge for natural clinoptilolite exchanged only with Cu^{2+} and as function of the reduction temperature. 1b) Average $\chi(k)\cdot k^2$ data calculated from the Cu–K absorption edge for $AgCu_3CLI$ at room temperature and as function of the reduction temperature. c) Average $\chi(k)\cdot k^2$ data calculated from the Cu–K absorption edge for $AgCu_9CLI$ at room temperature and as function of the reduction temperature. In all cases a Cu metal signal is included as a reference signal.

It seems that the volume ratio of dissolved $Cu(NO_3)_2$–$AgNO_3$ used for preparing the bimetallic samples does not influence Cu distances to its nearest neighbors significantly once reduced at the two temperatures. Furthermore the Ag incorporation favors the copper reduction at lower temperatures, and appears to be an efficient tool for the control of the dispersion of the resultant reduced Cu nanoparticles diminishing their size as compared with the sample without silver as will be shown by EXAFS analysis.

Figure 2 shows the magnitude of the Fourier Transform (FT) of the EXAFS signals (k^2 weighted data) of the studied samples as prepared (Cu^{2+} clinoptilolite and Ag–Cu binary mixtures) and the fits for the first shell of oxygen neighbors. This Figure shows also the FT of the EXAFS signal of the CuO standard sample at the top together with its fit assuming the first shell of oxygen neighbors as well. The fit model was based on simple oxygen in tetrahedral coordination for Cu as is in CuO [23].

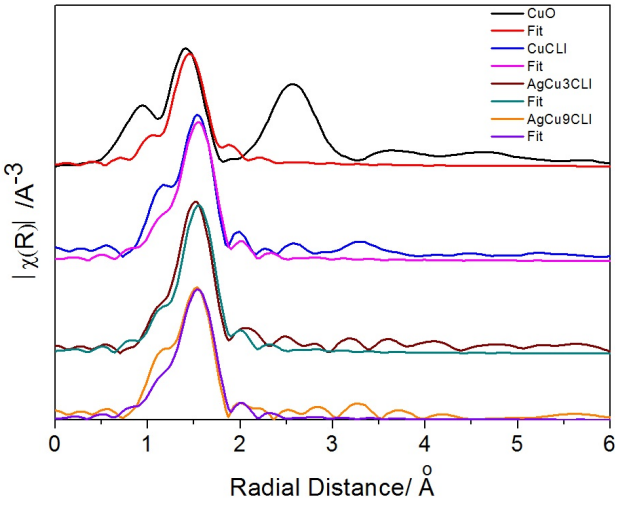

Figure 2. Magnitude of the Fourier Transform (FT) of the EXAFS signals (k^2 weighted data) of the Cu^{2+} clinoptilolite, Ag^+–Cu^{2+} binary mixtures and the CuO reference at room temperature, and fittings with the first shell of O.

Figures 3 and 4 show the FT of the EXAFS signals of the reduced samples at 150°C and 450°C respectively, the last one with fits for the metallic contributions. In each case the FT of the reference Cu metallic sample was included. From these fits and establishing a reasonable hypothesis of the geometrical shape for the nanoparticles is possible determine the size [20]. For a cuboctahedral shape is possible to affirm that CuCLI has a diameter of 1.2 nm, and $AgCu_3CLI$, $AgCu_9CLI$ has 1 nm and 1.4 nm respectively. These estimative can have an error around 20 percent.

Attending to the results shown in Figures 2-4, the samples, CuCLI, $AgCu_3CLI$, $AgCu_9CLI$ and $CuCLI_15_0$, exhibit a typical short-range order behavior. For these samples a single peak at 1.98 å is observed on the fits and it is related with the first coordination sphere of oxygen tetrahedral used as reference. It should be associated with the coordination of Cu^{2+} within the zeolites channels with 4 oxygen atoms of the framework, excluding the possibility of clustering or particle formation. It is in agreement with previous UV-Vis results

reported in [14].

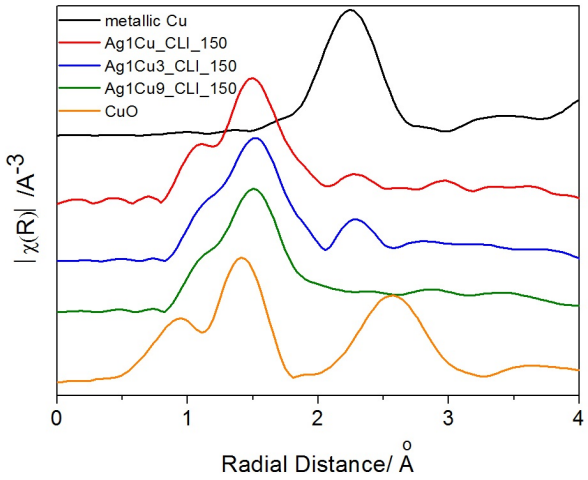

Figure 3. Fourier Transform (FT) of the EXAFS signal for metallic Cu (at the top) and for exchanged natural clinoptilolite samples reduced at 150°C. At the bottom is possible to see the EXAFS signal for a CuO reference.

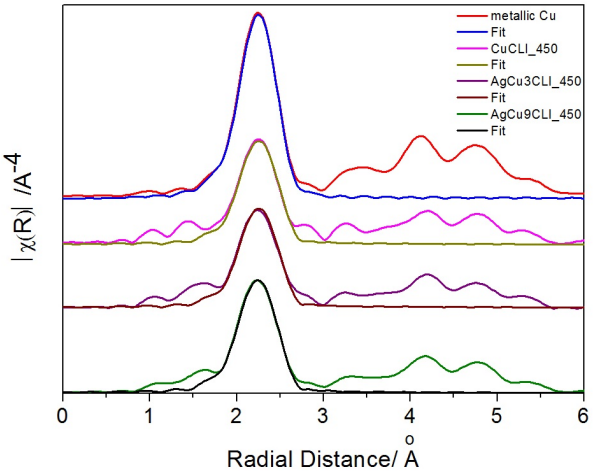

Figure 4. Fourier Transform (FT) and fits for the first shell of EXAFS signals (k^3 weighted data) for metallic Cu and exchanged natural clinoptilolite samples reduced at 450°C

A detailed analysis of the graphs reveals that for the $AgCu_3CLI_15_0$ and $AgCu_9CLI_15_0$ samples, additionally to the principal peak at 1.98 å, a small peak around 2.54 å occurs (obtained by the fit, in graph there is not phase corrected), while for the sample $CuCLI_15_0$ it does not appear. Moreover, with increasing reduction temperature the peak at 1.98 å reduces its amplitude, while for the $CuCLI_45_0$, $AgCu_3CLI_45_0$ and $AgCu_9CLI_45_0$ samples a second peak, at 2.54 å, increases its amplitude reaching its maximum values (Fig. 4). As can be observed from the graphs, the emerging peak as function of temperature must be associated to the first coordination sphere of the metallic copper foil used as reference. The described behavior supports the suggestion made before that the presence of Ag+ may facilitate the reduction of Cu^{2+} . As previously state, the FT of the sample $AgCu_9CLI$ shows the same trend as that described for $AgCu_3CLI$ as function of the temperature.

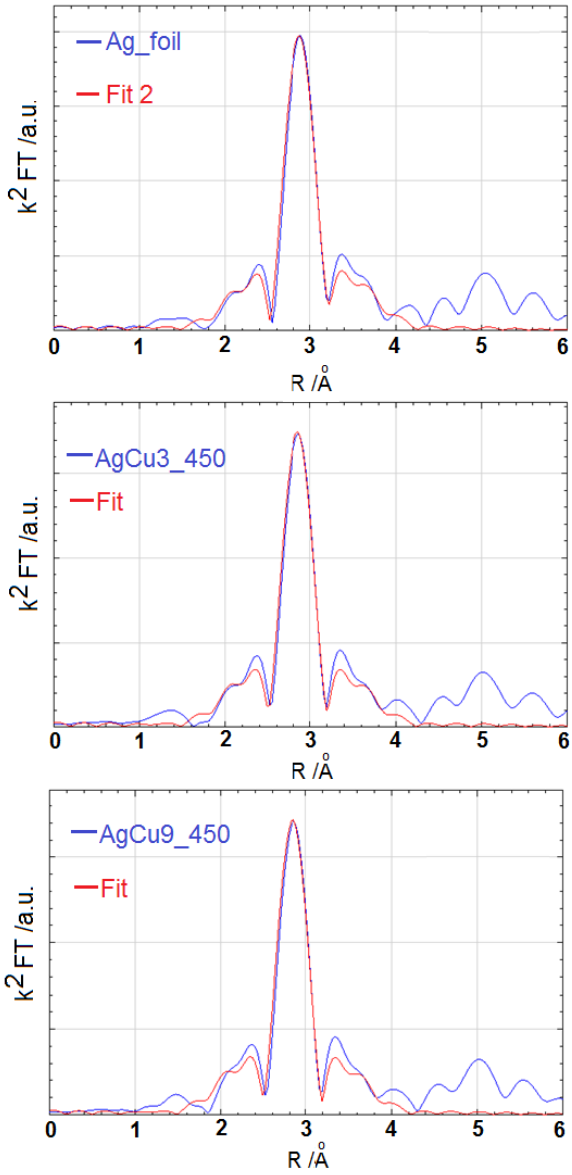

Figure 5. Fourier Transforms (FT) of EXAFS signals (at Ag−K absorption edge) for exchanged natural clinoptilolite samples reduced at 450°C and for the Ag foil used as reference (curves in blue). Fitting of the FTs based on the crystal structure of metallic Ag (fitted curve in red).

The distances associated with the second peak may be related with clustering of Cu−Cu, as commented earlier Cu-Ag particles formation are discarded, for be not compatible with the EXAFS signal in copper edge and not allowed in bulk for thermodinamical reasons [24].

The hypotheses for Cu−Ag nanoalloy formation can be excluded also taking into account the Fourier Transforms (FT) of EXAFS signals (from the Ag-K absorption edge) for exchanged natural clinoptilolite samples reduced at 450°C (Fig. 5). In this figure the FT of the Ag foil used as reference is also included. With increasing reduction temperature silver oxide become metallic Ag given reinforcement to the exclusion of Cu-Ag nanoalloy formation. The estimation for size in the Ag nanoparticles is the following: 2.5 nm for $AgCu_9$ CLI and 3 nm for $AgCu_3$ CLI.

For the reduction temperature of 450°C, most of the Cu and Ag appear as metallic species for exchanged samples, probably outside the zeolite channels. Moreover, the resolved peaks in the FT observed at large distances (long range order) in Fig. 4 and Fig. 5 are related to the subsequent coordination spheres of metallic copper and silver respectively. The former suggests the occurrence of both Cu and Ag nanoparticles.

On the other hand, the little peak still observed for both samples in the phase corrected distance of 1.98 at 450°C corresponds to remaining unreduced Cu^{2+} cations (Fig. 5), but it is not the case for Ag, where the reduction seems to be fully completed.

III.2. HR-XRD EXPERIMENTS

Figure 6 shows the X-ray diffraction patterns (XRD) of CuCLI (bottom of the figure) as well as of $AgCu_9CLI$ before and after reduction at 150°C and 450°C, i.e. $AgCu_9CLI_15_0$ and $AgCu_9CLI_45_0$, respectively. As stated before, the $AgCu_3CLI$ behaves as the $AgCu_9CLI$ one. The qualitative phase analysis of all diffraction patterns confirm that they preserve the C2/*m* and C *mcm* space groups of the main phases of the samples, clinoptilolite and mordenite respectively, after ion exchange. For clarity, only the characteristic maximum for the mordenite phase has been labelled with the Miller index (110)M, while only the maxima (020)C and (200)C have been chosen for representing the clinoptilolite phase.

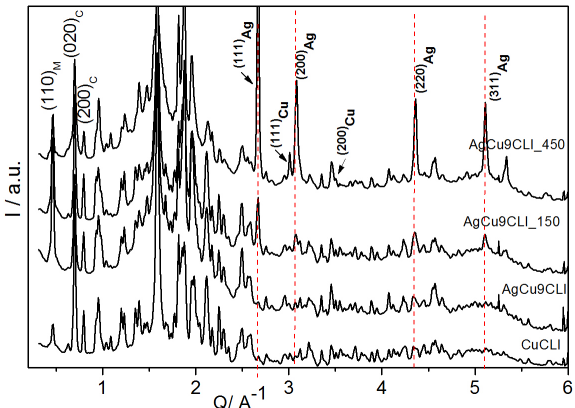

Figure 6. HR-XRDpatterns of the exchanged CuCLI and $AgCu_9CLI$ samples as well as the reduced $AgCu_9CLI_15_0$ and $AgCu_9CLI_45_0$ bimetallic.

For the Ag^+–Cu^{2+} binary sample reduced at 150°C, low intensity peaks corresponding to metallic silver are well observed (dashed vertical lines), while diffraction peaks of metallic copper are absent. It indicates that at 150°C long range order is still missing for Cu, but clustering of Cu–Cu particles with distances close to the first coordination sphere of the metallic Cu (short range order) is possible to sustain as shown in Figure 3.

At 450°C the metal silver (Ag) phase exhibits high and sharp intensity peaks, which in turn indicates that most of the silver appears as metallic Ag with a larger volume fraction in the sample. It is also supported by the results shown in Figure 5. On the other hand, low intensity peaks corresponding to metallic copper start to emerge at this reduction temperature. No alloying of the metallic species is observed. Additionally, the occurrence of well-defined peaks of the Ag – phase already at 150°C and the absence of Cu diffraction peaks allows neglecting the hypotheses previously made about the occurrence of Cu–Ag clusters. It was also confirmed by EXAFS analysis. Then only Cu–Cu clustering can be assumed as responsible for the changes observed in the EXAFS signals (Fig. 1) and in the FTs of the thermal treated $AgCu_3CLI$ and $AgCu_9CLI$ samples respect to the unreduced one (Fig. 2 – 4).

Table 2. Estimated FWHM values for (111)Cu and (200)Ag reflections.

sample	FWHM for (111)Cu	FWHM for (200)Ag
$CuCLI_45_0$	(0.173 ± 0.002)°	-
$AgCu_9CLI_45_0$	(0.179± 0.002)°	(0.301± 0.002)°

Another important feature of the HR-XRD patterns is presented in the Figure 7, where the peaks of metallic Cu and Ag in the range 2.5 – 5.2 å$^{-1}$ for $CuCLI_45_0$ and $AgCu_9CLI_45_0$ samples appear. Comparing the relative intensity of the Cu reflections for both samples it seems that agglomeration of reduced copper is inhibit in presence of silver as shown in the EXAFS results.

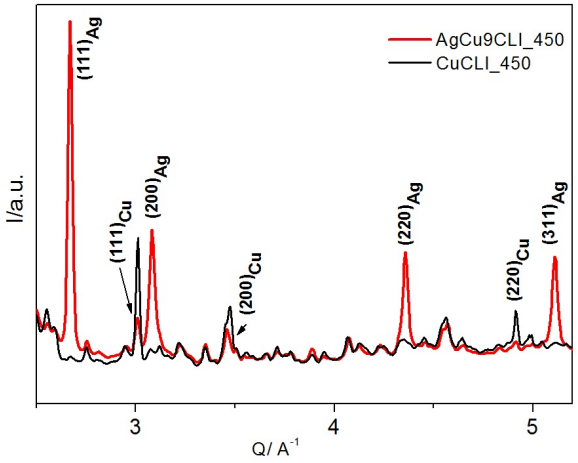

Figure 7. HR-XRD patterns in the range 2.5 – 5.2 å$^{-1}$ for the $CuCLI_45_0$ and $AgCu_9CLI_45_0$ samples.

Particle size determination from the diffraction profiles was not possible because the large degree of overlapping of peaks of different phases. However, an attempt for a qualitative analysis taking into account the Full Width at Half Maximum (FWHM) of the (111)Cu and (200)Ag peaks was made. Table 2 shows the estimated FWHM values for each reflection. The FWHM value for the reflection (111)Cu in both samples is unchanged, which in turn means no change in Cu particle size at this reduction temperature even in presence of Ag. On the other hand, Ag particles size seems to be smaller than Cu one.

IV. CONCLUSIONS

The EXAFS signals of both bimetallic samples show important changes of period and amplitude after their reduction at 150°C, indicating that Cu^{2+} coordination is

affected and that reduction of this cation occurs. It does not happen to Cu monometallic system one. Thus, the presence of silver promotes the Cu^{2+} reduction in Cu−Ag bimetallic systems that can be explained by the spillover phenomena. According to XRD and EXAFS results, only silver clusters are formed in both bimetallic samples reduced at 150°C. At higher reduction temperature (450°C) most of copper and silver appear as elemental metallic species for all samples, probably outside the zeolite channels. The study revealed that agglomeration of reduced copper is limited in presence of silver.

The metallic silver species formed during the reduction process drive the reduction of copper oxides in the ionic exchanged structure and finally drives the agglomeration of the reduced neutral copper atoms through small clusters at the surface, at lower temperatures of around 150°C, this process increases until higher size particles at higher temperature of 150°C occur.

ACKNOWLEDGEMENTS

EXAFS experiments have been supported by the Brazilian Synchrotron Light Laboratory (LNLS) under proposal D04B - XAFS1 7770. ICTP - Elettra Synchrotron, Trieste, Italy is also knowledge for financial support in the framework of the proposal: 20110280.

Authors thank the support from grants UNAM-PAPIIT-IN107817 and SENER-CONACYT-Hydrocarbons No 117373 (Mexico), and the project 18-53-34004 Russia-Cuba (RFBR-CITMA).This work was also supported in the framework of a scientific project associated to the national program of fundamental science (MES–UH-2018). F. Chavez-Rivas acknowledges support from COFAA-IPN-México.

REFERENCIAS

[1] R.E. Ramírez-Garza, I. Rodríguez-Iznaga, A. Simakov, M.H. Farías, F.F. Castillón-Barraza, Mater. Res. Bull. **97** 369, (2018).

[2] G. Yao, J. Lei, W. Zhang, C. Yu, Z. Sun, S. Zheng, S. Komarneni, Environ. Sci. Pollut. Res. **26**, 262782 (2019).

[3] L. Bacakova, M. Vandrovcova, I. Kopova, I. Jirka, Biomater. Sci., 6974 (2018).

[4] I. Rodríguez-Iznaga, V. Petranovskii, G. Rodríguez-Fuentes, C. Mendoza, A. Benitez-Aguilar, J. Colloid Interface Sci **316**, 877 (2007).

[5] B. Concepción-Rosabal, G. Rodríguez-Fuentes, N. Bogdanchikova, P. Bosch, M. Avalos, and V.H. Lara, Microporous Mesoporous Mater. **86**, 249 (2005).

[6] S.Y. Joshi, A. Kumar, J. Luo, K. Kamasamudram, N.W. Currier and A.Yezerets, Appl. Catal. B **226**, 565 (2018).

[7] J.F. Gelves, L. Dorkis, M.A. Márquez, A.C. Álvarez, L.M. González and A.L. Villa, Catal. Today **320**, 112 (2019).

[8] J. Vergara-Figueroa, S. Alejandro-Martín, H. Pesenti, F. Cerda, A. Fernández-Pérez and W. Gacitúa, Materials **12**, 2202 (2019).

[9] S. Chaturvedi and P. N. Dave, Chem. Methodol. **3**, 115 (2019).

[10] J.M. Fedeyko, H. Chen, T.H. Ballinger, E.C. Weigert, H. Chang, J.P. Cox, P.J. Andersen, SAE Technical Paper 2009-01-0899, (2009), https://doi.org/10.4271/2009-01-0899.

[11] M. Jablonska, R. Palkovits, Appl. Catal. B. **181**, 332 (2016).

[12] L. Zhang, Q. Wu, X. Meng, U. Müller, M. Feyen, D. Dai, S. Maurer, R. McGuire, A. Moini et. al., React. Chem. Eng. **4**, 975 (2019).

[13] Y. Shan, X. Shi, J. Du, Y. Yu and H. He, Catal. Sci. Technol. **9**, 106 (2019).

[14] I. Rodríguez-Iznaga, V. Petranovskii, F. Castillón-Barraza and B. Concepción-Rosabal, J. Nanosci. Nanotechnol. **11**, 1 (2011).

[15] I. Rodríguez-Iznaga, V. Petranovskii, F.F. Castillón and M.H. Farias, Opt. Mater. **29**, 105 (2006).

[16] P. Sánchez-López, Y. Kotolevich, S. Miridonov, F. Chávez-Rivas, S. Fuentes, and V. Petranovskii, Catalysts **9**, 58 (2019).

[17] M. Chen, Q. Sun, X. Yang, and J. Yu, Inorg. Chem. Commun. **105**, 203 (2019).

[18] B. Concepción-Rosabal, A. Pentón-Madrigal, E. Estévez-Rams, N. Bogdanchikova, M. Avalos-Borja. Rev. Cubana Fis. **25**, 136 (2008).

[19] S.J.A. Figueroa, J.C. Mauricio, J. Murari, D.B. Beniz, J.R. Piton, H.H. Slepicka, M. Falcao de Sousa, A.M. Espindola, and A.P.S. Levinsky, J. Phys.: Conf. Ser. **712**, 012022 (2016).

[20] B. Ravel and M. Newville, J. Synch. Rad. **12**, 537 (2005).

[21] A. M. Beale and B. M. Weckhuysen, Phys. Chem. Chem. Phys. **12**, 5562 (2010).

[22] R. Prins, Chem. Rev. 112, 2714 (2012).

[23] Inorganic Crystal Structure Database (ICSD), Version: 2008-1. https://icsd.products.fiz-karlsruhe.de/.

[24] G. Bergerhoff, I.D. Brown in "Crystallographic Databases", F.H. Allen et al. (Hrsg.) Chester, International Union of Crystallography, (1987).

DETERMINATION OF THE PLANCK CONSTANT THROUGH THE USE OF LEDS

DETERMINACIÓN DE LA CONSTANTE DE PLANCK MEDIANTE EL USO DE LEDS

C. Calvo-Mola, S. López-Pérez, E. García-Alfonso, J. Cerutti-Torres†

Facultad de Física, Universidad de La Habana, San Lázaro y L, La Habana 10400, Cuba. jcerutti@fisica.uh.cu†
† corresponding author

Recibido 14/5/2019; Aceptado 12/11/2019

Plancks constant plays a fundamental role in the quantum mechanics theory. The numerical value of this constant can be experimentally obtained by means of the study of a wide variety of physical phenomena. The main goal of the present laboratory exercise is the determination of the numerical value of the Planck constant using LEDs by means of two different theoretical models and an Arduino automatized measurement. To achieve this, four different LEDs spectra were provided and their current-voltage curves were measured. Results from the two proposed methodologies are compared and discussed.

La constante de Planck ocupa un papel fundamental en la mecánica cuántica. La determinación experimental de su valor numérico puede hacerse a través del estudio de diversos fenómenos y dispositivos. Se propone un ejercicio experimental cuyo objetivo es determinar el valor numérico de la constante de Planck de una manera simple y poco costosa, a partir de la construcción de la curva corriente-voltaje y el conocimiento del espectro de emisión característico de un conjunto de diodos emisores de luz (LEDs), en una práctica de laboratorio automatizada con Arduino. Se utilizan dos metodologías diferentes, y se comparan y discuten los resultados de cada una.

PACS: Determination of fundamental constants (determinación de constantes fundamentales), 06.20.Jr; Design of experiments (diseño de experimentos), 07.05.Fb; Data acquisition (adquisición de datos): hardware and software, 07.05.Hd; Photons (fotones), 14.70.Bh

I. INTRODUCTION

Planck constant (denoted by h) is a physical constant of great importance within Quantum Mechanics theory. It is usually defined as the quantum of electromagnetic action. Its numerical value has been fixed as exact by the International Bureau of Weights and Measures (BIPM, after the french name) in 2018 [1] to the number:

$$h = 6.62607015 \cdot 10^{-34} Js. \quad (1)$$

Planck constant owes its name to Max Planck, who introduced it in 1901 within his empirical formula for the Black Body radiation problem. Later in 1905, Einstein used it as the proportionality constant that related the frequency of light quanta (*photons*) and the energy they carried out, in his model for the photoelectric effect. Then, the fundamental relation stands:

$$E = h\nu = \frac{hc}{\lambda}, \quad (2)$$

being E the energy carried by a photon, ν and λ its frequency and wavelength, c the velocity of light and h the Planck constant.

Einstein received the Nobel prize in 1921 "for his services to theoretical physics, and especially for his discovery of the law of the photoelectric effect" [2] and Planck in 1918 "for the services he rendered to the advancement of physics by his discovery of energy quanta" [3].

The numerical value of this constant can be experimentally obtained by means of the study of a wide variety of physical phenomena [4]. A very straightforward and easy to implement way of doing so is by means of Light Emission Diodes (LEDs). LEDs are made of semiconductor materials that emits radiation as a result of a change of energy states, usually of electrons, when the sample is excited by an external energy source that do not vary significantly its temperature [5]. The Laboratory exercise we propose aims the determination of the numerical value of the Planck constant using LEDs by means of two different theoretical models and an Arduino automatized measurement.

Since last quarter of the past century, it is been common to find some studies regarding this topic [6–8]. Even experimental setups were designed and commercialized [9]. In recent years there can be also found similar publications [10, 11, 15, 16], one of them [10] with an automatized experimental proposal. Most of the above mentioned [6, 8, 10, 15, 16] use a rather incorrect approximation, i.e., assume the GAP energy is equal to the energy of the knee voltage, issue noted in [17]. It is discussed later in this paper why this is not correct, even when numerical results seem precise. Some of the above cited publications [7, 11] uses the same methodology we present as first method, with very accurate results. A different methodology can be also found on the internet mainly in students published Laboratory Reports (as an example, two students reports and an exercise program can be found on the links [12–14]). However, the methodology is never successfully explained nor correctly derived the equations of work and with not so accurate results.

Our present proposal has the advantage of combining two

different approaches, the first one focusing the student's attention on modeling the effect of light emission, while in the second one the focus is on the functioning of LEDs as electronic devices. Apart from that, a detailed explanation and accurate derivations of the expression for the working equations on both methods are presented. The uncertainty treatment is also discussed for both methodologies. Lastly, it is remarkable that our experimental set up is automatized by using the Arduino platform.

The present proposal is organized as follows. The first section presents a quick review on Solid State Physics and Semiconductor Theory, necessary to introduce the mathematical models. The next one introduces the mathematical models we use: we start with a simple model based on Einstein Photoelectric Effect equation, and then also propose a rather more complex based on Shockley diode model. Last two sections present the experimental set up and obtained results. Finally, conclusions are presented and discussed.

II. THEORETICAL BACKGROUND

II.1. Bands Theory

When classical ideas were applied to the study of solid state physics, the classical picture managed to explain the heat capacity in a certain range of temperatures for non conducting materials, and the electrical conduction of metals. However, a wide variety of experimental results in solids remained unexplained. One of them, the existence and behavior of semiconductors. Applying the principles of Quantum Theory to solids derives in the Bands Theory, which successfully explains the behavior of all solids [18].

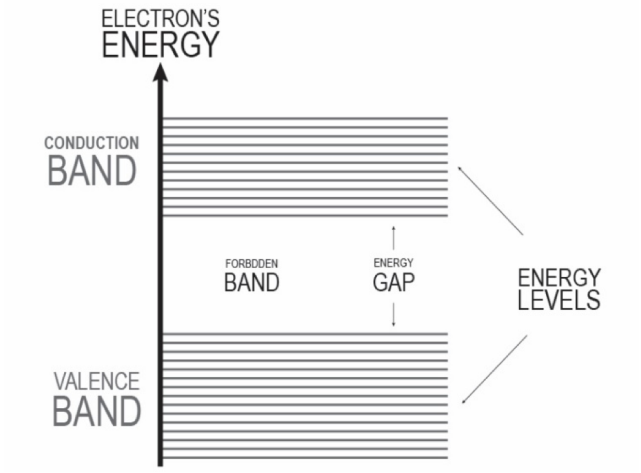

Figure 1. Schematic representation of energy bands within a solid.

Crystalline solids are a periodic arrangement of atoms which constitute a periodic potential for the movement of electrons. The solution of the Schrödinger equation to these periodic systems is a set of energy states clearly separated in bands of allowed and forbidden energies (Figure 1). In semiconductors and insulators electrons are occupying all states of the so called *valence band* and the next energetic region that they could occupy (*conduction band*) is separated by a forbidden region or bandgap (GAP). In general, the GAP of semiconductors is temperature dependent.

As all energy states are occupied in the valence band, the material can not conduct. In order to conduct electricity, the electrons must be able to "gain.[en]ergy, i.e., they must be in the conduction band where they have free energy states that they can occupy. Then, the semiconductor can conduct if it is possible to excite electrons from the valence to the conduction band.

II.2. Doping

In order to achieve greater efficiency in semiconductor materials, it is common to dope them with *impurities*. Impurities are any imperfection on the crystaline structure. They can be either the absence of an atom in a place of the structure, a displaced atom, or the substitution of an atom of the solid for another atom from a different chemical species. The latest is the one it is commonly used to dope semiconductors.

A *donor impurity* is an atom that possesses more valence electrons than the solid's constituent atoms and can "donate"these "excess.[el]ectrons to the conduction band more easily than the intrinsic atoms. Energetically, it is equivalent to say that the energy level of this "extra.[el]ectron is inside the GAP, near the conduction band. When a semiconductor material is doped with donor impurities, it means, is doped with electrons, it is called *n-type*.

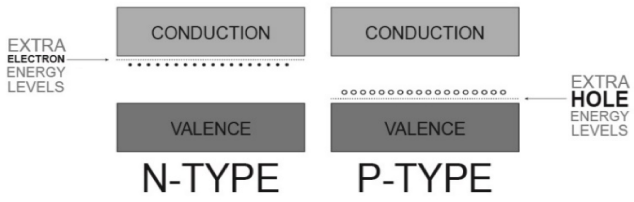

Figure 2. Schematic representation of the energy levels on typical *n-type* and *p-type* semiconductors.

An *acceptor impurity*, on the other hand, is an atom that possesses less electrons than constituent atoms. This kind of impurities creates "holes", vacancies of electrons in places where there should be. These holes are also in energetic states inside the GAP, near the valence band in a way electrons can occupy them easily, leaving mobile holes in the valence band. When a semiconductor material is doped with acceptor impurities, it means, is doped with holes, it is called *p-type*.

If the system has both kind of impurities, the material can decrease its energy by means of a recombination, for example when a free electron falls from the conduction band to a free hole in the valence band. Recombination process can

be accompanied by photon emission. This is the kind of processes that produces luminescence within a LED.

II.3. p-n junction

The most effective way to inject charges into a semiconductor, in order to produce light, is by means of a *p-n junction* [19]. As it is stated by the name, on one side of the junction there is an *n-type* semiconductor while on the other side there is a *p-type*, i.e., in one side of the semiconductor there are excess electrons near the conduction band while on the other side holes predominate near the valence band. If the system is excited (with room temperature, for example), the excess electrons in the *n-type* zone jump to the conduction band, and the holes of the *p-type* zone are filled due to electrons that jump from the valence band leaving free holes behind. Therefore, there is an excess of electrons within the conduction band in one side and an excess of mobile holes within the valence band in the other side.

At the moment of making the junction, the system tries to reach equilibrium between electrons and holes in both bands, and electrons start moving from the n to the p zone by diffusion. This process creates a negative net charge in the p zone and a positive net charge in the n zone, because the diffusion process has effectively created a charge unbalance in both sides of the junction. An electric field is then established and it equilibrates the diffusion movement. The region with unbalanced charge is called *depletion zone* or *space charge region*.

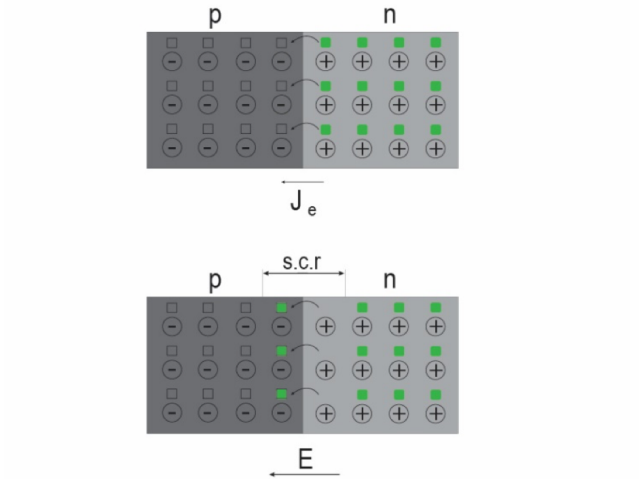

Figure 3. Schematic representation of a p-n junction and the creation of the *depletion zone*.

If the semiconductor is supposed to conduct electric current (or illuminate, in the case of LEDs), it must be forward-biased. It means it must be connected in a way external voltage is opposed to the internal voltage in the depletion zone (this is, the p zone should be wired to positive). Then, if the voltage applied is greater than the internal one, electrons will keep moving through the depletion zone from the n to the p zone, conducting electricity. The so called knee voltage is the minimum voltage needed for the LED to conduct. Therefore, the energy of knee voltage equals the energy of this electric field, which is not the same and can not be identified with the GAP energy, although they are indeed related.

If recombination of an electron and a hole occurs within the depletion zone, then energy is emitted. This energy loss can be radiative, in which case a photon would be emitted, or non radiative, in which case phonos would be produced. The radiated energy (if the first occurs) and therefore the frequency of the produced light, dependes on the GAP, it means, on the material.

III. MODELS

III.1. Method I

To make a numerical analysis of the light production phenomena within LEDs, we can start by using a model similar to the one used by Einstein for the Photoelectric Effect (FE) [20, 21]. Although these are two different phenomena, the logic followed by Einstein for the FE was based on the Conservation of Energy, which is a universal law. Then, the equation for the light emission within diodes would be:

$$K_{min} = E - W_0. \tag{3}$$

In our problem, we speak of a minimum kinetic energy, i.e., the minimum energy amount that is necessary for an electron to penetrate the depletion zone and that is provided by the external voltage. This can be expressed as:

$$K_{min} = eV_0, \tag{4}$$

where V_0 is the so called knee point voltage, i.e., the voltage for which current starts flowing trough the diode. The latest can be obtained by simple inspection on the IV curve, although there exits more refined methods, as the one that fits the lineal part of the curve to a line and takes the intersection with the abscissa as knee voltage.

This energy carried by electrons can be turned into radiation energy (E) as it is expressed by Eq. 3 where is also taken into account possible energy loss due to a wide variety of non radiative processes that can occur within the depletion zone (W_0). For simplicity, we asume this lost energy is the same for every LED. This term corrects the invalid assumption widely found in literature that $eV_0 = E$.

If we substitute E as in Eq. 2 and K_{min} as in Eq. 4, we obtain the linear model:

$$V_0 = \frac{hc}{e\lambda} - \frac{W_0}{e}, \tag{5}$$

in which, from the slope of a lineal fit to a set of values for the knee voltage and the wavelength of different LEDs, the numerical value of the Planck's constant can be computed.

III.2. Method II

A more detailed model can be constructed looking into the mechanisms of the diode itself. As they are complex devices, there are various mathematical models that tries to approximate the behavior of their IV curves. One of the most

commonly used is the Shockley diode model [19]. This relates the current and voltage flowing through the diode as:

$$I(V) = I_S\left(e^{\frac{eV}{\eta k_B T}} - 1\right), \tag{6}$$

where

I_S is the reverse saturation current,

e is the electronic charge,

η is the so called non-ideality factor, that is set to 1 if an ideal diode is under consideration, but for real diodes it is often a number higher than 1,

k_B is the Boltzmann constant,

T is the temperature, and

V, I are the voltage and current flowing through the diode.

However, even at rather low voltages and room temperature it is common to assume $V \gg \frac{k_B T}{e}$, where $\frac{k_B T}{e}$ is commonly named as thermal voltage. This approximation should not affect the value of the Planck constant, due to the very small value of the fraction (on the order of $10^{-2}V$ for room temperature) compared to the measured voltages (on the order of Volts). An inspection to Eq. 6 suggests that due to the presence of the non-ideality factor η within the exponential, this assumption should be done carefully, depending on the order of this parameter. However in worst case scenario (for our measurements, one of them is slightly higher than 10) the measured voltage remains at least an order higher than the thermal voltage. This clearly affects the expected result for the constant, even when only one of the LEDs presents the problem, because there are no enough LEDs to statistically corrects the deviation this one will cause.

If this above approximation is done, the previous relationship becomes:

$$I(V) = I_S e^{\frac{eV}{\eta k_B T}}. \tag{7}$$

The reverse saturation current is sometimes expressed in terms of the energy band gap as:

$$I_S \propto e^{-\frac{E}{\eta k_B T}}, \tag{8}$$

where E is the GAP energy. It is remarkable that there are lots of approximation for the saturation current as a function of the GAP energy and this is the simplest one. Some more accurate descriptions also include a temperature dependence factor instead of a simple proportionality factor. The substitution of expression 8 into Eq. 7 finally gives:

$$I(V) = Ae^{\frac{eV-E}{\eta k_B T}}, \tag{9}$$

with A being a proportionality constant.

If we take logarithm in both members, we obtain a lineal relation:

$$\ln\{I(V)\} = mV + b, \tag{10}$$

where

m is the slope of a line and is equal to $\frac{e}{\eta k_B T}$, and

b is the curve intercept with the vertical axis and is equal to $\ln\{A\} - \frac{E}{\eta k_B T}$.

In Equation 10 should be noted that the logarithm has been taken to the values of $I(A)$. There seems to be a dimensional error in this action, but this is not the case, because the term $\ln\{A\}$ in the intercept corrects the dimensionality of the equation.

A careful inspection on the expressions for the slope and intercept unravel their inner relation:

$$-\frac{be}{m} = h\nu - \ln\{A\}\eta k_B T, \tag{11}$$

where we have written $E = h\nu$.

Then, a lineal fit to measurements of $\ln\{I\}$ vs. V leads us to a new characterization of the LEDs, i.e, the values of m and b (Eq. 10). It must be taken care that measurements are done within the validity region of Eq. 6, the exponential grow part. Then if the characteristic m, b and ν for each LED are again plotted, the slope of a lineal fit to this set of values, as in Eq. 11, is exactly the Planck constant.

IV. EXPERIMENTAL SETUP

The spectra of the different LEDs were obtained in a Laboratory of the Physics Faculty using traditional methods. They are given to the students for them to find the wavelength and uncertainty of LEDs.

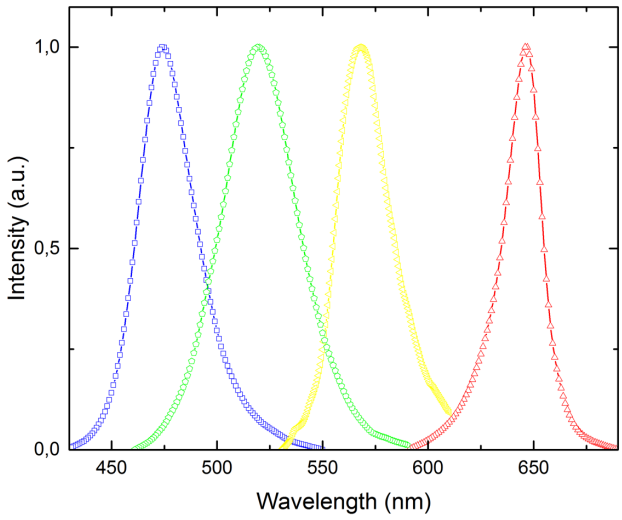

Figure 4. Measured LEDs spectra. The colors on the curves corresponds to the colors of each LED.

The wavelength of the LEDs is taken from the maximum of the spectra. The band width of the spectra was taken as the associated uncertainty for the wavelength of each LED. Table IV shows the different wavelengths obtained for our four LEDs with their uncertainties and Figure 4 shows the measured spectra.

Table 1. Wavelength value for each one of the LEDs in our experiment.

LED	Wavelength (nm)
Yellow	$567,80 \pm 24,14$
Green	$520,27 \pm 36,27$
Red	$646,40 \pm 18,61$
Blue	$474,29 \pm 27,33$

For the experimental setup the following elements are needed:

- LEDs of different colors (green, red, yellow and blue)
- Arduino Genuino UNO
- various 2 kΩ resistances
- a potentiometer
- an LCD 16×2 screen
- a protoboard
- conection cables
- remote control

IV.1. Experimental determination of the IV curve

For the measurement of the IV curve, a circuit like the one represented in the Figure 5 should be assembled. A program for the control of the measurement system has been implemented on Arduino. With a remote control it is possible to select the LED whose IV curve is going to be measured. With a lineal potentiometer the voltage applied to the terminals of the LED is varied. The values of voltage and current are shown in the LCD screen. It is important to remark once more that LEDs should be forward biased. The procedure is repeated 20 times for every LED.

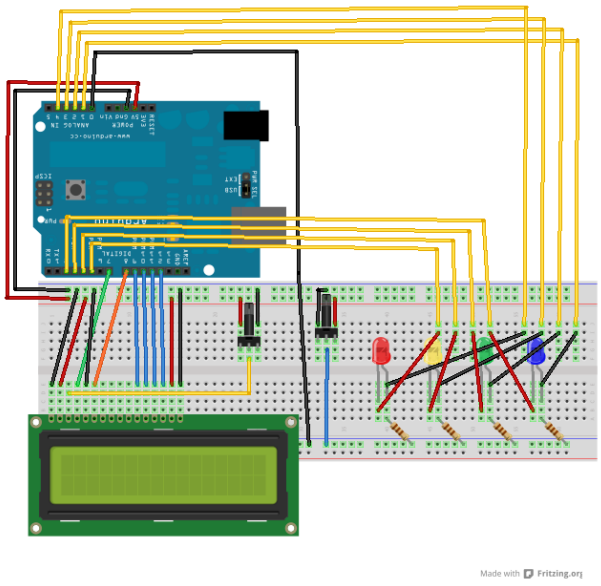

Figure 5. Circuit for the IV characterization of LEDs.

IV.2. A remark on uncertainties sources

The proposed experimental setup use an analog digital converter (ADC) from an Arduino Genuino Uno [22]. This is a successive approximation ADC, and those kind of converters are usually very precise. The least variation that the converter is able to detect is determined by the relation:

$$V_{min} = \frac{V}{2^N}, \tag{12}$$

where $V = 5V$ is the supply voltage and $N = 10$ *bits* is the resolution of the ADC. This implies that the minimum voltage variation that could be detected by the ADC is of $V_{min} = 4.88 \cdot 10^{-3} V$.

On the other hand, the LCD screen has a resolution of $V_{min}^{screen} = 1 \cdot 10^{-2} V$. This means that the screen is the main source of uncertainties in the measurement of voltage.

For the measurement of current, the voltage through a resistance of known value is measured. The value of the resistance is taken as exact. Therefore, it does not contributes to the uncertainties.

Taking the above considerations into account, we can establish that the uncertainties due to the measurement instrumenta is constant throughout the experiment and with an extremely low value, not comparable with the uncertainties that arise from the fitting process, and therefore will not be taken into account.

As it was mentioned before, the uncertainties related to the wavelength of the different LEDs were taken as the bandwidth of the emission spectra. This way the uncertainty is somehow overestimated, but it is important to take into account the fact that LEDs are not entirely monochromatic devices. With this, the uncertainty on the frequency is simply calculated by standard propagation of uncertainties.

For the knee voltage, the estimation of the uncertainties is rather complex. This is a factor that is highly dependent on the choices of the student, when inspecting the IV curve. However, if a line is fitted to the lineal part of the curve and the intercept is taken as the knee voltage, then the uncertainty of the intercept can be used to approximate the uncertainty of the knee voltage.

For the first method, the uncertainty on the value of the constant is the uncertainty associated with the slope of the fitted line, which was computed taking into account the measured uncertainties for the frequencies and the knee voltages.

As for the second method, the uncertainties needs to be propagated through all the steps of the methodology. The linearization of the IV curve gives the values of m and b for every LED, as in Eq. 10, with the associated uncertainties from the fitting process. Then the combination $-be/m$ is calculated and uncertainty propagated from the ones of b and m. That way, the uncertainties of the $-be/m$ factors as well as the frequencies, are used in the fitting process to compute the slope and its uncertainty, according to Eq. 11.

V. RESULTS

Figure 6 shows the experimental values for knee voltage and wavelengths as well as the lineal fit, with its parameters and related uncertainties. As it is stated by Eq. 5, conveniently selecting the quantities to plot (V_0 vs. $\frac{c}{e\lambda}$), the slope of the line is simply the Planck constant. Then,

$$h = (6.41 \pm 0.16) \cdot 10^{-34} Js, \tag{13}$$

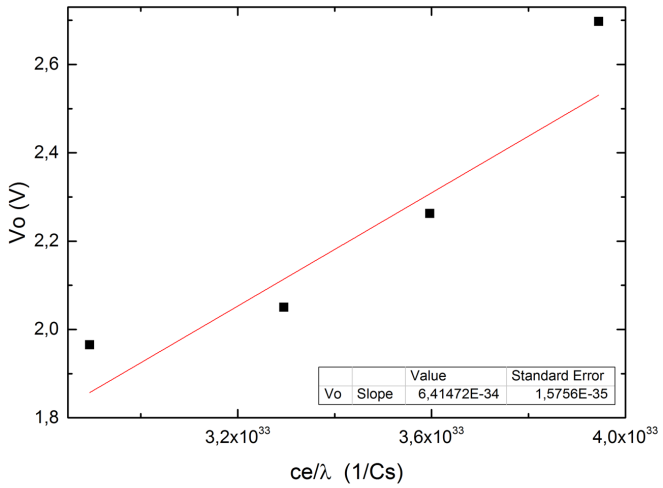

Figure 6. Lineal fit of knee voltage vs. $\frac{c}{e\lambda}$.

As for the second methodology proposed, Figure 8 shows the lineal fits to the IV curves for each of the measured LEDs. Table V shows the parameters m and b corresponding to the LEDs as well as the value of the combination $-be/m$ with its associated uncertainty.

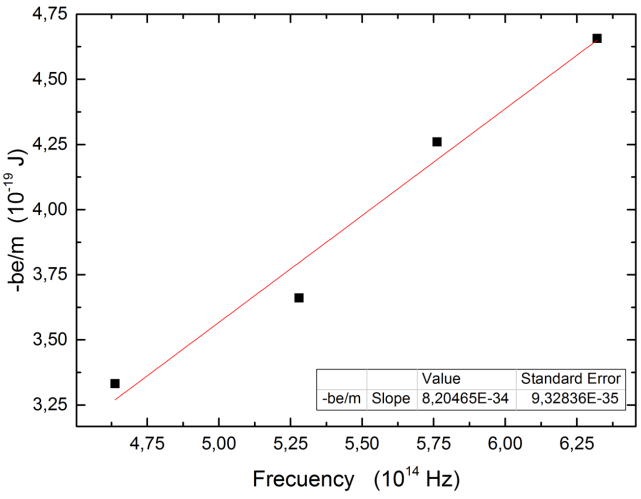

Figure 7. Lineal fit of $-\frac{be}{m}$ vs. ν according to Eq. 11.

Table 2. Intercept and slope values for the linear fit to the logarithmic IV curve, with the combination $-be/m$ and its associated uncertainty.

LED	b	m	$-be/m(10^{-19})$	$\Delta(10^{-20})$
Yellow	$-18,18$	$7,95$	3.66	$2,52$
Green	$-31,70$	11.92	4.26	$1,98$
Red	$-29,70$	$14,28$	3.33	1.39
Blue	$-34,87$	11.99	4.65	2.14

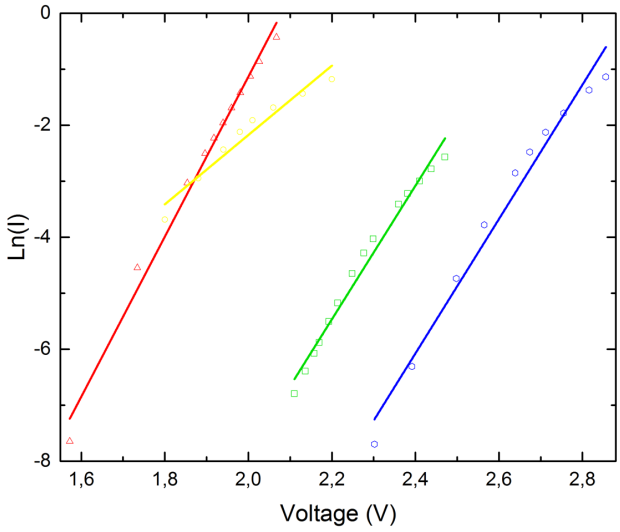

Figure 8. Lineal fits to the IV curves for each of the measured LEDs.

It is easily observed that the behaviour of the Yellow LED is different from the others, specially for the slope of the line. The only variation for the LEDs is the η parameter (temperature is considered constant through the experiment), which means the value of this parameter is considerably higher (an order of magnitude) with respect to the other three. However, as it was discussed previously, the measured voltages remains an order higher than the thermal voltage, so the Eq. 7 stands.

Figure 7 shows the experimental values and the lineal fit following Eq. 11, with the slope and related uncertainty. Then,

$$h = (8,20 \pm 0.93) \cdot 10^{-34} Js, \tag{14}$$

With none of the two methods is possible to obtain the value of the constant within the experimental uncertainty, however the results are close to it. It is remarkable that with the first method, despite its simplicity, it is possible to obtain a very good approximation to the numerical value of the Planck constant and with a reasonably low uncertainty, being not only a simple but also a precise method. The second one is less precise, in the sense that uncertainties are greater, which was an expected result due to the propagation that needs to be done, and also in the sense that the value obtained for the constant is further from the one reported in literature than the value obtained by the first method, also expected due to the influence that might be caused by the high η parameter on the Yellow LED.

VI. CONCLUSIONS

Two methods have been proposed that allow the student to compute the numerical value of the Planck constant with a reasonable good approximation to the one reported in literature. With the first method, widely found in literature, the student is able to compute the value of a universal constant by means of a simple mathematical

expression and general physical considerations on the rather complex phenomena that takes place within a LED. With the second one, not so commonly found in literature and rather successfully explained, the student deals with a more detailed overview of the functioning of LEDs as electronic devices. In a simple way the student is also put in contact with the Arduino platform, widely used in experimental measurements in the scientific research. The use of the Arduino also implies that the Laboratory Exercise can be implemented in any Physics Laboratory and it is an almost costless Exercise.

VII. ACKNOWLEDGMENTS

We'd like to thank the Physics Faculty of the Havana University which is the place where we study and where we've been able to develop this work. Also Prof. Gustavo Sanchez Colina and Prof. Gustavo Viera Lopez, from the Electronics Laboratory, for all the support in the realization of the experimental setup. Prof. Maria Sanchez Colina, as well as Msc. Yoandris Gonzalez and PhD. Arturo Abelenda, whose measurement system was used for the characterization of the LEDs. Finally the students of third year of Physics, who have done the exercise in their docent laboratories and have enriched us with their questions and comments.

REFERENCES

[1] Resolutions of the 26th CGPM. BIPM.org (https://www.bipm.org/utils/common/pdf/CGPM-2018/26th-CGPM-Resolutions.pdf). Fri. 26 Apr 2019.

[2] The Nobel Prize in Physics 1921. NobelPrize.org (https://www.nobelprize.org/prizes/physics/1921/summary/). Tue. 26 Mar 2019.

[3] The Nobel Prize in Physics 1918. NobelPrize.org (https://www.nobelprize.org/prizes/physics/1918/summary/). Tue. 26 Mar 2019.

[4] A.C. Melissinos, Experiments in Modern Physics, Academy Press, 1969.

[5] N. Zheludev, Nature Photonics **1**, 189 (2007).

[6] P. J. OConnor and L. R. OConnor, Phys. Teach. **12**, 423 (1974).

[7] J. W. Jewett Jr., Phys. Teach. **29**, 530 (1991).

[8] L. Nieves, G. Spavieri, B. Fernandez and R. A. Guevara, Phys. Teach. **35**, 108 (1997).

[9] D. F. Holcomb, Phys. Teach. **35**, 261 (1997).

[10] F. Zhou and T. Cloninger, Phys. Teach. **46**, 413 (2008).

[11] M. Andr and P. Andr, Science in School, **28**, 28 (2014).

[12] https://www.fisicarecreativa.com/informes/infor_mod/panck_diodos_2k1.pdf. Fri. 11 Oct 2019.

[13] https://rsef.es/images/Problemas/OEF2012/P-EXPERIMENTAL-OEF-2012.pdf. Fri. 11 Oct 2019.

[14] http://users.df.uba.ar/sgil/labo5_uba/inform/info/pautadas/led_const_plank2k1.pdf. Fri. 11 Oct 2019.

[15] A. Checchetti, A. Fantini, World Journal of Chemical Education, **3**, 87 (2015).

[16] C. O.Mosiori, D. A. Oeba and R. Shikambe, Path of Science, **3**, 2007 (2017)

[17] F. Herrmann and D. Schtzle, Am. J. Phys. **64**, 1448 (1996).

[18] A. Eisberg, R. Resnick, Quantum physics of atoms, molecules, solids, nuclei, and particles, Editorial Pueblo y Educacin, La Habana, 1984.

[19] W. Shockley, Bell Syst. Tech. J. **28**, 435489 (1949).

[20] The Nobel Prize in Physics 1921. Award ceremony speech. NobelPrize.org (https://www.nobelprize.org/prizes/physics/1921/summary/). Fri. 5 Apr 2019 5.

[21] A. B. Aarons and M. B. Peppard, Am. J. Phys. **33**, 367 (1965).

[22] M. Margolis, Arduino Cookbook, 2nd Edition, OReilly Media, 2012.

CONCEPCIONES ALTERNATIVAS EN EL ESTUDIO DE LAS LEYES DE NEWTON MEDIANTE CUESTIONARIO A ESTUDIANTES DE INGENIERA

ALTERNATIVE CONCEPTIONS IN THE STUDY OF NEWTONS LAWS THROUGH QUESTIONNAIRE TO STUDENTS OF THE CAREER OF ENGINEERING

J. Saquinaula-Brito and R. Pánchez Hernández

Facultad de Ciencias de la Ingeniería, Universidad Estatal de Milagro, Ecuador; jsaquinaulab@unemi.edu.ec
† autor para la correspondencia

Recibido 14/10/2019; Aceptado 14/11/2019

El bajo nivel conceptual que presentan los alumnos en el estudio de la física clásica ha llevado a un sinnúmero de investigaciones con el fin de mejorar el rendimiento académico. Entre las estrategias podemos citar la importancia que tiene conocer las concepciones alternativas previo a impartir la cátedra. Nuestro objetivo es el de elaborar y aplicar nuestro propio banco de preguntas para determinar errores conceptuales específicos sobre las leyes de Newton y determinar el nivel conceptual de 140 estudiantes del primer semestre de ingenieras. Los resultados reflejados en las justificaciones de sus respuestas muestran un bajo análisis conceptual acerca de la dinámica de partículas. Tal es el hecho de que solo el 4 % de los jóvenes responden correctamente a la definición de fuerza. Esto pone de manifiesto que en las clases se prioriza la resolución de ejercicios sin tomar en cuenta el raciocinio teórico.

The low conceptual level presented by students in the study of classical physics has led to a number of investigations in order to improve academic performance. Among the strategies we can mention the importance of knowing the alternative conceptions prior to teaching. The goal is to develop and apply our own test question pool to determine specific conceptual errors about Newton's laws and determine the conceptual level of 140 students in the first semester of engineering. The results reflected in the justifications of their responses show a low conceptual analysis about particle dynamics. Such is the fact that only 4 % of young people respond correctly to the definition of force. This shows that in the classes the resolution of exercises is prioritize without taking into account the theoretical reasoning.

PACS: Teaching of physics (enseñanza de la física), 01.40.-d; newtonian mechanics (mecánica newtoniana), 45.20.D-; forces in the newtonian mechanics (fuerzas en la mecnica newtoniana), 45.20.da

I. INTRODUCCIÓN

A través de los años, el proceso de enseñanza aprendizaje en los cursos de física clásica han sido ofrecidos mediante el modelo tradicional, donde el docente se preocupa por las clases magistrales, exponiendo conceptos, resolviendo ejercicios de manera mecánica, priorizando la matemática y dejando de lado la parte del razonamiento conceptual de la física.

Todos estos factores, incluyendo la falta de experimentación conlleva a que el estudiante se desmotive por aprender la disciplina [1].

En la elaboración de las clases no se deben apartar las concepciones alternativas o ideas previas que suelen tener los estudiantes, pues sirven como preámbulo para el aprendizaje mutuo entre los participantes, considerándose como conocimientos empíricosque ayudan a fomentar la investigación y el interés por despejar cualquier duda presentada en el proceso de enseñanza [2].

La tarea del docente se debe enfocar en conocer las concepciones alternativas para elaborar su plan de actividades académicas (clase, tarea y evaluación) con la finalidad de que los conceptos básicos se conviertan en concepciones científicas [3]. Por tal motivo, el presente trabajo muestra las justificaciones erróneas que presentan los alumnos al estudiar las leyes de Newton.

II. OBJETIVO DEL ESTUDIO

El trabajo pretende dos objetivos principales que son: Elaborar un cuestionario basado en las leyes de Newton con la finalidad de determinar concepciones alternativas específicas y estudiar la evolución de las ideas previas que poseen los estudiantes universitarios con respectoa la parte conceptual del estudio de la dinámica de partículas.

III. FUNDAMENTO TEÓRICO

III.1. Concepciones alternativas

Desde su nacimiento, las personas elaboran construcciones mentales con el propósitode dar respuesta a las experiencias del día a día [4]. Estas representaciones por lo general no son consonantes con las respuestas de rigor científico y conllevan a errores que con el pasar del tiempo son más difíciles de corregir. Por lo tanto, las concepciones alternativas son el conjunto de conocimientos previos que poseen los alumnos

sobre los fenómenos naturales que difieren del conocimiento científico [5].

La raíz de estas concepciones alternativas en el estudio de la física se debe a varios factores, siendo las más significativas: el lenguaje informal de la calle, la forma tradicional de enseñanza que prioriza la memorización, y errores conceptuales tanto de textos académicos como de los propios docentes [2].

La finalidad de detectar las concepciones alternativas es para provocar un cambio conceptual, el mismo que notrata simplemente de sustituir una concepción por otra, sino de generar una evolución conceptual [6].

III.2. Enseñanza de las leyes de Newton

El proceso de enseñanza aprendizaje en el campo de la física a lo largo de los años no ha cambiado significativamente a pesar de la existencia de metodologías con base en el constructivismo, la instrucción en pares donde se favorece el trabajo en equipo y el aprendizaje activo en el cual se realiza la experimentación para responder a estrategias educativas; puesto que se mantiene en cierto modo el dictado de las clases basadas en el método tradicional que prioriza la memorización, tanto en lo teórico como en las prácticas experimentales [3].

Estudios realizados en la década de los ochenta [7] muestran que esta manera histórica de enseñanza conlleva a que los estudiantes presentenideas comunes que son inconsistentes con la mecánica de Newton bajando su rendimiento académico sobre todo en la parte conceptual.

A raíz de este problema, profesores e investigadores pedagógicos desarrollan cuestionarios o banco de preguntas con la finalidad de medir el nivel de ganancia conceptual en la parte de cinemática y dinámica. Uno de los cuestionarios más utilizados es el llamado Force Concept Inventory (FCI) [8]. Todas las preguntas están vinculadas al movimiento, relacionando el concepto de fuerza y las tres leyes de Newton con las magnitudes cinemáticas, como son la velocidad y aceleración [1].

La aplicación de este instrumento de medición junto con otros estudios, muestra que los cursos basados en la metodología tradicional presentan un cambio conceptual poco significativo [9, 10]. Estos alumnos son buenos resolviendo de forma matemática los ejercicios, aunque presenten un bajo nivel conceptual de las leyes de Newton.

IV. MATERIALES Y MÉTODO

IV.1. Participantes (muestra)

Los participantes que conformaron la muestra a evaluar del estudio fueron 140 estudiantes (102 hombres y 38 mujeres) que formaron parte del primer semestre de las carreras de ingeniería industrial, sistemas y biotecnología de una Universidad Pública Ecuatoriana. La edad de los discentes oscila entre los 18 y 24 años (18 años es la edad que prevalece con el 48 %).

IV.2. Instrumento

El instrumento de evaluación consiste en una prueba de carácter teórico compuesta por 10 preguntas de opción múltiple (ANEXO 1) que debe ser respondido en un tiempo máximo de 40 minutos.

Tabla 1. Campo de acción y concepciones alternativas del instrumento de evaluación.

Pregunta	Campo de acción	Concepción alternativa
1	Primera ley de Newton	-Para mantener un cuerpo en movimiento es necesario aplicarle fuerza
2	Concepto de inercia	-Cuerpos que se mueven juntos con la misma velocidad presentan igual inercia
3	Concepto de fuerza	-Fuerza se define como el producto de la masa con su aceleración -Fuerza es la presión que se le aplica a los cuerpos
4	Fuerza gravitacional	-Todos los objetos en caída libre son atraídos con la misma fuerza
5	Segunda ley de Newton	-En un plano inclinado, la aceleración de un cuerpo depende de la velocidad inicial y la masa
6	Tercera ley de Newton	-La aceleración depende solo de la fuerza aplicada
7	Tercera ley de Newton	-Para que un objeto A mueva a otro B, la fuerza que aplica A sobre B debe mayor a la que B aplica a A
8	Diagrama de cuerpo libre	-La fuerza de rozamiento y la fuerza normal son fuerzas de origen distinto
9	Fuerza de rozamiento	-La ecuación $f = {}_kN$ siempre se aplica
10	Segunda Ley de Newton	-Para determinar la fuerza resultante es necesario conocer el valor de todas las fuerzas aplicadas

El cuestionario se divide en 2 ejercicios de desarrollo numérico y 8 preguntas conceptuales, de los cuáles en seis se tienen que justificar su opción de respuesta.

La finalidad de la prueba radica en analizar los errores conceptuales que llevan a que los jóvenes presenten concepciones alternativas. La tabla 1 detalla estas concepciones y su correspondiente campo de acción en el estudio de la dinámica.

V. RESULTADOS Y DISCUSIÓN

V.1. Concepción alternativa: "las fuerzas producen movimiento"

Pregunta 1: Lo que se persigue con esta pregunta es averiguar si persiste la idea Aristotélica de que, para mantener un cuerpo en movimiento tiene necesariamente que actuar una fuerza resultante.

De la tabla 2 observamos que la respuesta correcta es la segunda más acertada con un 32.9 % correspondiendo a un total de 46 estudiantes. Llama la atención de que el 47.1 % de ellos mantengan ideas erróneas que permanecen por años, por ejemplo: "Si no hay fricción no se disminuye solo se aumenta la velocidad", "El bloque se detendrá porque no hay alguien que le aplique fuerza constantemente".

Pregunta 2: El objetivo de esta pregunta es saber si creen que la inercia depende de la fuerza aplicada. Con asombro notamos que el 63 % de los participantes escoge la opción incorrecta.

De los resultados mostrados en la figura 1 podemos inferir que se piensa erróneamente que la inercia de un cuerpo está ligada a las interacciones con su entorno. De las respuestas erróneas a esta pregunta relativamente sencilla tal parece que aún no está del todo claro el concepto.

V.2. Concepción alternativa: "Fuerza se define como F = ma"

Pregunta 3: Este tema trata sobre el concepto de fuerza. En ella podemos observar con asombro que solo 5 jóvenes responden correctamente. Se tiene en la gran mayoría la idea errada de que fuerza, energía y presión son la misma cosa. Además, cerca del 36 % señaló la opción c), de lo cual se puede presumir que piensan que, para que exista fuerza es necesario acelerar al cuerpo.

Tabla 2. Justificación a las opciones seleccionadas para la pregunta 1.

Pregunta 1	Respuesta d)	
Sin marcar	9	
Número de estudiantes	**Opción elegida**	**Justificación**
16	a)	-"Porque el bloque tiene una velocidad y a lo que es tirado en un piso sin fricción su velocidad aumentaría." -"Si no hay fricción no se disminuye solo se aumenta la velocidad."
66	b)	-"Creo que se detendrá luego de una cierta distancia, -"Se detendrá a una cierta distancia porque su velocidad es pequeña. Aparte, la superficie es horizontal." -"Avanzará cierta distancia ya que depende de la fuerza que se haya lanzado." -"Porque debido a la gravedad en alguna parte se detendrá." -"El bloque se detendrá porque no hay alguien que le aplique fuerza constantemente." -"Se detendrá ya que cada objeto tiene cierta fuerza." la cual se terminará y el objeto se detendrá."
3	c)	-"No se detendrá porque viaja horizontalmente." -"Debido a que la velocidad del bloque es constante."
46	d)	-"La velocidad si es constante, aunque sea mínima." -"Al no tener cambios en la velocidad será constante y no se detendrá." -"Porque nada detiene el movimiento si no hay fricción." -"Porque el bloque no llega al suelo su velocidad en el aire es constante." -"No hay fuerzas que detengan o disminuyan la velocidad."

Pregunta 4: La finalidad de esta pregunta radica en averiguar si se mantiene la preconcepción de que los cuerpos en caída libre sufren la misma fuerza gravitacional. En su mayoría, el 73.6 % manifiesta que la fuerza que el planeta Tierra ejerce a todos los cuerpos tiene el mismo valor.

La posible causa de este resultado es el hecho de que confunden aceleración de la gravedad (que no depende de la masa) con fuerza gravitatoria, que como toda interacción depende de la masa del cuerpo y de la Tierra. Confirmamos nuestra hipótesis cuando encontramos justificaciones como estas: "Porque la gravedad es la misma y las dos tiran fuertemente ya que no depende de su peso".

V.3. Concepción alternativa: "La aceleración siempre depende de la velocidad" "a menor masa, mayor aceleración".

Pregunta 5: este ítem indaga la relación matemática entre fuerza y masa. No está clara la relación entre peso y masa ya que un grupo de estudiantes basa su afirmación en que el que tiene menos masa tendrá mayor aceleración y otro grupo

manifiesta lo contrario. Un total de 35 participantes indican correctamente la respuesta, aunque, fallen en su justificación, por ejemplo: "La aceleración de ambas es la misma ya que la esfera A tiene menos masa que la de B pero esta esfera tiene más velocidad inicial". Otros basan su respuesta en que ambas esferas son lanzadas con diferente velocidad, porque la esfera B comienza con mayor velocidad".

V.4. Concepción alternativa: "la acción mayor a la reacción"

Pregunta 6: lo que tratamos de averiguar con este tema es saber si se tiene claro la relación entre fuerza y masa para determinar la aceleración de un objeto. La pregunta en sí es básica pero curiosamente solo el 37.1 % responde correctamente. Como el 50.7 % indica la opción c) (la aceleración de los dos objetos es de igual magnitud), se podría asumir que se dejaron llevar por el enunciado de la tercera ley de Newton.

Pregunta 7: Este ejercicio conceptual es complementario del anterior, y en el que tratamos de investigar si queda claro los términos "acción-reacción". Los resultados confirman las respuestas de la pregunta 6, donde el 79 % que corresponde a 110 estudiantes manifiestan que para que un cuerpo desplace a otro, la fuerza de acción debe ser mayor a la de reacción. Solo 28 estudiantes marcan la respuesta válida.

V.5. Concepción alternativa: "la fricción y su dependencia con la normal"

Pregunta 8: El objetivo de este ítem es averiguar cuántos participantes tienen claro de que la fuerza normal y la de fricción son las componentes de una misma fuerza. Es preocupante de que solamente 29 estudiantes marcaron correctamente, aunque sus justificaciones como, por ejemplo: "Normal, fuerza de acción, gravedad", no estaban del todo bien sustentadas.

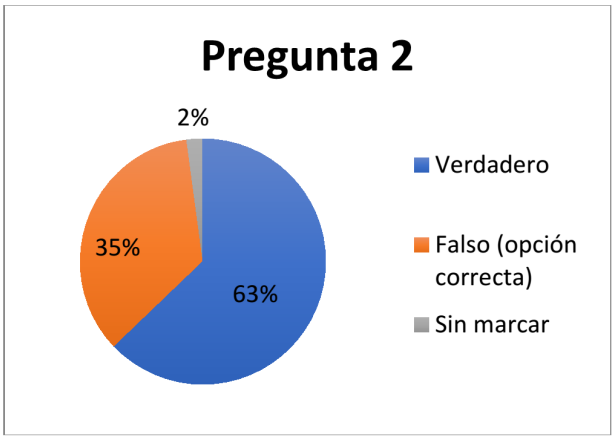

Figura 1. Gráfica de las opciones seleccionadas para la pregunta 2.

Aquí cabe hacer un "mea culpa", ya que por lo general al realizar un diagrama de cuerpo libre los profesores dibujamos estas fuerzas de manera aislada sin hacer énfasis que provienen de la misma interacción.

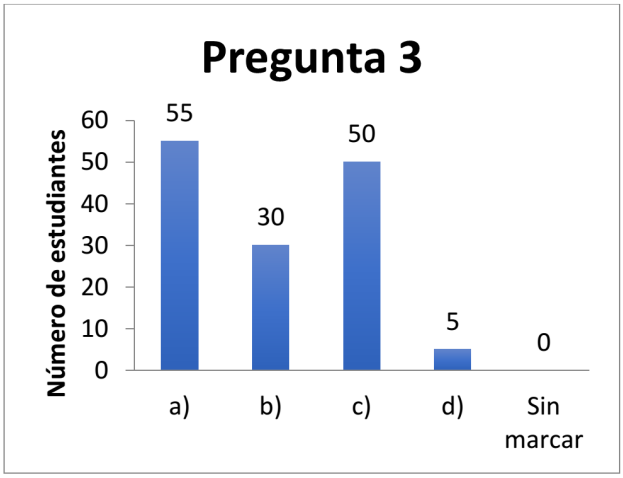

Figura 2. Gráfica de las opciones seleccionadas para la pregunta 3.

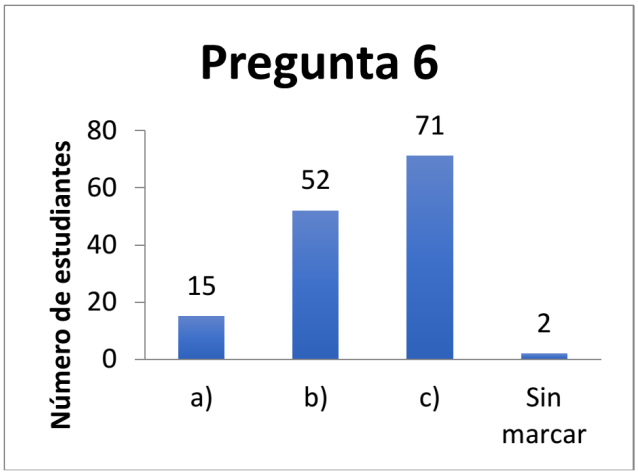

Figura 3. Gráfica de las opciones seleccionadas para la pregunta 6.

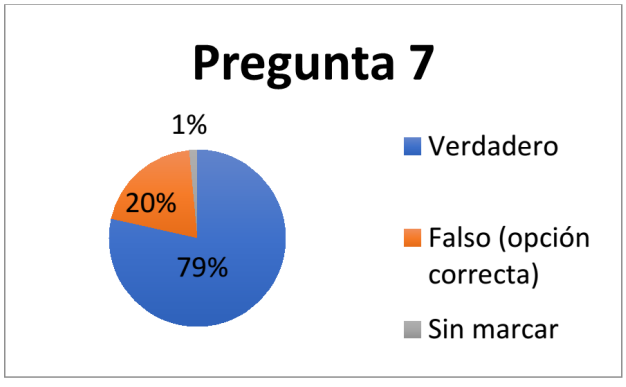

Figura 4. Gráfica de las opciones seleccionadas para la pregunta 7.

Tabla 3. Justificación a las opciones seleccionadas para la pregunta 4.

Pregunta 4	Respuesta b)	
Sin marcar	2	
Número de estudiantes	**Opción elegida**	**Justificación**
8	a)	-"La bola de tenis va a tirar más fuertemente, pero la que va a caer primero es la de bolos debido a su peso." -"El planeta tierra es más grande." -"Porque entre menos masa cae más rápido." -"Porque la pelota de bolos es más pesada y no puede ser lanzada con la misma fuerza que la de tenis."
27	b)	-"Porque su masa es mayor a la de tenis." -"Porque la bola de bolos es más pesada que la de tenis."
103	c)	-"Porque la gravedad es la misma y las dos tiran fuertemente ya que no depende de su peso". -"Porque tienen la misma gravedad." -"Porque la persona no le está aplicando ninguna fuerza a las dos bolas. - "Ambas caerán a la misma aceleración y tiempo" -"El peso no importa lo que importa aquí es la aceleración." -"Como es caída libre caen al mismo tiempo con la aceleración que no influye el viento y la gravedad pueden las dos caer al mismo tiempo." -"La fuerza de atracción gravitacional ejerce la misma fuerza para todos los objetos despreciando su masa."

Tabla 4. Justificación a las opciones seleccionadas para la pregunta 5.

Pregunta 5	Respuesta c)	
Sin marcar	17	
Número de estudiantes	**Opción elegida**	**Justificación**
38	a)	-"Porque va con menos peso." -"Un estudiante utilizó $v = ma$."
50	b)	-"Porque fue lanzada con mayor fuerza." -"Porque la esfera B comienza con mayor velocidad." -"La esfera B tiene mayor peso y por lo tanto una velocidad mayor." -"Ya que como tiene más masa tiene más aceleración."
35	c)	-"La aceleración de ambas es la misma ya que la esfera A tiene menos masa que la de B, pero esta esfera tiene más velocidad inicial." -"La aceleración es la misma ya que del mismo lugar solo con diferente velocidad." -"La división de masa para velocidad es casi la misma 0.01. Por eso tienen la misma aceleración." -"Son iguales ya que en la figura se muestra su aceleración." -"Se dedujo: $a = g\sin(?)$." -"Debido a que el ángulo para los dos es la misma."

Tabla 5. Justificación a las opciones seleccionadas para la pregunta 8.

Pregunta 8	Respuesta c)	
Sin marcar	12	
Número de estudiantes	**Opción elegida**	**Justificación**
10	a)	-"Solo se utiliza una fuerza." -"1 fuerza ya que se está aplicando sobre un bloque en un plano inclinado con fricción y por eso ejerce solo una fuerza."
19	b)	-"Dos fuerzas. La fuerza de fricción y la fuerza para mover el plano."
29	c)	-"Fuerza F, peso en x y y, normal." "Fuerzas en $x = aceleracion$, fuerza. Fuerza en $y = gravedad$." -"Normal, fuerza de acción, gravedad."
64 6	d) e)	-"Hay cuatro fuerzas. La fuerza F, la fricción, el peso y la normal"

V.6. Concepción alternativa: "siempre se utiliza f=N"

Pregunta 9: el ejercicio busca indagar la preconcepción de que las magnitudes de la fuerza de fricción y la fuerza normal siempre se relacionan mediante el coeficiente de rozamiento. Los 28 estudiantes (correspondiente nada más que al 20 % que seleccionaron la opción válida), justifican, pero, de manera errónea. Tal parece que tienen dificultades cuando se les presenta los dos coeficientes y saber con certeza si el cuerpo se encuentra en reposo o en movimiento.

Tabla 6. Justificación a las opciones seleccionadas para la pregunta 9.

Pregunta 9	Respuesta b)	
Sin marcar	44	
Número de estudiantes	**Opción elegida**	**Justificación**
13	a)	-"La fuerza de rozamiento no se expresa en la imagen." -"Porque la fricción estática es mayor por eso no se mueve."
28	b)	-"Aplicaron la primera ley de Newton." -"Porque es la fuerza que se aplica para obtener la fuerza de rozamiento." -"Es un par de fuerzas acción-reacción."
37	c)	-"Se aplicó la fórmula de fricción cinética."
18	d)	-"Aplicaron la fórmula de fricción estática."

Pregunta 10: La finalidad de este tema trata sobre visualizar la manera más rápida de resolver un problema que aparenta ser complicado por la cantidad de información que se le presenta. 76 jóvenes no recordaban la aplicación de la segunda ley de Newton y solo el 28 % lo resolvió de forma breve. Esto muestra que se tiene problemas en la elaboración de diagramas de fuerzas y de entender que se puede determinar la suma de todas las fuerzas sin la necesidad de tener la magnitud y dirección de cada una de estas interacciones.

Tabla 7. Justificación a las opciones seleccionadas para la pregunta 9.

Pregunta 10	**Número de estudiantes**	**Ópcion elegida**	**Justificación**
Respuesta c)	4	a)	Aplicó la fórmula *ma*
	4	b)	
	32	c)	
	9	d)	
	15	e)	
Sin marcar	76		

VI. CONCLUSIONES

Las conclusiones obtenidas del estudio basado en las justificaciones de los estudiantes son las siguientes:

(a) A pesar de su historial académico de varios años en formación secundaria y un curso de nivelación para ingresar a la universidad, los estudiantes mantienen pre conceptos en el campo de la física clásica. Esto se produce, debido a la manera de explicar la materia por parte de los docentes, basando su metodología solo en la forma tradicional que prioriza la memorización y sin tomar en cuenta las concepciones alternativas para elaborar su plan de clases. Además, podemos agregar la falta de laboratorios (región donde se realizó el estudio) o experimentos caseros de física que fortalezcan la teoría y motiven a nuestros jóvenes.

(b) El estudio muestra el bajo rendimiento de los estudiantes, al observar que la pregunta con mayor porcentaje de acierto es del 37 %, que corresponde a la ley de acción-reacción (ejercicio 6). La pregunta con el menor porcentaje de acierto es del 4 %, que tiene que ver con el concepto de fuerza (ejercicio 3). Estos resultados ponen de manifiesto que el plan de clases se fundamenta principalmente en la resolución de ejercicios, dejando de lado el análisis conceptual.

(c) Se consideran necesarias las siguientes sugerencias para reforzar la enseñanza conceptual en el estudio de la física:

- Comenzar la clase con preguntas de verdadero/falso o de opciones múltiples con la finalidad de determinar concepciones alternativas y de crear un conflicto en la forma de pensar del estudiante, que se den cuenta que un tema o concepto que aparentemente lo tenían claro, necesitan profundizar.
- Tomar una prueba de lectura previo a entrar a un tema, que puede ser leer ciertas páginas de un texto o analizar un vídeo. Ya queda a criterio del profesor si es una evaluación sumativa o formativa. Las preguntas deben ser sencillas.
- Uno de los principales libros de referencia debe tener un alto enfoque conceptual. Además, las evaluaciones deben tener un porcentaje de preguntas conceptuales o discrepantes.
- Al elaborar la guía de laboratorio es difícil aplicar al ciento por ciento metodologías constructivistas, nos dejamos llevar por lo que se denomina "receta de cocina" para que el estudiante complete la tabla de resultados. En la medida de lo posible se debe preguntar de tal manera que el joven tenga que pensar la manera de implementar el uso de los equipos para resolver el problema planteado.

REFERENCIAS

[1] M. Quibao, A. Silva, N. Almeida, R. Silva, S. Muniz y F. Paiva, Revista Brasileira de Ensino de Física [ISSN: 1806-9126], **41** 2, (2019). (http://www.scielo.br/pdf/rbef/v41n2/1806-9126-RBEF-41-2-e20180258.pdf), pp. 1-10.

[2] J. Carrascoa, Revista Eureka sobre Enseñanza y Divulgación de las Ciencias **2**, 183 (2005).

[3] J. Saquinaula, M. Guerrero and J. Ortiz, Espirales revista multidisciplinaria de investigación **2**, 1 (2018).

[4] S. Aguilar, C. Maturano and G. Nuez, Revista Electrónica de Enseñanza de las Ciencias **6**, 691 (2007).

[5] N. Menezes and J. Barrera, Lat. Am. J. Sci. Ed. **4**, 1 (2017).

[6] M. Moreira and I. Greca, Cincia & Educao (Bauru), **9** 301, (2003).

[7] I. Halloun and D. Hestenes, Am. J. Phys. **53**, 1043 (1985).

[8] D. Hestenes, M. Wells and G. Swackhamer, Phys. Teach. **30**, 141 (1992).

[9] E. Mazur, Peer instruction: a users manual, 1st Ed. (Upper Saddle River, New Jersey 07458, 1997).

[10] A. Lopes, CombinandoMetodología de Ensino Peer InstructioncomJust-in-Time Teaching para o Ensino de Física Universidade Federal de Viosa, Viosa, 2016.

SYMMETRY IN THE SYSTEM OF TWO BLOCKS CONNECTED BY A STRING WITH VARIABLE TENSION

SIMETRÍA EN DOS BLOQUES CONECTADOS POR UNA CUERDA CON TENSIÓN VARIABLE

D. Benitez[a], H. J. Herrera Suárez[b†], J. H. Muñoz[c]

a) Instituto de educación y pedagogía, Universidad del Valle, Ciudad Universitaria Meléndez Calle 13 Número 100-00, Cali, Colombia
b) Facultad de Ciencias Naturales y Matemáticas, Universidad de Ibagué, Carrera 22 Calle 67, barrio Ambalá,Ibagué, Colombia; hernan.herrera@unibague.edu.co†
c) Departamento de Física, Universidad del Tolima, A. A. 546, Ibagué, Colombia
† autor para la correspondencia

Recibido 19/10/2019; Aceptado 19/11/2019

In this paper we review the system made up by two blocks connected by a string over a smooth pulley with variable tension. One block lies on an horizontal surface and the another block is hanging vertically. We carry out a complete and systematic analysis for the tension of the string as function of the angle θ and the horizontal distance x, at static equilibrium. We find a simmetry-like that corresponds to two different configurations with the same tension and obtain the relationship that must satisfy two angles or two horizontal distances to obtain equal tension.

En este artículo revisamos el sistema conformado por dos bloques conectados por una cuerda sobre una polea sin fricción con tensión variable. Un bloque se encuentra sobre una superficie horizontal y el otro está suspendido verticalmente. Realizamos un análisis completo y sistemático para la tensión de la cuerda en función del ángulo θ y la distancia horizontal x, en equilibrio estático. Encontramos un tipo de simetría que corresponde a dos configuraciones diferentes con la misma tensión y obtuvimos la relación que deben satisfacer dos ángulos o dos distancias horizontales para obtener igual tensión.

PACS: Newtonian mechanics (mecánica newtoniana), 45.20.D; Tension measurement (medición de tensión), 07.10.Lw; Mechanical instrument equipment (equipo de instrumento mecánico), 07.10.-h.

I. INTRODUCTION

In this work we re-examine the system of two blocks of masses m and M connected by a string over a smooth pulley, at static equilibrium. The string is extensionless, uniform and its mass is negligible, and there is a coefficient of static friction between the mass m and the horizontal surface. In Figure 1 we show the forces acting on this problem.

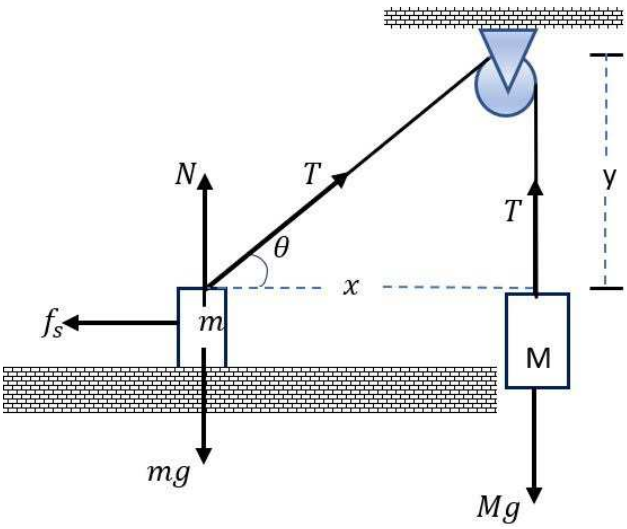

Figura 1. Two blocks tied to an extensionless rope. The mass of the string is negligible.

This system and similar versions are considered in fundamental physics textbooks [1–5], in some papers [6–10] and the website of A. Franco [11]. However, a complete analysis about the tension T in function of the angle θ or the horizontal distance x has not been considered in the literature.

The mentioned problem is important because the tension T and the normal force N are not constant, unlike what happens in the following systems: the Atwood's machine, a mass on an horizontal surface and the another mass suspended, a mass on an inclined plane and the another mass hanged, and two masses on two inclined planes.

The purpose of this work is to perform a complete analysis on the tension of the string, T, which is provided by the hanging mass M when the system is at static equilibrium, as function of the angle θ and the horizontal distance x, using trigonometric functions and elementary mathematical tools.

The paper is organized as follows. In section II we show the experiment arrangement built by us to model the system shown in Figure 1; in section III we present the theoretical analysis and the conclusions are given in section IV.

II. THE EXPERIMENT

Considering that only the reference [9] performed the experimental arrangement and took experimental data, corresponding to the system showed in Figure 1, and assuming that it is important because it articulates theory and experiment, we also carry out another arrangement.

We show, in Figure 2, the experimental arrangement used for obtaining the tension T in function of the angle θ. We use the linear air track, reference 337501, of the company Leybold [12]. We take $m = 1.3745$ kg and $M = 0.4$ kg, and put a digital dynamometer [13] over the mass m and the direction of the rope to measure the tension T. The mass of the dynamometer has been added to m. The angle θ was measured with the Angle Meter PRO+ free application of Play Store [14].

We obtained that the static friction coefficient between the mass m and the surface is $\mu_s = \frac{M}{m} = 0.29$. We show in Figure 3 our experimental results for the tension T in function of the angle θ, considering several static equilibrium configurations. The estimated errors in the measurements of the angle θ and the masses are 1^0 and 1 gr, respectively. The uncertainty of the tension T is obtained in quadrature:

$$dT = \sqrt{\left(\frac{\partial T}{\partial \theta}\right)^2 (d\theta)^2 + \left(\frac{\partial T}{\partial M}\right)^2 (dM)^2 + \left(\frac{\partial T}{\partial m}\right)^2 (dm)^2}$$

, given approximately $\Delta T = 0.02N$. In the next section we present the theoretical analysis about this figure.

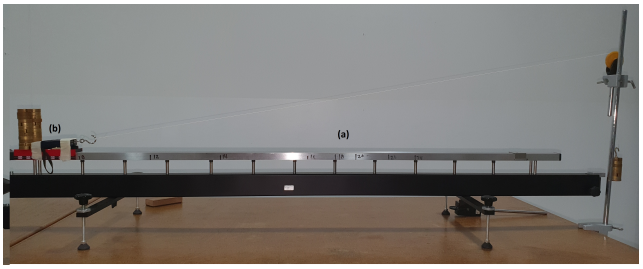

Figura 2. Experimental arrangement: (a) the linear air track; (b) the dynamometer

III. THEORETICAL ANALYSIS

Applying the Newton's second law to the mass m and assuming that the system is at static equilibrium, the tension of the string, T, in function the angle θ is given by [1,2,6–9,11]

$$T(\theta) = \frac{\mu_s mg}{\cos\theta + \mu_s \sin\theta}, \quad (1)$$

where μ_s is the coefficient of static friction, g is the gravity acceleration and θ is in the range $[0, \pi/2]$.The theoretical curve shown in Figure 3 was made with this equation. We can see that the experimental data agree, approximately, with the theoretical prediction.

The minimum value of this tension is reached when

$\theta_{min} = tan^{-1}(\mu_s)$.

This relation can be associated, in a pedagogical way, with the right triangle shown in Figure 5. By means of this figure it is easy to obtain $T_{min} = T(\theta_{min}) = \frac{\mu_s mg}{\sqrt{1+\mu_s^2}}$.

We display, in Figure 4, the tension $T(\theta)$ given by equation 1, with $m = 2kg$ and $\mu_s = 0.9$. In this Figure it is possible to identify *two extreme cases*: (1) When the string is parallel to the horizontal surface. In this case, $\theta \to 0$, then $\lim_{\theta\to 0} T(\theta) = \mu_s gm$; (2) When $\theta \to \pi/2$, then $\lim_{\theta\to\frac{\pi}{2}} T(\theta) = mg$. In this situation the rope is perpendicular to the horizontal surface and corresponds to the Atwood's machine at rest or at uniform motion.

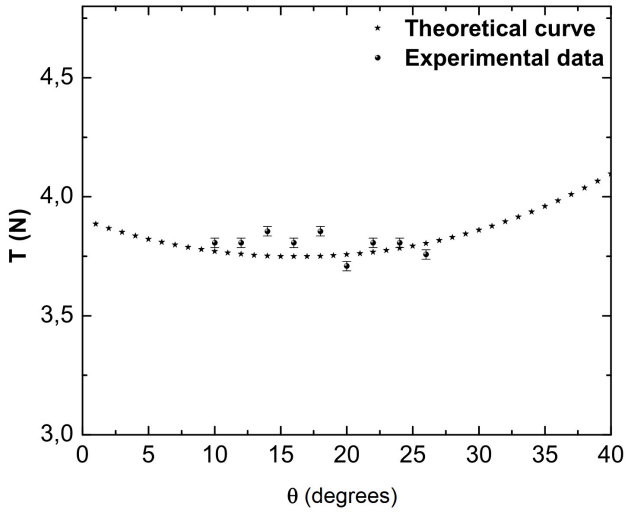

Figura 3. Experimental results for the tension T in function of Θ

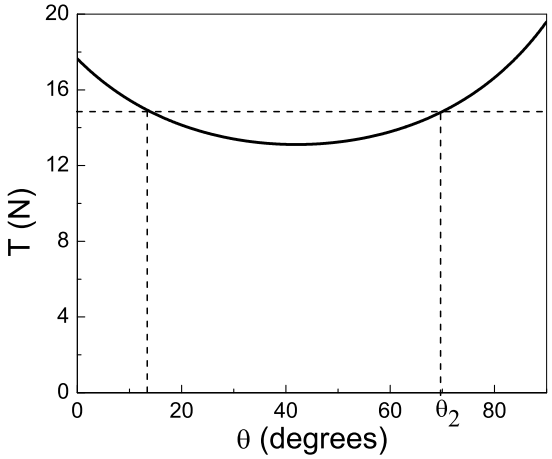

Figura 4. Tension T in function of the angle θ, with $m = 2$ kg, $y = 0.3$ m and $\mu_s = 0.9$.

III.1. *T as function of angle*

Let us consider an arbitrary tension $T = T_1$ and draw a parallel line to the horizontal axis at height T_1 in Figure 4. Clearly, we see that there are two angles (θ_1 and θ_2) for which the same tension is obtained . It means that for each selected angle θ_1 there is another angle θ_2 that $T(\theta_1) = T(\theta_2)$, i.e., there are two identical configurations for the static equilibrium (see Figure 6), indicating certain type of symmetry in the system. One of the aims of this note is to find the restriction that these angles must follow. From equation 1, we obtained

$$\frac{\mu_s mg}{\cos\theta_1 + \mu_s \sin\theta_1} = \frac{\mu_s mg}{\cos\theta_2 + \mu_s \sin\theta_2}. \quad (2)$$

Making a simple algebraic manipulation, we get

$$\mu_s = \frac{\cos\theta_1 - \cos\theta_2}{(\sin\theta_2 - \sin\theta_1)}, \tag{3}$$

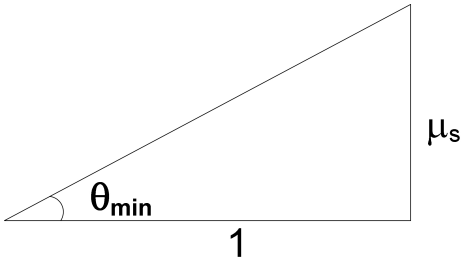

Figura 5. Right triangle associated to the relation $tan(\theta_{min}) = \mu_s$

and using the well known trigonometric identities,

$$\cos A - \cos B = -2\sin\left(\frac{A+B}{2}\right)\sin\left(\frac{A-B}{2}\right), \tag{4}$$

$$\sin A - \sin B = 2\cos\left(\frac{A+B}{2}\right)\sin\left(\frac{A-B}{2}\right), \tag{5}$$

we can rewrite the equation 3 as,

$$\mu_s = \frac{-2\sin\left(\frac{\theta_1+\theta_2}{2}\right)\sin\left(\frac{\theta_1-\theta_2}{2}\right)}{-2\cos\left(\frac{\theta_1+\theta_2}{2}\right)\sin\left(\frac{\theta_1-\theta_2}{2}\right)},$$

$$\mu_s = \tan\left(\frac{\theta_1+\theta_2}{2}\right), \tag{6}$$

finally getting

$$\theta_2 + \theta_1 = 2\tan^{-1}(\mu_s). \tag{7}$$

or equivalently

$$\theta_2 + \theta_1 = 2\theta_{min}. \tag{8}$$

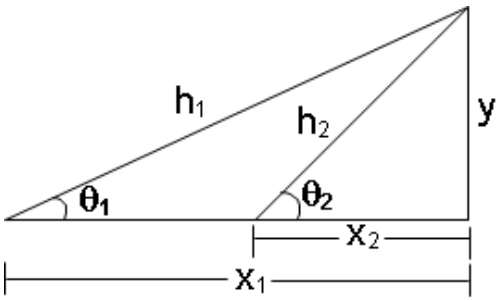

Figura 6. Configurations for the static equilibrium.

This equation establishes the relationship between the angles θ_1 and θ_2 that give the same tension. It provides us certain type of symmetry in this system.

III.2. T as function of x

It is also possible analyze the tension T in function of the horizontal distance x. For that, we use the following relations

$$\cos\theta = \frac{x}{\sqrt{x^2+y^2}}, \tag{9}$$

$$\sin\theta = \frac{y}{\sqrt{x^2+y^2}}, \tag{10}$$

in the equation (1) and obtained

$$T(x) = \frac{\mu_s g m\sqrt{x^2+y^2}}{x + y\mu_s}. \tag{11}$$

A graph of this equation is plotted in Figure 7.

Again, if we draw a parallel line to the horizontal axis at height T_2 we see that there are two different positions x_1 and x_2 that yield $T(x_1) = T(x_2)$ i.e., there are two similar configurations of static equilibrium (see Figure 7). The minimum value for T is obtained when $x_{min} = \frac{y}{\mu_s}$. In this situation is obtained $T_{min} = T(x_{min}) = \frac{\mu_s mg}{\sqrt{1+\mu_s^2}}$.

Thus, $T(x_{min}) = T(\theta_{min})$.

On the other hand, we can find the *two extreme cases* considered in the previous subsection: (i) We obtained that $\lim_{x\to 0} T(x) = mg$. This result is equivalent to $\lim_{\theta\to\frac{\pi}{2}} T(\theta)$; (ii) Furthermore $\lim_{x\to\infty} T(x) = \mu_s mg$. This situation agrees with $\lim_{\theta\to 0} T(\theta)$.

Now we are going to find the condition that must satisfy the horizontal positions x_1 and x_2 that yield $T(x_1) = T(x_2)$. We obtain this relation in three different forms:

- *First:* From equation 11 is obtained

$$\left(T^2 - g^2m^2\mu_s^2\right)x^2 + 2T^2y\mu_s x + \left(T^2 - g^2m^2\right)y^2\mu_s^2 = 0, \tag{12}$$

Resolving this quadratic equation in x, we get

$$x_1 = \frac{-T^2y\mu_s + gmy\mu_s\sqrt{T^2\mu_s^2 + T^2 - g^2m^2\mu_s^2}}{T^2 - g^2m^2\mu_s^2} \tag{13}$$

$$x_2 = \frac{-T^2y\mu_s - gmy\mu_s\sqrt{T^2\mu_s^2 + T^2 - g^2m^2\mu_s^2}}{T^2 - g^2m^2\mu_s^2}. \tag{14}$$

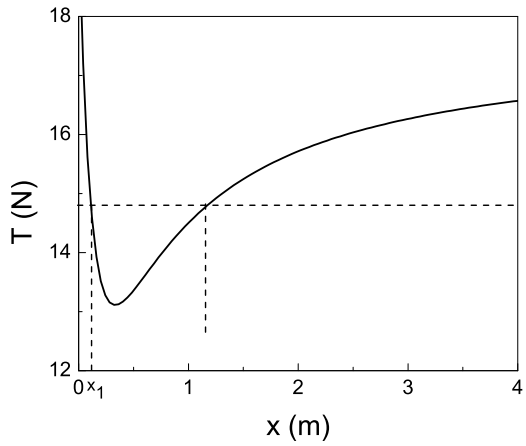

Figura 7. Tension T as function of x, with $m = 2$ kg, $y = 0.3$ m and $\mu_s = 0.9$.

The sum of these roots is

$$x_1 + x_2 = \frac{2T^2 y\mu_s}{g^2 m^2 \mu_s^2 - T^2}. \tag{15}$$

From this equation, x_2 can be obtained knowing x_1, the tension T, the coefficient of static friction μ_s and the vertical distance y.

- *Second:* From Figure 6 we can build Figure 8 and after applying the Law of Sines to obtain:

$$\frac{\sin\theta_1}{\sqrt{x_2^2 + y^2}} = \frac{\sin\theta_2}{\sqrt{x_1^2 + y^2}}, \tag{16}$$

or

$$x_1^2 \sin^2\theta_1 - x_2^2 \sin^2\theta_2 = y^2\left(\sin^2\theta_2 - \sin^2\theta_1\right). \tag{17}$$

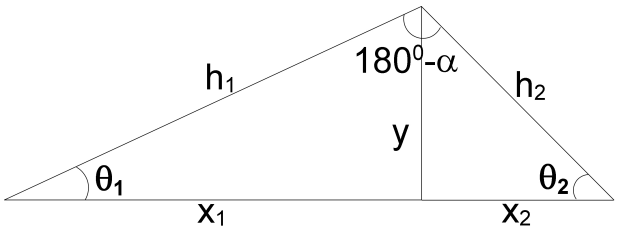

Figura 8. Reinterpretation of Figure 6.

Using the trigonometric identity $\sin^2(A) - \sin^2(B) = \sin(A+B)\sin(A-B)$, it is obtained

$$x_1^2 \sin^2\theta_1 - x_2^2 \sin^2\theta_2 = y^2 \sin(\theta_1+\theta_2)\sin(\theta_1-\theta_2) \tag{18}$$

or

$$x_1^2 \sin^2\theta_1 - x_2^2 \sin^2\theta_2 = y^2 \sin(2\theta_{min})\sin(\theta_1-\theta_2). \tag{19}$$

From this equation, we can obtained x_2 knowing x_1 and the angles θ_{min} and θ_1.

- *Third:* If $x_2 = kx_1$, $k \in \Re^+$: using $\tan\theta_1 = \frac{y}{x_1}$, $\tan\theta_2 = \frac{y}{x_2}$ in the trigonometric identity

$$\tan(\theta_1+\theta_2) = \frac{\tan\theta_1 + \tan\theta_2}{1 - \tan\theta_1\tan\theta_2}, \tag{20}$$

the following quadratic equation in x_1 is obtained:

$$k\tan(2\theta_{min})\,x_1^2 - y(k+1)\,x_1 - y^2\tan(2\theta_{min}) = 0,$$

which has the physical solution

$$x_1 = y\left(\frac{(k+1) + \sqrt{(k+1)^2 + 4k\tan^2(2\theta_{min})}}{2k\tan(2\theta_{min})}\right). \tag{21}$$

From this equation, it can be obtained x_1 for a given k and knowing the vertical distance y and the θ_{min} angle.

IV. CONCLUSIONS

We examined the static equilibrium problem of a block of mass m on a plane being pulled at an angle θ with the horizontal by a tension due to a suspended mass M from a pulley. We performed a complete analysis to the expression for the tension of the string, T, when the system is at static equilibrium. We found two different configurations with equal tension showing certain kind of symmetry, and showed that there are two extreme cases that can be related with the Atwood's machine and the system conformed by one mass on an horizontal surface connected with another mass suspended vertically from a pulley.

First, we analyzed the tension T in function of the angle θ. We found (except for $\theta_{min} = \tan^{-1}(\mu_s)$, where μ_s is the coefficient of static friction) that for each angle θ_1 there is another configuration of static equilibrium given by the angle θ_2 so that $T(\theta_1) = T(\theta_2)$ with the condition $\theta_1 + \theta_2 = 2tan^{-1}\mu_s = 2\theta_{min}$. Second, we analyzed, in a similar way, the tension T in function of the horizontal distance x. Again, we obtained that there are two horizontal distances x_1 and x_2 that give a configuration of the static equilibrium such that $T(x_1) = T(x_2)$. The condition that must satisfy x_1 and x_2 is given, in three different forms, by means of the equations 15 and (21). According to our knowledge, these results have not yet been published.

Additionally, we did a nice laboratory exercise in order to check experimentally the equation 1. The analysis carried out in this work is an important didactic tool that allows to articulate physics and mathematics, and theory with experiment, contributing to improve the learning of physics.

In this work we used simple and elementary mathematical tools as trigonometric identities and minima of a function, the free software Geogebra and the computer program Origin. Our results can be incorporated as additional questions to this problem in fundamental physics textbooks and introductory-level physics courses, and may help teachers to produce meaningful learning when teaching required, at the same time, the application of both trigonometric and statics.

ACKNOWLEDGMENTS

The authors acknowledgment to Juan Carlos Otavo for his collaboration in the experimental arrangement.

REFERENCES

[1] R. A. Serway and J. W. Jewett, Physics for Scientists and Engineers vol. 1, 9th ed, Cengage Learning, 2014, p. 148.
[2] F. A. González and M. Martínez Hernández, Problemas de física general, 1st ed, Tebar Florez, 1978, p.45.
[3] H. C. Ohanian and J. T. Markert, Physics for Engineers and Scientists, 3rd ed, W. W. Norton Company, 2009, p. 196.
[4] R. C. Hibbeler, Engineering Mechanics - Dynamics, 12th ed., Prentice Hall, 2010, p. 86.
[5] W. F. Riley and L. D. Sturges, Ingeniería mecánica: dinámica, 1st ed, Reverté, 1996, p.186.
[6] N. Lerman, Am. J. Phys. **32**, 927 (1964).
[7] S. Mak, Am. J. Phys. **55**, 929 (1987).
[8] D. Sutt, Phys. Edu. **29**, 249 (1994).
[9] W. H. van den Berg, Phys. Teach. **38**, 506 (2000).
[10] W. J. Leonard, Phys. Teach. **39**, 421 (2001).
[11] A. Franco García, [Online]. El mejor ángulo para arrastrar un bloque, (2016, May 1) Available: http://www.sc.ehu.es/sbweb/fisica3/dinamica/arrastra/arrastra.html
[12] https://www.leybold-shop.com/physics/physics-equipment/mechanics/dynamics-and-kinematics/air-track/air-track-337501.html
[13] https://www.amazon.co.uk/Skyeye-Digital-Handheld-Suitcases-Dynamometer/dp/B076FMHFQC
[14] https://apkpure.com/es/angle-meter-pro/iyok.com.anglemeterpro

STABILITY OF A NATURAL PALYGORSKITE AFTER A CYCLE OF ADSORPTION-DESORPTION OF AN EMERGING POLLUTANT

ESTABILIDAD DE UNA PALYGORSKITA NATURAL DESPUÉS DE UN CICLO DE ADSORCIÓN-DESORCIÓN DE UN CONTAMINANTE EMERGENTE

D. Hernández[a], L. Quiñones[a], C. Charnay[b], M. Velázquez[c], A. Rivera[a†]

a) Institute of Materials Science and Technology (IMRE), University of Havana, Havana, Cuba; aramis@imre.uh.cu†
b) Institut Charles Gerhardt Montpellier (ICGM), Université Montpellier, France
c) Research Center for Mining Metallurgy Industries (CIPIMM), La Havana, Cuba
† corresponding author

Recibido 15/10/2019; Aceptado 20/11/2019

PACS: Porous materials (materiales porosos), 78.55.Mb; Organic-inorganic hybrid nanostructures (nanoestructuras híbridas orgánicas-inorgánicas), 81.07.Pr; Environmental safety (seguridad medioambiental), 89.60.Ec; X-ray diffraction (difracción de rayos X), 61.05.cp.

The use of different types of supports for organic species adsorption [1, 2] in environmental applications is vital for decontamination. Special attention is given to naturals materials with adsorptive properties [3–6]. However, even when many authors work on the adsorption of organic pollutants by natural matrices, it is not common to investigate the physical and chemical properties of the matrices after being submitted to an adsorption-desorption cycle. The main motivation of this paper is to evaluate the structural stability of the natural clay palygorskite–an adsorbent of organic contaminants–after an adsorption–desorption process.

Natural Cuban clay type Palygorskite (*Pal*) is an excellent adsorbent of organic molecules [7]. It is a fibrous clay with structure 2 : 1 formed by tetrahedral silica sheets (SiO_4^{4-}) periodically inverted with respect to the tetrahedral bases leading to an interruption in the octahedral sheets ($AlO_3(OH)_3^{6-}$), and the formation of an open-channel structure [5, 8, 9]. Three water types are present in the structure (zeolitic, coordinated and structural water [10,11]), as well as exchangeable cations in the tunnels. From previous work [12] it is known that Pal acts like an effective adsorbent of sulfamethoxazole (SMX) at acid pH, room temperature and an initial concentration of 3 mg/mL. This drugs is classified as emerging contaminant, i.e., chemical species of common used present in water resources which have the potential to cause adverse ecological and (or) human health effects [13].

In order to demonstrate the possibility to reuse the Pal support in adsorption-desorption cycles, the material resulting of the desorption process (labeled as Pal DE) was characterized by X-ray diffraction (XRD), attenuated total reflection (ATR) infrared spectroscopy and zeta potential (ZP). The X-ray diffraction (XRD) experiments for the samples Pal and Pal DE were conducted on a Philips Xpert diffractometer, using Cu−Kα radiation (λ = 1.54 å) at room temperature for a range from 4 to 70°. ATR spectra were collected using a Perkin Elmer UATR Two FTIR Spectrometer in the range of 400 − 4000 cm^{-1}. The surface charge of clay particles was evaluated using a zeta potential analyzer (Malvern Zetasizer Nano NS Instrument). For the analysis, 1 mg of the samples (Pal or Pal DE) was dispersed fully in 2 mL of a deionized water suspension at different pH under ultrasonic stirring for 15 min. The measurements were made in triplicate and the averages were calculated.

As can be observed in figure 1, the main mineralogical phase present in the raw sample (*Pal*) and that resulting from desorption study (*Pal DE*) was palygorskite (*P*). Other mineral phases, montmorillonite (*Mt*) and quartz (*Q*), were also identified [14], which could be considered like spurious phases.

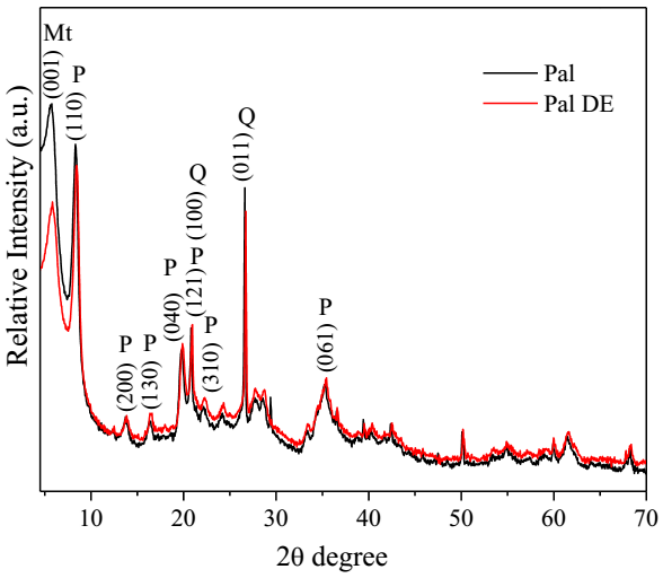

Figure 1. Diffraction patterns for Pal and Pal DE samples.

In the literature, the comparison between experimental and theoretical powder XRD patterns has allowed to note that most palygorskite samples are mixtures of

both monoclinic and orthorhombic polymorphs [15, 16]. Reflections corresponding to d-spacings between 4.0 and 4.5 å, called "Chisholm zone" [17], allow to determine if the palygorskite under study is mainly orthorhombic, monoclinic or either a mixture of both phases. However, in natural materials–as the *Pal* sample presented here–the presence in this zone of reflections associated to spurious phases (like quartz phase, *Q*) can difficult this analysis.

In addition, a decrease in the intensity of the 001 basal reflection of the montmorillonite spurious phase was detected in the sample *Pal DE*. This might be due to possible dissolution of the *Mt* spurious phase by the pH action during the SMX adsorption process, which takes place at acid pH (pH≈ 3) [18]. It can produce local changes in the material, which do not imply structural variation in the main phase, the paligorskite [19].

No significant variations were observed in the interplanar distances values of the characteristic diffraction maximums of palygorskite phase between the *Pal* and *Pal DE* samples. It suggests no structural changes in the material after an adsorption-desorption cycle, confirming its long range order stability.

ATR spectra of drug SMX (emerging contaminant from wastewater), the Pal-SMX composite, and the samples *Pal* and *Pal DE* are shown in figure 2. In the *Pal – SMX* spectrum, compared to the raw material (*Pal*), the appearance of signals associated with the presence of the organic molecule can be noted. However, for sample *Pal DE* these signals disappear as result of desorption process. As can be seen in the figure, very similar ATR spectra were obtained for the samples *Pal* and *Pal DE* (see figure 2): no variation in the characteristic bands of the clay were observed indicating the reversibility of the process as well as the possible reuse of the support material.

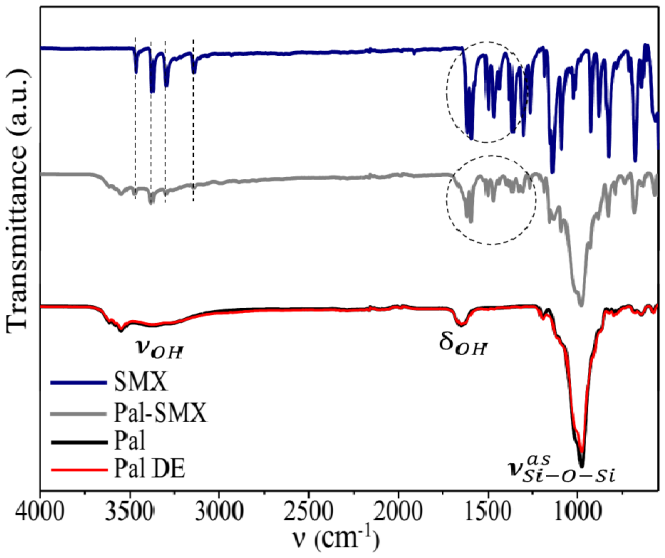

Figure 2. ATR spectra for samples of sulfamethoxazole (SMX), raw material (*Pal*), resulting composite of adsorption process (*Pal – SMX*) and material after the desorption process (*Pal DE*). In dotted lines the signals associated to the emerging pollutant.

Zeta potential results indicated that the surface charge of the samples Pal and Pal DE, before and after of the adsorption-desorption processes, was negative (≈ −25 mV at pH values from 4 to 10). Within the pH range studied, no isoelectric point was observed for both materials. These negative values are associated with dominance of permanent basal charge due to imbalanced isomorphous substitution in tetrahedral and octahedral sheets (for example, Al^{3+} substituting Si^{4+} in the crystal lattice). A similar result has been reported in the literature for 2:1 clays [20, 21]. In the present study, the quantitative and qualitative behavior obtained for both samples was basically the same. It could indicate the material capacity to recover its electrokinetic stability and thus the adsorptive properties, pointing to its potential reuse.

In summary, the different analysis support the hypothesis that the Pal raw material can be reused as an efficient adsorbent of the emerging contaminant SMX, based on the total material integrity and stability after the adsorption-desorption process.

REFERENCES

[1] L. Valdés, S. A. Martín, D. Hernández, L. Lazo, L. C. de Ménorval, and A. Rivera, Rev. Cubana. Fís. **34**, 35 (2017).

[2] D. Hernández, L. Lazo, L. Valdes, L. C. de Ménorval, Z. Rozynek, and A. Rivera, Appl. Clay Sci. **161**, 395 (2018).

[3] J. Akhtar, N. A. S. Amin, and K. Shahzad, Desalin. Water Treat. **57**, 12842 (2016).

[4] K.-L. Chen, L.-C. Liu, and W.-R. Chen, Environ. Pollut. **231**, 1163 (2017).

[5] S. Ismadji, F. Edi, and A. Ayucitra, in Clay materials for environmental remediation, edited by S. K. Sharma (Springer, London, 2015), pp. 5.

[6] M. Leal, V. Martínez-Hernández, R. Meffe, J. Lillo, and I. de Bustamante, Chemosphere 175, 534 (2017).

[7] S. A. Martín, L. Valdés, F. Mérida, L. C. de Ménorval, M. Velázquez, and A. Rivera, Clay Miner. **53**, 193 (2018).

[8] E. Galan, Clay Miner. **31**, 443 (1996).

[9] H. H. Murray, Clay Miner. **34**, 39 (1999).

[10] M. Suárez and E. García-Romero, Appl. Clay Sci. **31**, 154 (2006).

[11] D. A. McKeown, J. E. Post, and E. S. Etz, Clay Miner. **50**, 667 (2002).

[12] L. Quiñones, Tesis de Licenciatura, Universidad de La Habana, 2018.

[13] N. Bolong, A. F. Ismail, M. R. Salim, and T. Matsuura, Desalination **239**, 229 (2009).
[14] Mineralogy Database, http://webmineral.com/ (2019).
[15] J. E. Chisholm, Can. Mineral. **30**, 61 (1992).
[16] J. E. Post and P. J. Heaney, Am. Mineral. **93**, 667 (2008).
[17] J. García-Rivas, M. Sánchez del Río, E. García-Romero, and M. Suárez, Applied Clay Science **148**, 39 (2017).
[18] M. Rozalén, F. J. Huertas, and P. V. Brady, Geochimica et Cosmochimica Acta **73**, 3752 (2009).
[19] V. Gionis, G. H. Kacandes, J. D. Kastritis, and G. D. Chryssikos, American Mineralogist **91**, 1125 (2006).
[20] M. Duc, F. Gaboriaud, and F. Thomas, J. Colloid Interf. Sci. **28**9, 139 (2005).
[21] R. Rusmin, B. Sarkar, B. Biswas, J. Churchman, Y. Liu, and R. Naidu, Appl. Clay Sci. **134**, 95 (2016).

PHYSICAL COSMOLOGY GETS ITS FRECKLES: ABOUT PEEBLES'S NOBEL PRIZE IN PHYSICS 2019

LA COSMOLOGÍA FÍSICA SE HA MOTEADO: SOBRE EL PREMIO NOBEL DE FÍSICA DE PEEBLE EN 2019

C. Escamilla-Rivera†

Instituto de Ciencias Nucleares, Universidad Nacional Autónoma de México, Circuito Exterior C.U., A.P. 70-543, CDMX. 04510, Mexico; celia.escamilla@nucleares.unam.mx
† corresponding author

Recibido 20/5/2019; Aceptado 25/5/2019

PACS: Cosmology (cosmología), 98.80.-k; Background radiations (radiaciones de fondo), 98.70.Vc; Observational cosmology (cosmología de observación), 98.80.Es

I. INTRODUCTION: WHAT DO WE CALL PHYSICAL COSMOLOGY?

Cosmology is the study of the Universe on the largest scales. Up to the 1950s, cosmological data was scarce and generally so inaccurate that the British-Austrian mathematician and cosmologist H. Bondi claimed that if a theory did not agree with data, it was about equally likely the data were wrong [1].

Our current cosmological models are based on the solutions to Einstein General Relativity's equations, making some general assumptions of isotropy and homogeneity, the so-called *Cosmological Principle*, of the Universe at large scales. In other words: the assumptions on which the models are based, were certainly not inspired nor suggested nor even confirmed by the data a century ago. In fact, Einstein's static model was shown to be unstable and so the expansion of the Universe could have been a prediction of the theory; surely it would have ranked as one of the most amazing predictions of the physical world based on pure thought. As it happened, Hubble's observational discovery of the expansion around the same time relegated the models to describing the data. At the 30th Meeting of the International Astronomical Union (IAU), the members of the General Assembly decided by simple majority to support the resolution: "from now on the expansion of the universe [should] be referred to as the Hubble-Lemaître law" [2].

Novel observational techniques have revolutionised cosmology over the past decade. The combined power of galaxy redshift surveys, and Cosmic Microwave Background (CMB) [3] experiments have lead us into the era of *Precision Cosmology*, from where we start to test the theoretical models, and determine their cosmological parameters to percent level. The past years have seen the emergence of a standard model in cosmology, described by around six parameters. Given how recently this has all happened, we certainly need to keep our minds open for surprises, but the degree to which the models agree with the data is simply astonishing: the current cosmological model is based on the believe of a Hot Big Bang from where the observed structures grew, from scale invariant gaussian fluctuations amplified by gravity and presently dominated by dark energy and dark matter. This is called a spatially flat, scale-invariant ΛCDM model, where Λ denotes the cosmological constant (a special case of dark energy), and CDM stands for cold dark matter.

Questions that arise, and have been the chalice for many cosmologists remain: is the ΛCDM model the end of the road? Cosmology is almost unique in the physical sciences, therefore it also demands an answer to the question of why the cosmological parameters have the values they do. Is the Big Bang truly a singularity? What happened before that? Can these questions make sense? Not so long ago, most cosmologists would have mumbled that time was created in the Big Bang, that it makes no sense to talk about things which are in principle unobservable, such as other universes, or anything before this singularity. Yet there is currently a flurry of theoretical activity addressing precisely these issues, but it is not clear how we will distinguish each scenario based on different models. From proving the validity of the ΛCDM model, where factors like tensions phenomena are arising between Planck [4] and other cosmological measurements as: Cefeids (SH0ES), strong lensing time delays (H0LiCOW), tip of the red giant branch (TRGB), Oxygen-rich Miras and surface brightness fluctuations [5], only justify the study of possible alternatives to the ΛCDM model. One of the most interesting approaches seeks for dynamical properties of dark energy, which should be able to mimic Λ at the present time as required by the cosmological observations. Some approaches start from quintessence scenarios [6,7], dark energy parameterisations [8–12], modified gravity [13, 14], extended theories of gravity [15], equations of state $w(z)$ reconstructions [16], non-parametric reconstructions of $w(z)$ [17, 18], to Bayesian reconstruction of a time-dependent $w(t)$ [19] or dynamical w_x from alternative gravity models [20], which represents a large overview on how we are trying to explain the effects of Λ. Furthermore, with the increase of computational techniques, many alternative options have emerged using machine learning techniques [21]. However, a consensus of a unique model is still missing and all

the proposals imply a model dependency which can be significantly different by imposing a different theoretical scenario. Clearly, current and future data from the surveys will certainly clarify all the issues or at least shed some light on them.

All the above work has been possible thanks to original discoveries in the theoretical framework of cosmology over the past century. This year's Nobel Laureate James Peebles has made seminal contributions in this science [22]. Through detailed modelling, with the help of analytic methods, he has explored fundamental properties of our Universe and discovered unexpected new physics. We have now at hand an unified model capable of describing the Universe from its earliest fraction of a second up to the present and into the distant future. Let us take a general look how these ideas were develop.

II. IF EVERYTHING STARTED WITH A BIG BANG...

Our current understanding of the Universe is based upon the successful Hot Big Bang theory, which explains its evolution from the first fraction of a second to our present age, almost 14 billion years later (see Figure 1). This theory rests upon four strong pillars, a theoretical framework based on General Relativity, as was put forward by A. Einstein and A. Friedmann in the 1920s, and three observational facts: first, the expansion of the Universe, discovered by E. Hubble in the 1930s, as a recession of galaxies at a speed proportional to their distance from us. Second, the relative abundance of light elements, explained by G. Gamow in the 1940s, mainly that of helium, deuterium and lithium, which were cooked from the nuclear reactions that took place at around a second to a few minutes after the Big Bang, when the Universe was a few times hotter than the core of the sun. Third, the CMB, the afterglow of the Big Bang, discovered in 1965 by A. Penzias and R. Wilson as a very isotropic blackbody radiation emitted when the Universe was cold enough to form neutral atoms, and photons decoupled from matter, approximately 500 000 years after the Big Bang. Today, these observations are confirmed to within a few percent accuracy, and have helped establish the Hot Big Bang as the preferred model of the universe.

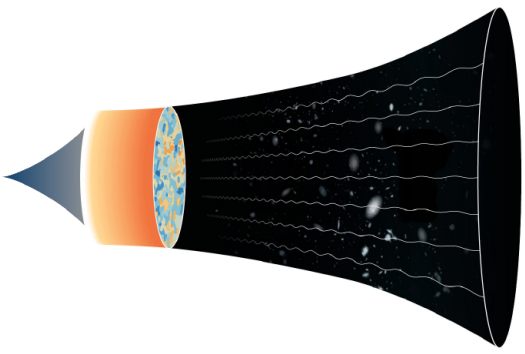

Figure 1. Schematic timeline of our Universe extending from an unknown origin on the left to a darkening future on the right. Figure from [22].

Even today, this CMB ancient radiation is all around us and, coded into it, many of the universe's secrets are hiding. Using his theoretical tools and calculations, J. Peebles was able to interpret these traces from the infancy of the Universe and discover new physical processes.

III. THE COSMOLOGICAL CHALICE: ON HOW TWO QUESTIONS OPEN THE DISCUSSION OF THE CENTURY

If we consistently follow a model where the CMB has an origin in a cosmological Big Bang, then we should be able to observe different values when measured in different directions. This is what we call *anisotropies* – where physical cosmology gets its freckles –, which should indicate deviations of the real Universe with respect to a homogeneous and isotropic idealisation. This is fundamental, since otherwise we would not observe cosmological structure.

Due to our inherent inability to experiment with the universe, its origin and evolution has always been prone to wild speculation. However, Cosmology was born as a science with the advent of General Relativity and the realization that the geometry of space-time, and thus the general attraction of matter, is determined by the energy content of the universe. Therefore, since 1915, the first question that came as a consequence was *where are we in the universe?* An expert in the field starts with Einstein's equations to give an answer to this question,

$$G_{\mu\nu} \equiv R_{\mu\nu} - \frac{1}{2} g_{\mu\nu} R + \Lambda g_{\mu\nu} = 8\pi G T_{\mu\nu}, \tag{1}$$

but let us generalise these non-linear equations as the relationship between the geometry ($G_{\mu\nu}$) of the universe and the matter ($T_{\mu\nu}$) that its contained in it. Around the 1920s, the known (observed) universe extended a few hundreds of parsecs away, to the galaxies in the local group, Andromeda and the Large and Small Magellanic Clouds: the universe looked extremely anisotropic. Nevertheless, both Einstein and Friedmann speculated that the most reasonable symmetry for the Universe at large should be homogeneity at all points, and thus isotropy. It was not until the detection, a few decades later, of the CMB radiation that this important assumption was finally put onto firm experimental ground. So, what is the most general metric satisfying homogeneity and isotropy at large scales? The Friedmann-Robertson-Walker (FRW) metric

$$ds^2 = -dt^2 + a(t)[d\psi^2 + f(\psi) d\Omega^2], \tag{2}$$

where $f(\psi)$ represents a curvature constant K as $f(\psi) = [\sin^2\psi, \psi^2, \sinh^2\psi]$. The dynamics of the metric is contained in one function: the scale factor $a(t)$, which is related to the redshift z of the light that came from others galaxies as $a = 1/(1+z)$. We can also define the Hubble parameter, $H = \dot{a}/a$, where the dot stands for time derivation. If we introduce this metric in Einstein's equations we should verify not only the dynamics, but also the matter content, which is represented by a perfect fluid. The entire dynamic is determined by

$$H^2 = \frac{8\pi G}{3} \sum_i \rho_i + \frac{\Lambda}{3} - \frac{K}{a^2}, \tag{3}$$

where ρ_i is the energy density of each component of matter in the Universe (radiation, baryons, neutrinos, Λ – possibly associated with the vacuum energy of quantum field theory –, etc.) and we can establish whether the universe has a closed ($K = 1$), flat ($K = 0$) or open ($K = -1$) topology. The latter can be written as

$$\Omega_K \equiv \frac{K}{a^2H^2} = \sum_i \Omega_i - 1, \tag{4}$$

where all the density parameters are defined as $\Omega_i = \rho_i/\rho_{\rm crit}$, with $\rho_{\rm crit} = 3H^2/8\pi G$. To illustrate how the evolution of the universe works, we can write (3) as

$$\frac{\dot{a}^2}{2} - \frac{GM}{a} - \frac{\Lambda}{6}a^2 = -\frac{K}{a} = \text{constant}, \tag{5}$$

where $M \equiv 4\pi/3\rho a^3$ is the equivalent of mass for the whole volume of the universe. In other words, (5) can be understood as the energy conservation law $E = T + V$ for a test particle of unit mass in the central potential

$$V(r) = -\frac{GM}{r} + \frac{1}{2}kr^2, \tag{6}$$

which corresponds to a Newtonian potential plus a harmonic oscillator potential with a negative spring constant $k \equiv -\Lambda/3$. On the one hand, we notice that, for vanishing Λ, a critical universe, defined as the division between indefinite expansion and recollapse, corresponds to a flat universe. On the other hand, a spatially open universe corresponds to an eternally expanding universe and for a spatially closed universe to a recollapsing one in the future. Only in a case when $\Lambda \neq 0$, spatially open universes may recollapse while closed universes can expand forever. In Figure 2 we can observe some possible evolutions of the scale factor in a $(\Omega_\Lambda, \Omega_m)$ concordance region.

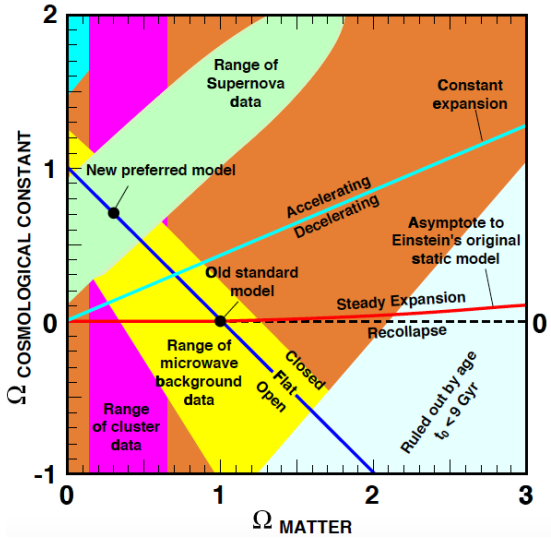

Figure 2. Evolution of a with respect to t for different values of matter and cosmological constant. Color regions stand for the range of observations. The current best cosmological model is a flat scenario with a third of the energy density in the form of non-relativistic matter and two thirds in the form of vacuum energy or a Λ. Figure from [23].

Now we are ready to address the second question that arises as a direct consequence of the general covariance of the theory: the conservation of energy, or *what is the universe made of?* To follow the above discussion, we can write this conservation of energy in terms of the FRW metric and the perfect fluid tensor as

$$\frac{d}{dt}(\rho_i a^3) + p_i \frac{d}{dt}(a^3) = 0, \tag{7}$$

where ρ_i and p_i represent the density and pressure of matter components, respectively. Now, to find an analogy between the above expression and the Second Law of Thermodynamics, $TdS = d(\rho a^3) + pdV$, we observe that (7) implies that the universe is expanding adiabatically ($dS = 0$), therefore the entropy per comoving volume is $S = a^3(\rho_i + p_i)a^3/T$, which is conserved. The consequence of this conservation is that, during the adiabatic expansion of the universe, the scale factor grows as $a \propto T^{-1}$. This implies that in the past the universe must have been much hotter and denser and eventually it would be colder and dilute. Since a can be written in terms of the redshift, we can measure the temperature of the CMB at high redshift as $T = T_0(1+z)$. These measurements have been carried out systematically, however the results do not ensure that the temperature of the CMB has varied as expected [24].

To track the consequences of the above ideas, we should go back in time, when the universe started to become hotter and hotter and thus the amount of energy available for particle interactions increased. At this point, the interactions goes from those described at low energy by gravitational and electromagnetic physics, to atomic physics, nuclear physics till high energy physics at the electroweak scale, followed by a speculative grand unification epoch and finally the not well understood quantum gravity. And here comes Peebles's idea [25]: a connection between temperature and the density of matter. Based on the observed temperature of the Universe, it is possible to constrain the amount of matter that consists of nucleons (baryonic matter), which in the early 1965 observations showed less matter than predicted by Peebles. And the solution is one of the most remarkable achievements in the history of science: observational data matches perfectly the predictions of a theoretical model. The theoretical model presented by Peebles et al. in [26] states: "A critical factor in the formation of galaxies may be present as a black-body radiation content of the universe". In other words, emitted radiation by the early universe (for our purposes, the 'body') should be distributed between the various wavelengths of the electromagnetic spectrum, and the shape of that spectrum depends entirely on temperature. Therefore, if we know the temperature of such a black-body we can precisely predict what the resulting spectrum should look like. Twenty four years after this publication was released, NASA launched the Cosmic Background Explorer (COBE) satellite, and got the first results after a mere nine minutes of observations. The accumulated data points formed a perfect black-body spectrum – the universe is a perfect emitter and absorber of radiation. From this, we were able to measure the fluctuations temperature in the CMB to date 2.726 K, and therefore in which epoch the matter in the universe began to aggregate. The story did not end with COBE. Missions as BOOMERang and Maxima added even more details to the CMB. Later

the WMAP project supplied the best values for such critical cosmological parameters as the actual age of the universe, the curvature of spacetime, and when the first atoms and stars began to form. The Planck 2015 mission, as the successor to COBE and WMAP, reveals a map where dark matter makes up about 26.8 percent of our universe, an increase from the previously measured 24 percent, while normal matter contributes 4.9 percent rather than 4.6 percent. The results also indicated that dark energy constitute 67.9 percent of the universe rather than the 71.4 percent previously estimated [4].

IV. OUR LOPSIDED UNIVERSE

With these results a new window opened in the 1980s, where researchers realised the impact of indications of unknown components of matter in the Universe. In addition, calculations based on an open universe, with a density less than ρ_{crit}, did not predict anisotropies compatible with observations at hand. If the universe had been open, the anisotropies would already have been discovered. Yet there was no sign of them. As an extension, if the density of ordinary matter had been at the critical value, the galaxies we have observed could never have formed. In [27], Peebles proposed a scenario with a non-relativistic cold dark matter in order to couple the anisotropies in the CMB to large-scale structures in the universe. Small as it is, $\delta T(\theta,\phi)/T(\theta,\phi) = 5\times10^{-6}$, but consistent with the measurements given by the COBE. According to the position in the sky, these anisotropies can be written as an expansion of spherical harmonics

$$\delta T(\theta,\phi) = \sum_{l,m} a_l^m Y_{lm}(\theta,\phi), \tag{8}$$

where $\theta = \pi/l$ gives the relationship between the observed angle and the multipole index. The spectrum derived has acoustic peaks as Fourier modes of the primordial plasma (the epoch where the radiation and the baryons were coupled). This spectrum shows the evolution of the amplitude of the nodes until the decoupling time. As a result, we can extract information about the shape of the universe and the matter and energy it contains. According to the Planck 2018 results (see Figure 3), (a) the first peak shows that we live in a universe with a small curvature $\Omega_K = 0.001\pm0.002$. The (b) second peak shows that baryonic matter is just $\Omega_b h^2 = 0.0224\pm0.0001$ of the matter and energy in the universe. The (c) third peak shows that $\Omega_{\rm CDM} = 0.120\pm0.001$, corresponding to dark matter. From these peaks, it is possible to compute the last component to fulfil the requirement for a flat universe, a dark energy with $\Omega_\Lambda = 0.679 \pm 0.013$.

V. OVERVIEW

The essence of *Precision Cosmology* allows us to deepen the explanation of the structure and evolution of the Universe and to discover New Physics. It is a universally acknowledged fact that we still do not understand the physics of the cosmological constant – perhaps its value is not constant – and perhaps a time-varying dark energy plays an important role in the evolution of the Universe. J. Peebles has already contemplated this possibility many years ago – a scientist ahead of his era. The nature of dark matter is not known either. Some interesting explanations include new particles, but until such a new particle is discovered, we cannot be sure that any of the current theoretical explanation of cold dark matter is the right one.

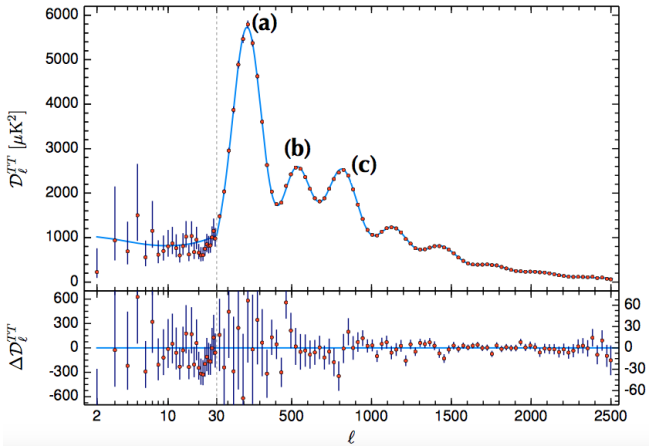

Figure 3. Anisotropies in the temperature of the CMB as measured by the Planck mission. Modified from [4].

The progress on how the theory and observations now fit is notable and there are few cosmological parameters. Still, there are observations that cannot be entirely explained at present and measurements of the Hubble parameter in the late-time Universe do not quite match predictions of CMB physics [28]. This issue perhaps hints to new physics that is hiding somewhere. As the measurements become more precise, new and unexpected phenomena are likely to be discovered, therefore *Physical Cosmology* will have unexpected things on the front, and J. Peebles is the one who has shown us the path to discover them. As his Shaw Prize citation states "He laid the foundations for almost all modern investigations in cosmology, both theoretical and observational, transforming a highly speculative field into a precision science".

ACKNOWLEDGMENTS

CE-R thanks M. Alcubierre and W. Bietenholz for their interesting comments on the manuscript. This work is supported by the Royal Astronomical Society as FRAS 10147, PAPIIT Project IA100220 and ICN-UNAM projects.

REFERENCES

[1] Oral History interview transcript with Hermann Bondi 1978-03-20, American Institute of Physics, Niels Bohr Library and Archives. American Institute of Physics.

[2] `https://www.iau.org/static/archives/announcements/pdf/ann18029e.pdf` Accessed 12.12.2019.

[3] T. Matos and L. Ureña. La Radiación Cósmica de Fondo. Colofón Ed. Académicas. IAC. 2019.

[4] N. Aghanim *et al.* [Planck Collaboration], arXiv:1807.06209 [astro-ph.CO].
[5] L. Verde, T. Treu and A. G. Riess, arXiv:1907.10625 [astro-ph.CO].
[6] B. Ratra and P. J. E. Peebles, Phys. Rev. D **37**, 3406 (1988).
[7] C. Armendariz-Picon, V. F. Mukhanov and P. J. Steinhardt, Phys. Rev. Lett. **85**, 4438 (2000).
[8] I. Sendra and R. Lazkoz, Mon. Not. Roy. Astron. Soc. **422**, 776 (2012).
[9] G. B. Zhao, D. Bacon, R. Maartens, M. Santos and A. Raccanelli, arXiv:1501.03840 [astro-ph.CO].
[10] C. Escamilla-Rivera, Galaxies **4**, no. 3, 8 (2016).
[11] M. Rezaei, M. Malekjani, S. Basilakos, A. Mehrabi and D. F. Mota, Astrophys. J. **843**, 65 (2017).
[12] C. Escamilla-Rivera and S. Capozziello, Int. J. Mod. Phys. D (2019).
[13] L. G. Jaime, L. Patiño and M. Salgado, Phys. Rev. D **89**, 084010 (2014).
[14] R. Lazkoz, M. Ortiz-Baños and V. Salzano, Eur. Phys. J. C **78**, 213 (2018).
[15] T. Harko and F. S. N. Lobo, Int. J. Mod. Phys. D **21**, 1242019 (2012).
[16] J. Alberto Vazquez, M. Bridges, M. P. Hobson and A. N. Lasenby, JCAP **1209**, 020 (2012).
[17] M. Seikel, C. Clarkson and M. Smith, JCAP06 (2012).
[18] A. Montiel, R. Lazkoz, I. Sendra, C. Escamilla-Rivera and V. Salzano, Phys. Rev. D **89**, 043007 (2014).
[19] G. B. Zhao *et al.*, Nat. Astron. **1**, 627 (2017).
[20] L. G. Jaime, M. Jaber and C. Escamilla-Rivera, Phys. Rev. D **98**, 083530 (2018).
[21] C. Escamilla-Rivera, M. A. C. Quintero and S. Capozziello, arXiv:1910.02788 [astro-ph.CO].
[22] `https://www.nobelprize.org/prizes/physics/2019/press-release/` Accessed 12.12.2019.
[23] J. Garcia-Bellido, Phil. Trans. Roy. Soc. Lond. A **357**, 3237 (1999).
[24] M. Lopez-Corredoira, astro-ph/0310214.
[25] (a) P.J.E. Peebles, Phys. Rev. Lett. **16**, 410 (1966). (b) P.J.E. Peebles, Astrophys. J. **146**, 542 (1966).
[26] R.H. Dicke, P.J.E. Peebles, P.G. Roll and D.T. Wilkinson, Cosmic black-body radiation, Astrophys. J. **142**, 414 (1965).
[27] P.J.E. Peebles, Astrophys. J. **263**, L1 (1982).
[28] E. Di Valentino, A. Melchiorri and J. Silk, Nat. Astron. (2019), doi:10.1038/s41550-019-0906-9.

FINDING NEW WORLDS: DIDIER QUELOZ AND MICHEL MAYOR'S NOBEL PRIZE IN PHYSICS 2019

ENCONTRANDO NUEVOS MUNDOS: LOS PREMIOS NOBEL DE FÍSICA 2019 DE DIDIER QUELOZ Y MICHEL MAYOR

R. CÁRDENAS†

Planetary Science Laboratory, Universidad Central "Marta Abreu" de Las Villas, Santa Clara, Cuba; rcardenas@uclv.edu.cu†
† corresponding author

Recibido 20/11/2019; Aceptado 23/11/2019

PACS: Astrometry (astrometría), 95.10.Jk; Instrumentation (instrumentación), 95.55.Br; Astrobiology (astrobiología), 91.62.Fc, 96.55.+z

I. INTRODUCTION

Since ancient times, humans have speculated on the potential existence of other Solar Systems, with planets orbiting a parent star [1, 2]. In 1952 a method based on the measurement of stellar radial velocities was proposed to detect exoplanets [3]. However, formidable technical challenges remained a major obstacle for several decades. In 1992 –40 years later– the first observational detection of exoplanets was reported by astronomers Aleksander Wolszczan and Dale Frail [4]. Using the Arecibo radio telescope, they detected two giant planets orbiting the pulsar PSR B1257+12 in the constellation of Virgo. Many astronomers were surprised, as they expected to find such planets only around main sequence stars.

II. THE METHOD OF STELLAR RADIAL VELOCITIES TO DETECT EXOPLANETS

As mentioned above, the first method to detect exoplanets was based on the measurement of stellar radial velocities. A star and its exoplanet revolve around the centre of mass of the system (the barycenter), as illustrated in Figure 1.

Due to the Doppler effect, an observer on Earth will receive blue-shifted light when the star is moving towards him (or her), and red-shifted light when the star is moving away from him (or her). Including relativistic effects, the redshift z can be calculated as,

$$z = \frac{\lambda_0 - \lambda}{\lambda_s} = \sqrt{\frac{1+\beta}{1-\beta}} - 1, \tag{1}$$

where λ_0 is the wavelength detected by the observer on Earth and λ_s is the wavelength in the reference frame of the star, and the parameter β is defined as:

$$\beta = \frac{V}{c}, \tag{2}$$

where V is the radial velocity of the star relative to the observer on Earth (taken positive if the star is receeding, and negative if it is approaching), and c is the speed of light in vacuum. For the non-relativistic limit, it can be shown that,

$$z \sim \beta = \frac{V}{c}, \tag{3}$$

which is the classical expression for the radial redshift caused by Doppler effect (we note that motion in the transverse direction causes the so called transverse Doppler effect, so far of little or no use for exoplanet detection).

As follows from equations 1 and 2, measuring z would allow calculating V, the velocity of the star. However, this is strictly true only if the stars woobles in the line of sight of the observer on Earth, so the inclination i of the planet's orbit respect to the line perpendicular to the line-of-sight should be considered:

$$V = \frac{V_D}{\sin i}, \tag{4}$$

where V_D is the observed (Doppler) velocity of the star. Also, the period of motion of the star can be determined using Doppler spectroscopy, while its mass is typically determined using the well-known mass-luminosity relationship. Once the stellar properties are determined (radial speed V, period T and mass M), it is possible to determine some properties of the exoplanet.

First we may apply the third Kepler's law (the square of the orbital period T of a planet is directly proportional to the cube of the semi-major axis of its orbit r):

$$r^3 = \frac{GM}{4\pi^2} T^2, \tag{5}$$

where G is the gravitational constant and, as both periods are equal, in 5 it is used the observed period of the star, T. Having determined r, the velocity of the planet v around the star can be calculated using Newton's law of gravitation and the orbit equation:

$$v = \sqrt{\frac{GM}{r}}. \tag{6}$$

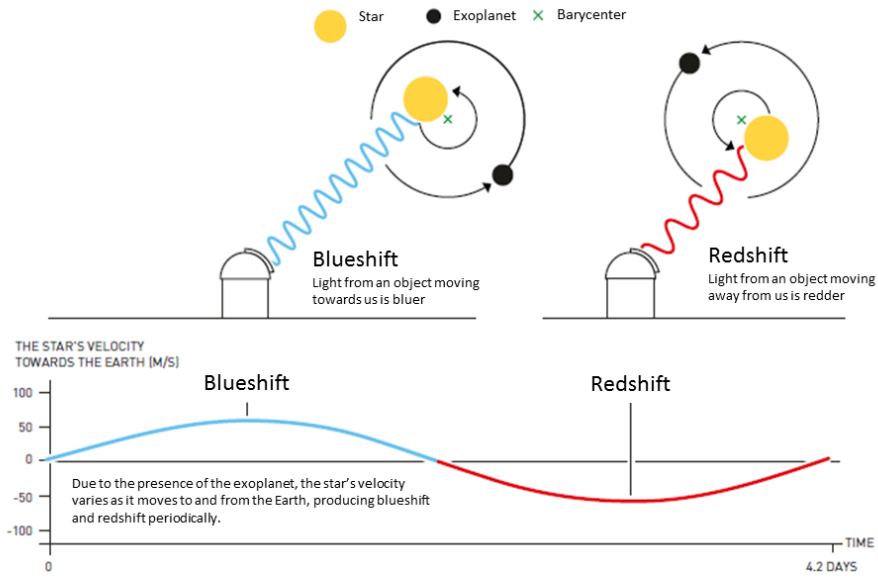

Figure 1. Use of the Doppler effect to estimate the radial velocity of a star, as seen from Earth. Figure modified from [5].

Then, application of the conservation of linear momentum allows determining the mass m of the planet:

$$m = \sqrt{\frac{MV}{v}}. \tag{7}$$

There are other methods to detect exoplanets. For instance, Transit Photometry, which uses the decrease of the intensity of star's light when the planet passes through the line of sight of an observer from Earth. Also Gravitational Lensing and other more recent methods [5].

III. A NEW EPOCH IN EXOPLANET DETECTION

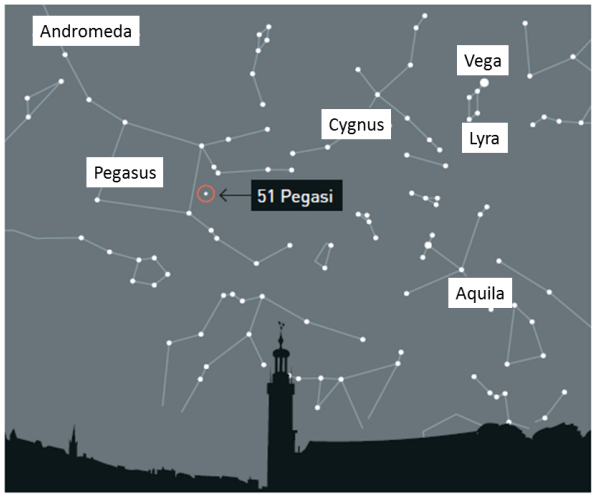

Figure 2. Position of 51 Pegasi b, the first exoplanet detected orbiting a main sequence star. The sketch represents the sky over Stockholm in October. Figure adapted from [5].

Someone monitoring our Solar System would observe a radial velocity change of ±13 m/s of the Sun over 12 years due to the orbital motion of Jupiter [1]. Of course, this tiny variation imposes a severe challenge from the observational point of view.

Michel Mayor at the University of Geneva, André Baranne from the Marseilles Observatory and collaborators designed a new echelle spectrograph: the ELODIE instrument [6, 7]. Using it on a sample of 142 stars, and surveying around 5000 spectral lines for Doppler spectroscopy, they found that the radial velocity of the star 51 Pegasi (in the Pegasus constellation), had variations with a period of about four days (see Figure 2). In 1995 Didier Queloz and Michel Mayor announced the discovery of 51 Pegasi b, the first detected exoplanet orbiting a main sequence star [8]. Because of this breakthrough discovery, they have been awarded the Nobel Prize in Physics 2019 (shared with Jim Peebles for theoretical findings in Cosmology; see the corresponding article in this issue).

IV. IMPLICATIONS FOR ASTROBIOLOGY

The first announcement of a confirmed exoplanet [4] was taken with caution by the Astrophysics community: several previous claims of discovery had been later rejected because of experimental noise. Additionally, theory predicted only a very small fraction of planets orbiting a pulsar (which has been confirmed late on). Thus, the discovery of Michel Mayor and Didier Queloz of the first exoplanet orbiting a Sun-like star opened a new door in Astrophysics and Astrobiology. Five years after the discovery, when the first review "post–51 Pegasi" appeared, 34 exoplanets had been discovered orbiting

Sun-like stars [1, 2], and as of 7 November 2019, there are 4093 confirmed exoplanets, and more than 3000 expecting for confirmation [9].

An inmediate question arose: are exoplanets habitable? It motivated a closer link between astrobiologists, planetary scientists and environmentalists. It also contributed to further development of the quantification of habitability, with three (complementary) approaches: the astrobiological one, the biogeochemical one and the ecological one. Based on metrics of quantitative habitability, there exists a catalog of potentially habitable exoplanets, maintained by the Laboratory of Planetary Habitability of the University of Puerto Rico at Arecibo [10]. So far, it acknowledges 55 potentially habitable exoplanets using climatological criteria, especially the possibility of having liquid water at the planetary surface [11]. However, it should be noticed that, in our planet, it is estimated that the subsurface biosphere is comparable in mass and volume to the surface one, a fact that multiplies the possibilities of existence of living entities in other planetary bodies. Of special interest is the so-called chemolitoautotrophic life, which uses chemosynthesis instead of photosynthesis to fuel its metabolism, being independent of the availability of sunlight. Therefore, at the Planetary Science Laboratory of Universidad Central "Marta Abreu" (Santa Clara, Cuba), habitability metrics for chemolitoautotrophic life are being developed [12].

V. NAMING EXOPLANETS

The frequent discovery of exoplanets has promoted campaigns to name them [13], led by the International Astronomical Union (IAU). In Cuba, a commission of 5 scientists is working to name the star BD-17 63 (an orange dwarf star) and its exoplanet BD-17 63 b. This system is located at the constellation Cetus (the Whale) and, as ruled by IAU, is visible from Cuba, the naming country.

VI. CONCLUSIONS

The breaktrough Discovery of Didier Queloz and Michel Mayor changed forever our points of views concerning our place in this vast Universe. In particular, the possibility of life in some of these "strange new worlds" has motivated a revolution in Astrophysics and Astrobiology, implying collaborations between astrobiologists and environmentalists [12, 14–16].

ACKNOWLEDGEMENTS

R. Cárdenas and E. Altshuler acknowledge the revision of this manuscript by Nobel laureate M. Mayor.

REFERENCES

[1] The Nobel Committee for Physics, Scientific Background on the Nobel Prize in Physics 2019 (2019).
[2] M.A.C. Perryman, Rep. Progr. Phys. **63**, 1209 (2000)
[3] O. Struve, Observatory **72**, 199 (1952)
[4] A. Wolszczan and D. A. Frail, Nature **355**, 145 (1992)
[5] https://en.wikipedia.org/wiki/Exoplanetology#Indirect%20methods Accessed 12.12.2019.
[6] Joanna Rose, Popular Science Background on the Nobel Prize in Physics 2019 (2019)
[7] A. Baranne, D. Queloz, M. Mayor, G. Adrianzyk, G. Knispel, D. Kohler, D. Lacroix, J.-P. Meunier, G. Rimbaud and A. Vin, Astron. Astrophys. Suppl. Ser. **119**, 373 (1996)
[8] M. Mayor and D. Queloz, Nature **378**, 355 (1995)
[9] https://en.wikipedia.org/wiki/Lists_of_exoplanets Accessed 12.12.2019.
[10] http://phl.upr.edu/projects/habitable-exoplanets-catalog
[11] R. Kopparapu, R. Ramirez, J. Schotel, J. Kasting, S. Domagal, V. Eimet, Astrophys. J. Lett. **787**, L29 (2014)
[12] R. Cárdenas, D. Avila-Alonso, N. Pérez-Díaz, O. Martin-González, R. Nodarse-Zulueta, On the quantification of habitability: current approaches, Proceedings of the 2nd International Conference on BioGeoSciences - Modeling Natural Environments, (Springer-Nature, 2019), pp 1-8
[13] https://www.iau.org/public/themes/naming_exoplanets/
[14] A. Méndez, The First Billion Years: Habitability 2019, https://www.hou.usra.edu/meetings/habitability2019/pdf/1033.pdf (2019) Accessed 12.12.2019.
[15] M. López-Águila, R. Cárdenas-Ortiz, L. Rodríguez -López, Rev. Cubana Fis. **30**, 77 (2013)
[16] A. González, R. Cárdenas-Ortiz and J. Hearnshaw, Rev. Cubana Fis. **30**, 81 (2013)

DE CÓMO LAS VENTANAS PUEDEN SER INTELIGENTES: TERMOCROMISMO APLICADO

ABOUT HOW WINDOWS BECOME SMART: APPLIED THERMOCHROMISM

A. A. Iribarren Alfonso, Y. Agustín, J. Rodríguez González-Elipe†

a) Instituto de Ciencia y Tecnología de Materiales, Universidad de La Habana, La Habana; augusto@imre.uh.cu†
b) Instituto de Ciencia de Materiales de Sevilla (CSIC-Univ. Sevilla), España
† autor para la correspondencia

Recibido 25/10/2019; Aceptado 5/11/2019

PACS: Optical coatings (revestimientos ópticos), 42.79.Wc; Thermo-optic effects (efectos termo-ópticos), 78.20.N-; Optical constants (constantes ópticas), 78.20.Ci; Day lighting/natural lighting of buildings (iluminación diurna / iluminación natural de edificios), 88.40.mx

I. INTRODUCCIÓN

Las construcciones y mantener el confort de quienes permanecen en ellas consumen enormes cantidades de energía para mantener iluminación, ambiente y temperatura adecuada [1]. Ese consumo de energía crece continuamente en el sector comercial y residencial y en algunos países ha superado a los gastos de energía de sectores como el de transporte y hasta el industrial y se ha estimado que consumen un tercio de la energía total consumida [2]. Por otra parte, no puede olvidarse el consumo energético por climatización, o sea, refrigeración, calefacción y ventilación. El consumo de energía eléctrica en los sectores comercial y residencial es de alrededor de la mitad del consumo de energía eléctrica mundial, solo superados por el sector industrial [3]. Cuantitativamente se ha estimado que la iluminación artificial consume aproximadamente el 20 % de la electricidad en el mundo lo que representa alrededor del 6 % del consumo mundial de energía. El gasto en climatización de edificaciones representa dos tercios de lo que estos consumen [4–6] y eso representa alrededor del 22 % del consumo mundial total y seguirá aumentando [4]. Todo esto en medio de las crisis que se avecinan más agudas por la escasez de los combustibles fósiles y el calentamiento global entre otros daños que la civilización actual propicia.

Una forma de reducir algo los gastos de climatización es la construcción con materiales termoaislantes que disminuyen las transferencias indeseables de energía térmica desde y hacia el exterior de las edificaciones. Esto se explica a partir de que luego de alcanzar la temperatura de confort deseada, las bajas fugas térmicas permiten mantener el confort con poco gasto de energía. Estas soluciones, lamentablemente, son opacas, o sea, bloquean el paso de la luz solar. Así hay que tener en cuenta otro aspecto que conspira contra el ahorro o disminución general del gasto energético que es la iluminación necesaria en el interior de las edificaciones. Aparte del posible uso de iluminación artificial a la que estamos habituados se recomienda el uso de la iluminación natural, o sea, la proveniente del sol que de hecho posee todos los componentes de la luz visible necesarios para un confort visual dado el hecho de que el propio ser humano evolucionó en medio de este mismo flujo luminoso. Sin embargo, el flujo luminoso solar que llega a la superficie terrestre (Fig. 1), además del casi 45 % de la deseable luz visible, posee aproximadamente un 6 % de luz ultravioleta (UV) y casi el 50 % de luz infrarroja (IR). La componente ultravioleta, invisible a nuestros ojos, que es la radiación de menor longitud de onda o mayor energía es perjudicial a la piel humana, pero puede ser absorbida por el vidrio de una ventana común.

La componente infrarroja, también invisible, con longitud de onda larga, puede transferir grandes cantidades de calor al interior a través de las ventanas comunes, pues son fotones de baja energía que al ser absorbidos por los objetos ocasionan calentamiento y elevan su temperatura contribuyendo al calentamiento general del espacio en que se encuentra. Para regiones frías puede ser beneficioso, pero en las cálidas llega a ser agobiante.

Para controlar la luz solar y disminuir la transferencia térmica a interiores se han utilizado diversas variantes convencionales como quiebrasoles, cortinas, recubrimientos simples y múltiples, colorantes, fotodispersores y otras variantes y mecanismos. Sin embargo, estas soluciones que básicamente clasifican dentro de las estáticas, resuelven parcialmente el problema térmico, pero afectan la iluminación, como también pueden ser caras o poco prácticas, por lo que no resultan óptimas. Actualmente, además, existe la tendencia a utilizar grandes ventanas y elementos transparentes y translúcidos en fachadas y hasta en techos de las construcciones que impone la creación de soluciones eficientes que mejoren el confort visual y el térmico a la vez que no impliquen aumentos en gastos de energía. En el presente trabajo se da una panorámica sobre las ventanas inteligentes y sus características generales así como que refleja las motivaciones que han llevado a enfocar investigaciones y colaboración científica en este tema por diversos grupos de investigación incluidos los de los

autores.

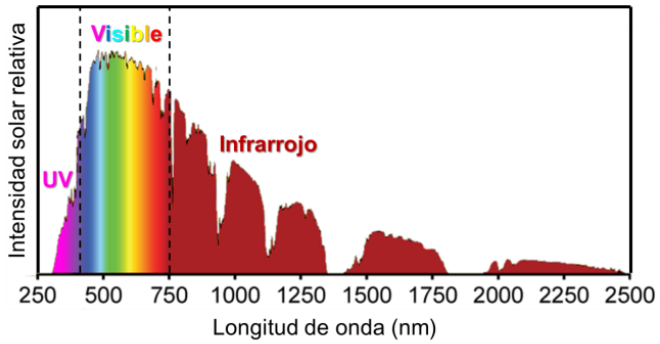

Figura 1. Espectro de intensidad relativa de la radiación solar que llega a la superficie de la Tierra.

II. VENTANA "IDEAL"

En la actualidad se desarrollan trabajos de investigación que persiguen el desarrollo de una ventana ideal mediante la aplicación de tecnologías novedosas no convencionales capaces de ahorrar energía y, simultáneamente, aumentar el confort ambiental de manera más eficiente que las variantes convencionales [7]. Una ventana ideal debe ajustar su diseño y función al clima donde se utiliza. En un lugar cálido, sería muy conveniente que este elemento constructivo permita la entrada de luz visible a los espacios interiores, pero refleje la luz infrarroja exterior sin absorberla. En lugares fríos, sería conveniente que este elemento constructivo permita pasar la luz natural, incluida la radiación infrarroja, desde el exterior. En ambos casos este elemento constructivo debe ser térmicamente aislante para evitar la transmisión de calor en uno u otro sentido.

Son muchos los materiales, orgánicos e inorgánicos, y tecnologías que se utilizan para lograr diversas funciones en las ventanas, incluyendo las de disminuir o retener la radiación infrarroja que entra en un local o reducir el exceso de iluminación y deslumbramiento entre otros objetivos. En el presente trabajo nos referiremos al desarrollo de ventanas que utilizan vidrios con recubrimientos avanzados cuyas características cambian de manera autónoma cuando lo hacen las condiciones ambientales.

III. VENTANAS INTELIGENTES

El flujo de radiación solar varía durante el día, de forma que para lograr el confort deseado se impone el uso de elementos constructivos que, aunque permitan siempre el paso de la luz visible, varíen selectiva y convenientemente la transmisión y la reflexión de la luz de las regiones ultravioleta e infrarroja. Se ha acuñado el término de ventanas inteligentes (smart windows en inglés) para designar las tecnologías capaces de controlar la cantidad y tipo de radiación que penetra en los edificios a través de ventanas y cubiertas transparentes. Las tecnologías típicas usadas en las ventanas inteligentes están basadas en recubrimientos [8] y se clasifican en:

(a) Tecnologías bajo-emisivas basadas en recubrimientos que filtran la radiación infrarroja. Sin embargo, son pasivos e invariables frente a cambios en las condiciones ambientales.

(b) Tecnologías fotocrómicas basadas en recubrimientos que se oscurecen automáticamente al ser irradiados con luz de alta energía, generalmente ultravioleta. Su eficacia depende de la intensidad de esta radiación y no son fáciles de aplicar a grandes superficies.

(c) Tecnologías termocrómicas basada en recubrimientos que se oscurecen automáticamente, cambian de color o reflejan la radiación infrarroja al alcanzar determinada temperatura.

(d) Tecnologías electrocrómicas basadas en materiales que se oscurecen, cambian de color o aumentan la reflexión en todo el rango espectral mediante la aplicación de polarización eléctrica. Para su funcionamiento requieren de capas que actúen como electrodos y electrolitos, por lo que técnicamente son más complejos, de costos elevados en grandes superficies y requieren mantenimientos a veces complicados.

Los sistemas (b) y (c) responden de manera autónoma a cambios de temperatura o radiación, aunque no pueden ser modulados directamente. Las tecnologías a y b pueden ser de bajo costo, pero no responden a los cambios térmicos y en el caso de los recubrimientos fotocrómicos se produce una caída en transmisión tanto en el visible como en el infrarrojo.

Las tecnologías electrocrómicas se consideran activas por ser dependientes y controlables mediante la aplicación de una polarización eléctrica. Existen otras variantes de tecnologías activas como la gasocrómica, la de partículas suspendidas o cristal líquido, entre las más comunes. Estas tecnologías, aunque pueden ser eficientes y se acercan más a lo que podría considerarse una ventana ideal, poseen desventajas como su costo y su mayor complejidad técnica. Las tecnologías por recubrimientos termocrómicos pueden ser de gran interés para climas calientes y de alta irradiación solar como el nuestro. La base de la respuesta autónoma de los recubrimientos termocrómicos es una transición de fase que transforma el comportamiento de la capa de aislador a conductor eléctrico, reflejándose la radiación infrarroja cuando se encuentras en esta situación. En concreto, al calentarse el recubrimiento termocrómico, este cambia sus propiedades ópticas, afectando a penas a la transmisión de luz visible, mientras que el coeficiente de energía solar térmica trasmitida al interior en forma de radiación infraroja es deseablemente bajo.

Los recubrimientos inteligentes como los electrocrómicos y los termocrómicos tienen la posibilidad de cambios de características ópticas como color, transparencia, fotodispersión, etc. bajo la acción de estímulos eléctricos, térmicos o de otro tipo, de ahí que las posibilidades de aplicación van más allá que su uso en ventanas inteligentes.

IV. VENTANAS INTELIGENTES CON RECUBRIMIENTOS TERMOCRÓMICOS

El funcionamiento de los recubrimientos termocrómicos se basa en una transición de fase reversible que tiene lugar al superar una temperatura determinada Tt. Por encima de la misma se produce un cambio desde un estado semiconductor, en que la capa es transparente, a un estado metálico que reflejan la radiación infrarroja pero mantienen casi inalterada la transparencia a la luz visible. En la Fig. 2 se ilustra cómo trabaja el recubrimiento termocrómico en una ventana inteligente. La reflexión de la radiación infrarroja reduce el calentamiento al evitarse la absorción de esa radiación. Para que esta función sea operativa y de interés práctico, es necesario que el material del recubrimiento presente ese cambio de fase a una temperatura cercana a la temperatura ambiente que se considere adecuada para conseguir confort ambiental. Materiales inorgánicos como algunos óxidos y yoduros metálicos y materiales organometálicos poseen transiciones termocrómicas semiconductor-metal. Sin embargo, de ellos, el único que presenta una temperatura de cambio de fase cercana a la ambiente es el dióxido de vanadio, VO_2, con $Tt \approx 68°C$ [8–10]. Al alcanzar esta temperatura, la red cristalina del VO_2 cambia de monoclínica, que ópticamente se comporta transparente a la radiación infrarroja, a la tetragonal, en que se produce una disminución de la transmisión y aumento de la reflexión en la región infrarroja cercana.

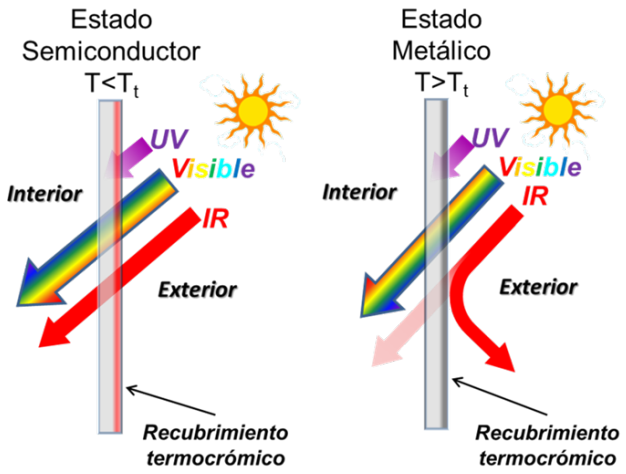

Figura 2. Funcionamiento de un recubrimiento termocrómico.

En ambos casos este recubrimiento absorbe la componente ultravioleta, lo que también hace, por ejemplo, el vidrio de la ventana. En consecuencia, la modulación de radiación solar que atraviesa un elemento recubierto de VO_2 puede ocurrir automáticamente al alcanzarse la temperatura de transición de fase. Aunque el VO_2 se perfila como material sobresaliente en las aplicaciones solares termocrómicas, sus propiedades típicas en forma de compuesto másico no son las óptimas para su uso para el control de la radiación en ventanas "inteligentes". En concreto, las investigaciones que se siguen desarrollando en este campo tienen como objetivo fabricar recubrimientos para los cuales la transición de fase tenga lugar a temperaturas más próximas a la ambiente [9, 11]. Estas investigaciones persiguen modificar la nanoestructura y morfología de las capas con el fin de mejorar su desempeño a temperaturas de operación deseadas.

Los materiales termocrómicos pueden ser también orgánicos o híbridos [12], o sea, una mezcla de orgánicos e inorgánicos. Los materiales orgánicos investigados son variados, pero presentan inconvenientes como su inestabilidad, alta temperatura de transición, colores inicial y final diferentes, falta de reversibilidad, degradación y poca eficiencia de modulación de sus propiedades ópticas, que limitan su uso generalizado.

V. APLICACIONES

La aplicación más generalizada de los recubrimientos termocromáticos se encuentra en su uso para ventanas y cubiertas transparentes y traslúcidas de edificios que combinen confort visual con la reducción de la radiación infrarroja que penetra a través de ellos en el caso de climas cálidos o la penetración y retención en el interior de tal radiación en climas fríos. El ahorro energético que posibilita el uso de estos recubrimientos es alto debido a la reducción del empleo de sistemas de climatización y ventilación. Los recubrimientos termocromáticos pueden también tener otros usos. Por ejemplo, el control de la radiación en los calentadores solares de agua doméstica sirve para prevenir averías por sobrepresión de agua cuando su temperatura es muy elevada. De la misma manera, en invernaderos, los recubrimientos termocrómicos pueden controlar inteligentemente la radiación infrarroja que llega a las plantas. También, el uso de pinturas termocrómicas se puede considerar para limitar el incremento de temperatura en superficies expuestas a la radiación solar como en el caso de los vehículos que poseen superficie y cubierta metálicas que se calientan al estar bajo la radiación solar. También pueden aplicarse tales pinturas como recubrimiento de materiales sintéticos, telas, cerámicas, etc. Materiales termocrómicos orgánicos podrían usarse como indicadores de temperatura usados en seguridad alimentaria.

VI. CONCLUSIONES Y PERPECTIVAS

En resumen, los esfuerzos de investigación presentes y futuros sobre recubrimientos termocrómicos presentan un gran interés y deben potenciarse. Su uso es relevante para el desarrollo de nuevas generaciones de ventanas inteligentes que contribuyan a aumentar el ahorro energético. Aunque ya ha habido numerosos estudios sobre el uso de recubrimientos de óxido de vanadio VO2 sobre áreas grandes, se requiere continuar con el estudio de nuevos materiales compuestos basados en el VO_2 entre otros para propiciar un mejor control ambiental y su producción masiva de manera eficaz. El bajo costo de producción de ventanas inteligentes o recubrimientos de ventanas, específicamente de VO2, estimula el desarrollo de estudios fundamentales por la academia y el de investigación aplicada desarrollada por la industria, resultando muy promisorio y factible

para países con recursos limitados. En Cuba, donde no se emplean las ventanas inteligentes, a pesar de que llega alta radiación solar, los trabajos en este tema, aunque son aún incipientes, ya se realizan y perfilan estudios que incluyen obtención de nanopartículas de VO_2, estudio de posibles matrices poliméricas y modificaciones morfológicas en películas delgadas.

REFERENCIAS

[1] P. Bhusal, E. Tetri, L. Halonen, Lighting and energy in buildings, Espoo, Finland, Helsinki University of Technology, Department of Electronics, Lighting Unit, Report 47 (2008).

[2] InfoConstrucción, El 33 % del consumo energético mundial tiene lugar en los edificios, (March 6th, 2019) (https://www.infoconstruccion.es/noticias/20190306/edificios-consumo-energetico) Accessed 12.12.2019.

[3] D. Stolik Novgorod, Energía Fotovoltaica para Cuba (Editorial Cubasolar, La Habana, 2019), p. 17.

[4] The Future of Cooling, International Energy Agency, OECD/IEA (2018). (https://www.iea.org/publications/freepublications/publication/The_Future-_of_Cooling.pdf).

[5] Rockwool, El 66 % del consumo energético de los edificios corresponde a aire acondicionado, ventilación y calefacción, (July 26, 2018) (https://www.rockwool.es/quienes-somos/noticias/2018/el-66-del-consumo-energetico-de-los-edificios-corresponde-a-aire-acondicionado-ventilacion-y-calefaccion/).

[6] I. G. Mardones, La demanda de aire acondicionado disparará el consumo eléctrico en el mundo, Geotermiaonline (2018) (https://geotermiaonline.com/2018/05/aire-acondicionado-refrigeracion/) Accessed 12.12.2019.

[7] S. D. Rezaei, S. Shannigrahi and S. Ramakrishna, Sol. Energy Mater. Sol. Cells **159**, 26 (2017).

[8] M. Kamalisarvestani, R.Saidur, S.Mekhilef, F.S.Javadi, R. Saidur, S. Mekhilef and F.S. Javadi, Renew. Sust. Energy Rev. **26**, 353 (2013).

[9] Sh. Wang, K. A. Owusu, L. Mai, Y. Ke, Y. Zhou, P. Hu, Sh. Magdassiand Y. Long, Appl. Energy **211**, 200 (2018).

[10] M. M. Seyfouri and R. Binions, Sol. Energy Mat. Sol. C. **159**, 52 (2017).

[11] Sh. Wang, M. Liu, L. Kong, Y. Long, X. Jiang and A. Yu, Prog. Mater. Sci. **81**, 1 (2016).

[12] J. Faucheu, E. Bourgeat-Lami and V. Prevot, Adv. Eng. Mater. 1800438 (2018).

BREAKING THE SOUND BARRIER: CUBANS AT CAM19

ROMPIENDO LA BARRERA DEL SONIDO: CUBANOS EN EL CAM19

J. Cerutti†

Facultad de Física, Universidad de La Habana, 10400 La Habana, Cuba; jcerutti@fisica.uh.cu

Recibido 10/11/2019; Aceptado 20/11/2019

In august 2017, a group of 14 cuban postgraduate students participated for the first time in the Canadian American Mexican Graduate Students Physics Conference (CAM), in Washington, D.C. As Maria Sanchez Colina, president of the Cuban Physical Society (SCF) and head of the delegation said at that time, the Cuban participation in CAM 2017 showed that Science is a powerful force allowing women and men to transcend frontiers, walls and prejudices of any kind [1]. The participation of a Cuban delegation was appreciated both by the Cuban students and by the CAM regular organizers. Immediate positive feedback from that experience was the organization of the First Cuban Physics Meeting for Graduate Students, that took place in La Habana in 2018, and the possibility of a new invitation for Cuban students to participate in further CAM editions.

The American Physical Society (APS), who supported the Cuban participation in Washington, generously made once again the offer to support the expenses of registration and travel for the Cuban participation in the 2019 edition of CAM in Sudbury, Ontario, Canada.

Figure 1. Cuban posgraduate students dressed properly to walk through a nickel mine where a laboratory on dark matter and neutrino physics is located. Picture taken at the entrance of SNOLAB, 2km underground. From left to right: Joeluis Cerutti Torres (UH), Michael Hernandez Bertrán (UH) and Jorge Alberto Cardenas (UCLV).

However, this time an unexpected barrier appeared: health problems suffered by some US and Canada diplomats in Havana (surprisingly associated to "sonic attacks" at the time they were made public around August 2017[1]), had caused a drastic decrease in the diplomatic personnel of the corresponding embassies in Havana. Then, Cubans had to travel to a third country to get visas in order to travel to the US and Canada. As a result, a very small representation of Cuban graduate students was able to participate. Three students, two from the Physics Faculty, University of Havana, and one from the Central University of Las Villas were able to physically take part in the event in Canada, and one more student, from ICIMAF, was able to virtually participate. In addition, a professor from CNEURO traveled as an invited plenary speaker.

We must underline the constant care of both the APS and the Organizing Committee, as well as the SCF, into solving every problem and make possible that Cuba could be present in Sudbury. Once again, science proved to be an efficient tool braking political and conventional barriers into fruitful cooperation.

Parallel sessions for oral presentations of the students and a poster session occupied the most part of the CAM2019 schedule. Two Cuban students presented their research results in the poster sessions and the other two presented oral talks, one of them via Skype. A Cuban student was also invited to be part of the judging team for the poster competition that took place in the event. The poster session had the particularity that it was preceded by a Poster Jam: a mini-session in which every poster presenter had 60 seconds to "sel" her/his poster –for the Cuban poster presenters it was a challenging, but interesting experience.

Besides the opportunity to share their research projects, participants were able to learn about recent research topics, with the plenary talks given by professors of the four participating countries. The Cuban professor Eduardo Martinez Montes gave a talk about Neuroscience. Also, the last plenary talk, talking about job opportunities for PhD in physics, gave the students the opportunity to start thinking about post-doctoral life.

Besides academic activities, the agenda included three discussion panels and two interactive workshops. The first two panels dealt mainly with the vision that students have of themselves as PhD students and their future: Career Planning and Funding in Science. The third one was about

[1] See "Havana Syndrome" in Wilkipedia https://en.m.wikipedia.org/wiki/Havana_syndrome

Publications. As for the workshops, the first one was about how to write effective Curriculum Vitae, and the second one about gender and racial integration in science.

Figure 2. Cuban students and Prof. Martinez Montes (CNEURO), inside the facilities of SNOLAB, in Sudbury, Ontario.

It is impossible not to mention a very interesting activity organized by CAM2019 –arguably the most popular among all participants. Two kilometers under Sudbury, within an active nickel mine in Vale Creighton, is located a science laboratory specialized in neutrino and dark matter physics: SNOLAB. The original Sudbury Neutrino Observatory (SNO) experiment has ended but the facilities remained as a permanent laboratory that hosts today five more experiments, looking for neutrino characterization or dark matter detection, and at least four more are under construction or starting to run. The current director of SNOLAB, Arthur McDonald, was awarded the Nobel Prize in 2015, precisely for his research on neutrinos. The tour to SNOLAB was extremely interesting from a scientific perspective and also seemed like an adventure for all the participants.

I had the pleasure to be one of the students who was able to represent Cuban science among fellow master and doctoral students of the region. CAM2019 was an experience of collaboration, starting way before the Conference itself, and moreover during the days of scientific discussions. Almost everyone –from organizers and participants— were eager to meet us; the Cuban students. Most of them wanted to talk about science, society and politics, but some of them were also looking for a partner to dance! I must confess that critical thinking, science and research, as well as political and social positions of Cuban students were better represented than our ability to dance.

REFERENCES

[1] M. Sánchez-Colina, Rev. Cubana. Fis. **34**, 98 (2017).

EL PREUNIVERSITARIO ASALTA LA FACULTAD DE FÍSICA

Foto de grupo de la Primera escuela de Verano "Física para todos", celebrada del 8 al 12 de julio de 2019 en la Facultad de Física de la Universidad de La Habana.

Durante la semana del 8 al 12 de julio, La Facultad de Física de la Universidad de La Habana se llenó literalmente de jóvenes de enseñanza preuniversitaria. Esta vez los jóvenes no estaban asistiendo a oír o ver, sino a hacer: todos pusieron sus manos y su intelecto en diversos proyectos propuestos por los profesores de la Facultad de Física. Los temas eran realmente eclécticos: construcción un dispositivo para medir el campo magnético terrestre, escribir un programa en Python (sin saber programar en Python a priori) para seguir a una hormiga sobre el suelo, determinar experimentalmente la resistencia mecánica de un preservativo, determinar si un ser humano puede moverse en línea recta, con los ojos vendados, utilizando una silla de ruedas... Este eclecticismo, que podría haber conducido al caos, realmente tuvo el efecto contrario: la mayor parte de los participantes se tomaron muy muy en serio el reto. Como colofón, el 12 de julio se realizó una jornada científica donde los estudiantes de preuniversitario expusieron sus trabajos ante un tribunal, y se confirieron premios. A continuación, se cita textualmente la casi totalidad del el informe que la decana de Física, Dra. Aimé Peláiz-Barranco, envió a la Rectora de la Universidad de La Habana.

La 1ra Escuela de Verano "Física para Todos" se desarrolló en la Facultad de Física de la Universidad de La Habana del 8 al 12 de Julio de 2019. Contó con la asistencia de 47 estudiantes de preuniversitario: 20 de 10mo grado y 27 de 11no grado, de 15 preuniversitarios de La Habana (11), Mayabeque (2) y Matanzas (2).

Se impartieron dos charlas: "Viajando al nanomundo" por el Dr. Osvaldo de Melo Pereira y "El universo: al infinito y más allá" por los Dres. Gretel Quintero-Angulo y Daryel Manreza-Paret. Se desarrollaron 16 Proyectos Experimentales en tríos, con la participación de 19 profesores y 1 técnico docente de la Facultad de Física, 2 investigadores y 1 técnico del IMRE, y 4 estudiantes de Física (1 de 1ro, 1 de 4to, y 2 de 5to)[1]*. A través de estos proyectos todos los estudiantes fueron evaluados satisfactoriamente por sus respectivos profesores considerando el interés, desempeño y responsabilidad mostrados en todas las actividades incluidas en cada proyecto. En*

[1]Participaron en los proyectos los profesores Alberto Batista, Vicente Díaz, Teresita Molina, Antonio Serrano, Gustavo Viera, Gretel Quintero, Alfredo Reyes, Frank Corrales, Ernesto Altshuler, Félix Martínez, Alfredo de la Campa, Jael Faloh, Gustavo Sánchez, René Fundora, Francisco Gutiérrez, Saúl Larramendi, María Sánchez, Osvaldo de Melo, Arbelio Pentón, Daryel Manreza. Igualmente los trabajandores del IMRE Lídice Vaillant, Beatriz Concepción y Nicolás Sirgado. Julio Vidal, Armando Pérez y Reinaldo Font. Estuvieron vinculados a la organización antes y durante la Escuela: Nelia López, Roberto Mulet, Arbelio Pentón, y otros colegas. Es importante mencionar también la participación de los estudiantes de Física Karen Alonso (1er año), Carlos Calvo (4to año), Jesús Alba (5to año) y Josué Benavides (5to año) en los proyectos experimentales, así como David Machado (5to año) y Bárbara Pérez (5to año) en el apoyo logístico.

el día final de la Escuela se celebró una intensa Jornada Científica, en la que cada equipo presentó su trabajo ante un tribunal de tres experimentados profesores –que no fueron parte de los proyectos: los doctores Julio Vidal, Armando Pérez y Reinaldo Font.

Los estudiantes, además, recibieron información sobre la carrera y la Facultad, realizaron un recorrido por la universidad, y se realizó una reunión con los padres con vistas a ofrecer información sobre el plan de estudio de licenciatura en Física y lo que representa esa carrera para el futuro de los jóvenes interesados.

Se aplicaron encuestas a los participantes con resultados muy alentadores. Los estudiantes calificaron positivamente la organización y nivel científico de la Escuela, y la calidad de los proyectos desarrollados. Confirmaron un buen cumplimiento de sus expectativas y un aumento de su motivación por la física. Pidieron que la Escuela se mantuviera, se incrementara el número de días y las actividades a desarrollar (tanto científicas como extensionistas).

Al cierre de la Escuela, del total de 44 estudiantes (1 de ellos ya tenían asignada nuestra carrera y el Colegio Universitario), 21 solicitaron estudiar la carrera (14 de 10mo grado y 7 de 11no grado), y de ellos 17 hacer el 12 grado en el Colegio Universitario (13 de 10mo grado y 4 de 11no grado). Esto representa para nosotros un magnífico resultado para esta 1ra Escuela de Verano.

El desarrollo de la Escuela fue gracias al apoyo de la dirección de la Universidad de La Habana, la beca de 12 y Malecón, Extensión Universitaria, el IMRE, la Sociedad Cubana de Física, el Taller Iberoamericano de enseñanza de la Física (TIBERO), y claro está, los profesores, trabajadores y estudiantes de la Facultad de Física. Contamos con cobertura divulgativa en el Canal Habana y la Revista Juventud Técnica. Debemos agradecer también a la Dra. Daybel Panellas Alvarez por su apoyo para la divulgación en el Canal Habana y la elaboración de las encuestas aplicadas a los estudiantes participantes, y a la estudiante de 5to año de diseño Yohana Carvajal Escobar por el apoyo en el diseño del logo de la Escuela.

La experiencia de esta 1ra Escuela nos ha mostrado que existe mucho potencial en nuestros adolescentes hacia las ciencias, pero carecen de la información necesaria (incluyendo a sus padres) y las actividades vocacionales que le permitan decidirse por este tipo de carreras. En este sentido, se hace necesaria la elaboración de una estrategia vocacional con actividades a los largo del curso, para llegar a un número mayor de estudiantes, y que tenga como cierre la Escuela de Verano, cuya concepción evaluaremos también atendiendo a los resultados derivados de las encuestas.

E. Altshuler

LA SOCIEDAD CUBANA DE FISICA REPRESENTADA EN LA VIII ASAMBLEA DE FEIASOFI

Participantes en la VIII Asamblea de FEIASOFI. María Sánchez-Colina, presidenta de la Sociedad Cubana de Física y vice-presidenta de la FEIASOFI, es la tercera de izquierda a derecha.

La ciudad de Zaragoza (España) acogió la VIII Asamblea de la Federación Iberoamericana de Sociedades de Física (FEIASOFI), el día 19 de julio de 2019. La Sociedad Cubana de Física estuvo representada por su presidenta, Dra. María Sánchez-Colina –también vice-presidenta de la FEIASOFI. Además, hubo representaciones de similares organizaciones de Argentina, Brasil, Chile, Colombia, Costa Rica, República Dominicana, España, Guatemala, Honduras, México, Uruguay, y Venezuela. En la Asamblea se informó de las actividades realizadas desde la reunión de La Habana de febrero de 2018. En la VIII Asamblea se adoptaron importantes compromisos destinados a fortalecer el papel de la FEIASOFI en su área de influencia, incluyendo un acuerdo de reciprocidad de derechos entre las asociaciones integrantes. Se adoptó un nuevo criterio para las cuotas de membresía y el compromiso de realizar reuniones bianuales coincidentes con el congreso de alguna asociación de los países miembros. También se decidió redoblar el apoyo a la organización de la Olimpiada Iberoamericana de Física y a la Olimpiada Latinoamericana de Física (OLUF) que, como sabemos, es una iniciativa de Cuba. Los presidentes y representantes de las Sociedades de FEIASOFI aprovecharon su estancia en Zaragoza para mantener encuentros bilaterales.

E. Altshuler

(Adaptado de la Revista Española de Física, julio-septiembre 2019)

EINSTEIN PARA PERPLEJOS

La Sociedad Cubana de Física, la Sociedad Cubana de Historia de la Ciencia y la Tecnología y la Biblioteca Nacional "José Martí" auspiciaron la presentación del libro "Einstein para Perplejos" de José Edelstein, el 16 de agosto de 2019 en los salones de ésta última. El autor, además, obsequió ejemplares del trabajo a las instituciones auspiciadoras.

Si me plegara ante las bondades omnipresentes de Wikipedia, costaría apenas un par de teclazos informar que el autor José Edelstein Glaubach, es un físico y divulgador de la ciencia nacido en Argentina en 1968, que hoy labora en el departamento de Física de Partículas de la Universidad de Santiago de Compostela. Licenciado del Instituto Balseiro –un hecho nada inesperado cuando se trata de un brillante físico argentino– se doctoró en la Universidad Nacional de La Plata, y realizó estancias post-doctorales en centros académicos de nivel mundial, como la Universidad de Harvard. Haciendo un esfuerzo por distanciarme un poco de la elocuencia de Wikipedia, me permitiría agregar que el trabajo científico de José aborda algunos de los temas de la Física en los que estarían trabajando Galileo o Newton, en

caso de que fueran nuestros contemporáneos. Y lo digo, porque asuntos como la Teoría de Cuerdas y la posible unificación entre la Mecánica Cuántica y la Teoría de la Relatividad pujan por abrir nuevos senderos en la cosmovisión del ser humano en este mismo instante.

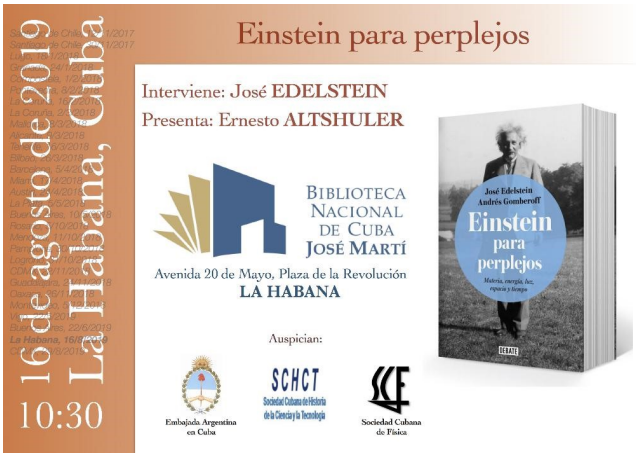

Anuncio de la presentación del libro "Einstein para perplejos".

Si me animara a separarme aún más del facilismo *wikipédico*, podría aventurar que quizás el hacer ciencia justamente en el borde de la cosmovisión humana, allí donde la Física intenta secuestrar a la Filosofía hacia el mundo de las ecuaciones matemáticas, es lo que ha motivado a José a sacar un pie de la Física pura, y probar la temperatura de las aguas del otro mundo; el de las letras.

Pero lo que difícilmente podría encontrarse en Wikipedia, es el cómo conocí a nuestro invitado, allá por la época aciaga de la última década del siglo XX cubano, conocida eufemísticamente como "Período Especial". José, formando parte de un grupo de colegas argentinos que se auto-denominaban "Chau Bloqueo", organizaba sistemáticamente envíos de papel, lápices, goma de pegar y otras modestas pero cruciales donaciones para nuestro laboratorio en la Universidad de La Habana. En medio de la etapa más competitiva de sus carreras científicas, esos colegas ponían su dinero pero, sobre todo, su precioso tiempo, para que los del lado de acá pudiéramos hacer ciencia en "condiciones de alta tropicalidad". Esta imagen, que resulta más cercana a mi corazón, es la que primero me viene a la mente cuando se menciona el nombre del autor de "Einstein para perplejos".

Se trata, en una palabra, de un libro que no sólo es capaz de amortiguar las perplejidades presentes de sus lectores, sino que creará nuevas e inesperadas perplejidades. Pues la perplejidad es, junto a la curiosidad y el asombro, una gran instigadora del avance científico.

E. Altshuler

EN LA IBERO, *CASI* LLEGAMOS AL ORO

La XXIV Olimpíada Iberoamericana de Física tuvo lugar en El Salvador, del 9 al 13 de septiembre de 2019. Los 4 participantes cubanos se agenciaron medallas, aunque esta vez ninguna fue de oro: Reynaldo Pupo Osorio, Victor M. Michel González y Angel R. Sánchez ganaron medallas de plata (el primero fue la primera plata, a sólo 0.5 puntos de los oros), mientras que Carlos E. González Carballosa se alzó con un bronce.

J. Mora
IPVCE "Carlos Marx"
Matanzas

LLENO COMPLETO EN LA 402

El profesor Carlos Cabal se dirige al cosmonauta cubano Arnaldo Tamayo-Méndez (de frente, al fondo) durante un encuentro que éste último tuvo con estudiantes y profesores en la Facultad de Física de la Universidad de La Habana el pasado 6 de noviembre de 2019 (Foto: E. Altshuler).

Ocurrió el pasado 6 de noviembre. Hacía muchos años no se veía un auditorio tan multitudinario en el aula 402 del último piso del edificio de Física, en la Universidad de La Habana: de hecho, fue necesario agregar sillas a las ya existentes. Y no era para menos: se trataba de una presentación del cosmonauta cubano Arnaldo Tamayo-Méndez, organizada por la dirección y el PCC de la facultad de Física. Tamayo, tras hacer una introducción sobre su histórico viaje, que tuvo lugar en 1980, presentó el documental "El Primero", y luego respondió preguntas realizadas por la audiencia, compuesta esencialmente por estudiantes y profesores de la facultad de Física. El cosmonauta recordó los experimentos que científicos cubanos diseñaron para realizar en condiciones de micro-gravedad durante el vuelo, como el crecimiento de cristales semiconductores y de sacarosa, en los cuales habían tenido un papel protagónico colegas de la Facultad de Física de la Universidad de La Habana y del ININTEF (hoy ICIMAF), entre otras instituciones. Ha de resaltarse el tono riguroso, pero salpicado de humor, que mantuvo el cosmonauta durante todo el encuentro –incluyendo su respuesta a alguna que otra pregunta incisiva realizada por la audiencia.

E. Altshuler

CELEBRANDO LOS 90 DE UN ARTÍFICE DE LA REFORMA UNIVERSITARIA

El Prof. Altshuler, junto a un grupo de colegas, ex alumnos y amigos, unos instantes antes de que comenzara el acto en el Aula Magna. De izquierda a derecha: Fabito Grobart, Esperanza Purón, Roberto Valdés, Miguel González, Roberto Díaz-Martín, Olimpia Arias, José Altshuler-Gutwert y Wilfredo Torres (Foto: Victor Márquez).

El pasado 21 de octubre, auspiciado por la Cátedra de Cultura Científica Félix Varela, se celebró en el Aula Magna de La Universidad de La Habana el aniversario 90 del Profesor José Boris Altshuler-Gutwert. Pocas veces se tiene la oportunidad de efectuar celebraciones de este calibre, sobre todo porque el homenajeado desempeñó un relevante papel en la elaboración de la Ley de Reforma Universitaria de 1962 y su labor en nuestra universidad alcanzó tal protagonismo que fue el primer Vicerrector luego de la puesta en vigor de dicha ley, siendo Rector el eminente intelectual y luchador social Juan Marinello. Como artífice de la especialidad de Electrónica y Telecomunicaciones después del triunfo revolucionario, la Universidad Tecnológica de La Habana le confirió en 2004 el Doctorado Honoris Causa. El listado de las obras donde ha dejado su impronta es demasiado extenso para resumirlo en pocas líneas. Baste señalar que es Académico de Honor y preside actualmente la Sociedad Cubana de Historia de la Ciencia y la Tecnología, que ha sido Vicepresidente de nuestra Academia de Ciencias, Presidente de la Comisión para el Estudio y el Uso Pacífico del Espacio Ultraterrestre, y Fundador del Movimiento Cubano por la Paz, y también que ha recibido, entre otros galardones, las Distinciones Rafael María de Mendive y Educador Destacado del Siglo XX en Cuba, y la Medalla de Combatiente de la Lucha Clandestina.

El acto dio inició con una palabras de elogio del Profesor Hugo Pérez Rojas, compañero de muchos años, quién reseñó pasajes de la vida de José y su legado a quienes lo conocieron y admiraron. También hizo el elogio, a nombre de la Cátedra de Cultura Científica Félix Varela, su presidente, el Dr. Ernesto Estévez Rams. Pero el momento inesperado de la velada lo constituyeron las palabras que el propio homenajeado dirigió a los presentes, rememorando distintos episodios y motivaciones importantes de su vida. Con todo, la conversación informal que, una vez concluido el acto, tuvo lugar entre el homenajeado y un grupo de jóvenes universitarios, resultó quizás lo más especial de la tarde.

José Boris Altshuler-Gutwert nació el 25 de septiembre de 1929. En el contexto "espacio temporal" en el que creció, Cuba era una isla ajena en lo fundamental a la ciencia. Ciencia que en épocas anteriores había dado muestras de la pujanza de nuestro sujeto nacional cuando intelectuales de la colonia vieron en ella parte integrante de la conformación de la nacionalidad cubana. Entrados el siglo XX y la "república de corcho", fue la inexistencia social de desarrollo científico y técnico autóctono lo que marcó el distanciamiento entre las formas culturales en el país.

Militante de la Juventud Socialista desde mediados de la década de 1940, el homenajeado nos contó en sus palabras improvisadas, como la vista de personas paupérrimas, incluidos niños y ancianos, durmiendo a la intemperie en los portales del Centro Asturiano, hoy Sala Universal del Museo de Bellas Artes, se contó entre los hechos que le llevaron a decirse que había que hacer algo para cambiar el orden social responsable de tales miserias. Al recibir en 2013 la condecoración por el aniversario 50 de la UPEC, Jorge Risquet narraba cómo fue juzgado, junto a otros colegas de la redacción del "Magazine Mella" por publicar en 1950 un "violento artículo" contra la corrupción gubernamental. Entre los sometidos a juicio, menciona a José Altshuler-Gutwert, quien tenía entonces 21 años.

Como parte del proceso revolucionario cubano en el poder desde 1959, la educación superior comenzó su propia revuelta: en este caso, retomar la reforma inconclusa, tras la derrota de la tiranía batistiana, de Julio Antonio Mella. Hasta entonces invalidados en la práctica para impartir docencia en La Universidad, los primeros intelectuales comunistas pudieron acceder al claustro profesoral, entre ellos Carlos Rafael Rodríguez, Mirta Aguirre y José Altshuler-Gutwert. El 31 de diciembre de 1960 se creó el Consejo Superior de Universidades, encargado de elaborar la Ley de Reforma Universitaria. Como representantes del Gobierno Revolucionario fueron nombrados Armando Hart, Regino Boti, Pedro Cañas y el homenajeado, para entonces, ya profesor titular de la Escuela de Ingeniería. Respecto a la Ley de Reforma Universitaria, en el texto de Armas, Torres Cuevas y Cairo dedicado a la historia de la educación superior en Cuba, se lee "Utilizando varios folletos de las actas de discusiones de especialistas y de las reuniones del Consejo Superior de Universidades, el homenajeado, con ayuda del ingeniero Albert [asesor de la Junta Central de Planificación…], elaboró un proyecto con unidad de estilo, que con algunas modificaciones finales hechas en la sesión en que se le dio lectura, constituyó el texto de la ley". Y se añade en el texto mencionado: "El ingeniero Altshuler y el ingeniero Diosdado Pérez Franco elaboraron los planes de estudio de las Escuelas de Ingeniería Eléctrica y Civil, respectivamente, y sobre los hombros del primero recayó la responsabilidad de coordinar todos los planes de estudios de la futura facultad de tecnología".

La primera dirección universitaria de la Revolución posterior a la Ley de Reforma Universitaria la encabezó como Rector el eminente intelectual y dirigente comunista Juan Marinello y como Vicerector, José Altshuler-Gutwert. En esa alquimia feroz que es la Revolución cubana, a tres años de su triunfo, esta rescataba la alianza interrupta desde el siglo XIX entre humanismo y ciencia: Marinello, pensador, poeta y literato, y Altshuler, investigador en el campo de la ciencia y la tecnología. En 1962, en una intervención titulada "El ingreso en las carreras universitarias y las necesidades urgentes de nuestro desarrollo" este último comenzaba diciendo "La ley de reforma de la enseñanza superior en Cuba sitúa (con toda justicia) como primera obligación de la universidad nueva, formar profesionales de nivel superior en el

número y con la calidad que demandan las necesidades de la nación. La torre de marfil queda derribada."

Las revoluciones no las hacen personas que asienten: las hacen los rebeldes. Las revoluciones son asunto de inconformes, los que creen que hay algo que arreglar y que se puede arreglar, aun si es a un costo muy alto. El homenaje que le ofrecimos a José Altshuler-Gutwert fue un homenaje a los soldados de ese NO fundador sin el cual no habrían ni ciencia, ni educación superior, ni justicia, ni patria para todo el pueblo cubano, sin exclusiones.

E. Estévez-Rams
Facultad de Física
Universidad de La Habana

Revista Cubana de Física
ISSN 0253-9268
Online ISSN 2224-7939